2018-12-05

Surface Chemistry and Spectroscopic Studies of Enzymatic, Non-Enzymatic Molecules and their Applications

Shiv K. Sharma
University of Miami, sk.edu46@gmail.com

Recommended Citation

Sharma, Shiv K., "Surface Chemistry and Spectroscopic Studies of Enzymatic, Non-Enzymatic Molecules and their Applications" (2018). *Open Access Dissertations*. 2218.
https://scholarlyrepository.miami.edu/oa_dissertations/2218

UNIVERSITY OF MIAMI

SURFACE CHEMISTRY AND SPECTROSCOPIC STUDIES OF ENZYMATIC, NON-ENZYMATIC MOLECULES AND THEIR APPLICATIONS

By

Shiv K. Sharma

A DISSERTATION

Submitted to the Faculty
of the University of Miami
in partial fulfillment of the requirements for
the degree of Doctor of Philosophy

Coral Gables, Florida

December 2018

UNIVERSITY OF MIAMI

A dissertation submitted in partial fulfillment of
the requirements for the degree of
Doctor of Philosophy

SURFACE CHEMISTRY AND SPECTROSCOPIC STUDIES OF ENZYMATIC, NON-ENZYMATIC MOLECULES AND THEIR APPLICATIONS

Shiv K. Sharma

Approved:

Roger M. Leblanc, Ph.D Professor of Chemistry	Françisco M. Raymo, Ph.D. Professor of Chemistry
Jamie D. Walls, Ph.D. Associate Professor of Chemistry	Guillermo Prado, Ph.D. Dean of the Graduate School
Jean-Marie Parel, Ph.D Associate Professor of Ophthalmology	

SHARMA, SHIV K. (Ph.D., Chemistry)
Surface Chemistry and Spectroscopic Studies of (December 2018)
Enzymatic, Non-Enzymatic Molecules
and their Applications

Abstract of a dissertation at the University of Miami.

Dissertation supervised by Professor Roger M. Leblanc.
No. of pages in text. (121)

The content of this thesis is an investigation into physicochemical, photophysical, and interfacial properties of β-galactosidase, a crucial enzyme, its conjugate with CDs, interaction of β-galactosidase with X-gal, and surface chemistry and spectroscopic study of toxins, Cholera toxin B (CTB) and Fumonisin B1 (FB1). The objective of the work was to understand the surface chemistry behavior of the important enzyme, conjugates and toxins in a model systems representing vaguely cell membrane environments, to prove the activity of the deposited enzyme, its conjugate, and toxins in a form of the monolayer. We also studied the effect of green LED light on the FB1 Langmuir monolayer which will be useful for possible future treatment of fungal keratitis without any side effects. Furthermore, this approach can be employed to understand the property of transmembrane receptors, to study the cell adhesion, and its implications. Besides that, this information is relevant for the successful deposition of Langmuir-Blodgett (LB) film. The Langmuir monolayer isotherm of enzyme, conjugate and the toxin were studied using the surface chemistry and spectroscopy at the air-water/subphase interphase.

We employed the pressure (π)-area (A) isotherm measurement which is typically the very first step in the study of these enzymatic and non-enzymatic molecules floating at

the subphase surface as it gives useful information on the existence of different phases, phase transitions and the stability of Langmuir monolayer at fixed temperature and pH.

During our study we found that β-galactosidase as well as its conjugate form stable Langmuir monolayer. We observed that during the interaction of the enzyme with X-gal, its secondary structure changes. This does not mean that the overall structure of the enzyme gets changed. This is because enzyme structure is determined by primary, secondary, tertiary, and quaternary structure. The interfacial study of CTB showed that the molecule is very stable at the air-subphase interface. In performing surface chemistry and spectroscopic study of FB1 molecule, the interesting finding that came out of the FB1 Langmuir monolayer investigation was that the analyte adopted stability (without irradiation of green LED light) at the monolayer and remained degraded with subsequent effect of the green LED light (525 nm) at air-water interface.

To my family and my advisor

ACKNOWLEDGEMENTS

Firstly, I would like to express my sincere gratitude to my research advisor, Professor Roger M. Leblanc and would like to dedicate my dissertation to him for his matchless supervision, guidance, and continuous support during my doctoral studies at University of Miami (UM). His excellence in mentoring and marvelous skills as a scientist have given directions to my scientific career. His dedication as a role model has been the paradigm which I will follow in my future career. I truly thank him for his constant encouragement and motivation throughout my graduate studies and research at UM. Professor Leblanc's patient guidance showed me the way to be a good scientist and a good human being; this work wouldn't have been accomplished without his presence.

Besides my advisor, I would like to express my sincere appreciation to the members of my doctoral committee, Professor Francisco Raymo, Professor Jamie D. Walls, and Professor Jean-Marie Parel for their insightful comments, encouragement, and valuable support in my research career and academics. I would also like to extend my thanks to Dr. Chengshan Wang ((Middle Tennessee State University) and Dr. Elsayed M. Zahran for their advice, discussions, and help with my thesis and defense.

I am grateful to every faculty member and staffs in the Department of Chemistry for their help during the past five years, especially Professor Burjor Captain, Professor Rajeev Prabhakar, Dr. Tegan Eve, Ana Parr, Juanita Hernandez, Raul Hernandez, Noel Urbina, and Edward Torres.

I thank my fellow labmates Yiqun Zhou, Sajini Hattiarachchi, Piumi Liyanage, Keenan Mintz, Elif S. Seven, Suraj Paudyal for the stimulating discussions and collaboration. I would also like to extend my sincere thanks to my previous group members Zhili Peng, Eric Waideley, Yiwen Ji, Lorenzo Sansalone, Han Xu. Most importantly, I would like to thank Shanghao Li who was always there with me at the start of my research studies and helped me to initiate good lab techniques.

Last, but certainly not least, I would like to thank my parents, whose love and guidance are with me in whatever I pursue. They are the ultimate role models. Most importantly, I wish to thank my loving and supportive wife, Sijan, and my wonderful baby boy, Roger, who provide unending happiness and inspiration.

TABLE OF CONTENTS

Page

LIST OF FIGURES………………………………………………………………….x

LIST OF TABLES…………………………………………………………….….….xiv

LIST OF SCHEMES……….……………………………………………..…...……...xv

LIST OF ABBREVIATIONS……………………………………………...…xvi

Chapter 1: Introduction

1.1 Surface Chemistry and Langmuir Monolayer…………………………………1

1.2 Importance of Surface Chemistry and Spectroscopic Studies to Investigate the Properties of Enzymatic and Non-enzymatic Molecules…………..………….2

1.3 States of Monolayer on the Subphase…………………………...……….…5

1.4 Advantages of Langmuir Monolayer Approach…………………………...….7

Chapter 2: Study of β-galactosidase Langmuir Monolayer at Air/X-gal Subphase Interface

2.1 Background……………………………………………………………9

2.2 Experimental Section……………………………………………………...13

2.2.1 Chemicals……………………………………………………..…13

2.2.2 Equipment……………….……………………………………………13

2.2.3 Langmuir Monolayer Preparation………………..………………..14

2.2.4 Infrared Reflection-Absorption Spectroscopy (IRRAS).………..…14

2.2.5 Brewster Angle Microscopy (BAM)……………………………………...15

2.3 Results and Discussion……………………………………………………..…15

2.3.1 Surface pressure and surface potential-area isotherms……….……15

2.3.2 Concentration effect of X-gal in the aqueous subphase…………..….17

2.3.3 Compression-decompression cycles..…………………………..…19

2.3.4 Infrared Reflection-Absorption Spectroscopy (IRRAS)…………….22

2.3.5 Brewster Angle Microscopy (BAM)……………..…………...……26

2.4 Summary……………………………………………………..…………28

Chapter 3: Probing of interaction between β-galactosidase and X-gal at Air/X-gal Subphase Interface by Experimental and Theoretical Methods

3.1 Background……………………………………………………………………..29

3.2 Experimentation…………………………………………...……………30

3.3 Result and Discussion………………………………………………….32

3.3.1 Sum Frequency Generation Study..……………..………………32

3.3.2 Infrared Reflection Absorption Spectroscopy (IRRAS)…………....33

3.4 Computer Simulation to Investigate the Interaction of β-galactosidase and X-gal………………...…………………………...…………………36

3.4.1 Method……………………………………………...………………………36

3.4.2 Results and Discussion……………………..……………………37

3.4.3 Study of the Active site…………………………………………………...39

3.5 Proposed Mechanism of Interfacial Interaction of β-galactosidase and X-gal..41

3.6 Summary……………………………………………………………………..43

Chapter 4: Surface Chemistry and Spectroscopic Studies of Conjugate of β-Galactosidase-Carbon Dots and it's Use in Biosensing

4.1 Background…………………………………………………………….….44

4.2 β-galactosidase-CDs conjugation for biosensing ……………………………46

4.3 Experimental…………………………………………………………………47

4.3.1 Conjugation of β-galactosidase with CDs………………………….……47

4.3.2 Characterization of the Biocomposite…………………………..…….48

4.3.2.1 UV-vis Spectra of the Conjugate…………………………48

4.3.2.2 Fluorescence Spectra…..………………..……………….……49

4.4 Cytotoxicity Study of the Conjugate on Sea Urchin Embryo.………………50

4.5 Surface Chemistry and Spectroscopic Studies of the Conjugate……..………51

4.5.1 Surface Pressure and Surface Potential……………...……………51

4.5.2 Effect of concentration of X-gal on β-galactosidase-CDs conjugate Langmuir monolayer………..…..…………………….…...…52

4.5.3 In situ UV-vis Spectrum of the Langmuir Monolayer……….……..53

4.6 Monitoring Reaction of the Conjugate and Lactose…………………………55

4.7 Development of a Biosensing Platform……………………………...……56
4.7.1 Cyclic Voltammetry Study……………………………………….57
4.8 Summary………………………………………………………..………61

Chapter 5: Surface Chemistry and Spectroscopic Study of Cholera Toxin B (CTB) Langmuir Monolayer

5.1 Background……………………………………….………………62
5.2 Materials and Methods……………………………….……………65
5.2.1 Chemicals…………………….……………………….………65
5.2.2 Equipment………………………..…………..…………………65
5.2.3 Langmuir Monolayer Preparations…………………..…………66
5.2.4 UV-vis Spectroscopy……………………………………………67
5.2.5 Fluorescence Spectroscopy……………………………….……..67
5.2.6 Infrared Reflection Absorption Spectroscopy (IRRAS)…………..…..67
5.3 Results and Discussions……………………………..…………………68
5.3.1 Surface Pressure and Surface Potential-Area Isotherms…………68
5.3.2 Compression-Decompression Cycles and Stability Curves…...……70
5.3.3 UV-vis Absorption Spectroscopy…………………...…………....72
5.3.4 Fluorescence of Langmuir Monolayer………….…………………74
5.3.5 Infrared Reflection Absorption Spectroscopy (IRRAS)…………….…77
5.4 Summary…………………………………………………………...…80

Chapter 6: Surface Chemistry and Spectroscopic Study of Fumonisin B1 and Impact of Green Irradiation on its Langmuir Monolayer

6.1 Background……………………………………………..………………82
6.2 Experimental……………………………………………………………85
6.2.1 Materials and Reagents ……………………………………………85
6.2.2 Equipment……………………………………….…………………85
6.3 Methods………………………………………………………………86
6.3.1 Surface Pressure−Area Isotherms Preparation…….………..……86
6.3.2 UV−visible Absorption Spectroscopy………………………………86

6.3.3 Fluorescence Spectroscopy……………………………………...……87

6.3.4 Compression−Decompression Cycles………………...…………87

6.3.5 Solution Work…………………………………………………………87

6.4 Results and Discussion……………………………………………….………88

6.4.1 Surface Chemistry Study………………………………….………..88

6.4.1.1 Surface Pressure vs Area Isotherm…………………….…..88

*6.4.1.2 Compression-decompression of FB1 Langmuir Monolayer.*90

6.4.1.3 In situ UV-vis Absorption Spectroscopy of Langmuir Monolayer……………………………………………..93

6.4.1.4 In situ Fluorescence Spectroscopy of Langmuir Monolayer…………….…...……….……………………95

6.4 The Effect of LED Light on the FB1 Langmuir Monolayer…………....96

6.6 Comparative Study of the Effect of 525 nm LED Light on the FB1 in Solution Phase…………………………..……………………………98

6.7 Summary………………………………………………………………..…103

Chapter 7: Future Directions

7.1 Investigation of Reactivity of Monolayers…………………………………104

7.2 Understanding of Surface Reactions…………………………...………104

7.3 Carbon dots in Polymerization Process as Initiators………………………..106

7.4 Quantification of Fumonisin B1 toxin Using Carbon Dots…………………106

References……………………………………………………………..………....111

LIST OF FIGURES

Chapter 1

Figure 1.1 Image of two different Langmuir troughs (namely KSV Nima and Kibron) in our lab……………………………………………………………………3

Figure 1.2 Langmuir isotherm of arachidic acid……………………………………...…5

Figure 1.3 Structure of cell membrane showing membrane proteins………………....8

Chapter 2

Figure 2.1 Different applications of β-galactosidase enzyme………………………...9

Figure 2.2 Surface pressure and surface potential versus area/molecule when the subphase was NaCl (0.1M) and X-gal (9.78× 10^{-3} M)……………….…16

Figure 2.3 Surface pressure versus mean molecular area isotherms for 3.7×10^{-7} M β-galactosi--dase spread on 0.1M NaCl and (2.45, 4.89, 7.34 and 9.78) × 10^{-3} M of X-gal……………………………………………………………..18

Figure 2.4 Compression-decompression of Langmuir isotherm of β-galactosidase. **Column A:** absence of X-gal in the subphase maintained at the surface pressure of 5, 15 and 30 mN/m. **Column B:** presence of X-gal (4 mg/mL, 9.78 × 10^{-3}M) in the subphase maintained at surface pressure of 5, 10 and 15 mN/m…………………………………………………………………21

Figure 2.5 Normalized p-polarized IRRAS spectra at the air-subphase interface of the β-galactosidase Langmuir monolayer compared at different surface pressures in absence and presence of X-gal in the subphase at a 45° incident angle…………………………………………………………………....24

Figure 2.6 Brewster angle micrographs for β-galactosidase spread on the (A) 0.1 M NaCl, (B) 0.1 M NaCl + 2.45 × 10^{-3} M X-gal and (C) 0.1 M NaCl + 9.78 × 10^{-3} M X-gal at different surface pressures during compression. The scale bar represents 100 μm…………………………………………………….27

Chapter 3

Figure 3.1 SFG spectra for presence and absence of X-gal in the subphase………...32

Figure 3.2 p-Polarized IRRAS spectra at the air-subphase interface of the β-galactosidase Langmuir monolayer in absence of X-gal in the subphase at a 45° incident angle……………………………………………………...33

Figure 3.3 p-Polarized IRRAS spectra at the air-subphase interface of the β-galactosidase Langmuir monolayer in presence of X-gal (2.45, 4.89, 7.34

and 9.78) × 10^{-3} M of X-gal in the subphase at a 45° incident angle……………………………………………….……………………..35

Figure 3.4 X-ray crystallographic structure of β-galactosidase showing four monomeric units (a), The most representative structure derived from the 100ns MD simulation on β-galactosidase-X-gal complex with specific interactions of X-gal (shown in ball and stick) at the X-gal binding site (b)……………………………………………………………………...38

Figure 3.5 Superposition of the conformation of the active site derived from the most representative structure of the complex simulation (yellow color) with the corresponding X-ray structure (grey color)…….………………………...39

Figure 3.6 Root mean square deviation (RMSD) of amino acid residues. The RMSD is commonly used as an indicator of convergence of the structure towards an equilibrium state……….…………………………………...….…40

Figure 3.7 RMS fluctuation of residues of enzyme……………………………….....41

Figure 3.8: **(a)** Showing the pocket in the enzyme from the where X-gal fits into it **(b)** The transfer of a proton (red) of enzyme to the X-gal by opening C-O bond **(c)** Completion of enzyme catalyzed reaction. Here, the weakened C-O bond in X-gal is susceptible to nucleophilic attack by a water molecule (in green) to produce 5-bromo-4-chloro-3-indolyl and galactose…………....42

Chapter 4

Figure 4.1 The different changes in color after treating the x-gal with the native and conjugated enzyme stored in room temperature after a week and two months, respectively…….……………………..……………….....46

Figure 4.2 Absorption spectra of the conjugate. Here, the concentration of EDC and CDs was same in both cases….………………………………………..48

Figure 4.3 Fluorescence spectrum of β-galactosidase-carbon dots conjugate……....49

Figure 4.4 Cytotoxicity study of the conjugate…….………………………………...51

Figure 4.5 Surface pressure and surface potential isotherm of β-galactosidase-CDs Langmuir monolayer……………………………………………………..52

Figure 4.6 Langmuir isotherms of β-galactosidase-CDs conjugate with different concentrations of X-gal and 0.1 M NaCl subphase. The spread volume was 45 µL at room temperature……………….………………………....53

Figure 4.7 In-situ UV-vis spectra of the conjugate (0.1 mg/mL) on the subphase of 0.1 M NaCl…………………………………………………………...………54

Figure 4.8 Fluorescence spectra of the conjugate with different concentration of lactose……………….…...……………………………….................55

Figure 4.9 Cyclic voltammogram of conjugate on glassy carbon electrode with Ag/AgCl standard electrode in absence and presence of lactose……..…59

Figure 4.10 Cyclic voltammogram of glassy carbon electrode (adsorbed with β-galactosidase/Carbon Dots conjugate) with different concentration of lactose in Fe^{2+} solution……………………………………….………...60

Figure 4.11 Plot of concentration of lactose versus current…………………………..60

Chapter 5

Figure 5.1 CTB (top view, protein data bank ID: 1XTC) with CTA subunit removed……………………………………………………………..62

Figure 5.2 Langmuir monolayer of CTB (0.2 mg/mL) obtained after spreading on the 20 mM citrate phosphate buffer subphase (pH 5.5)………………..…….69

Figure 5.3 Compression-decompression Langmuir monolayer curves of CTB (0.2 $mg.mL^{-1}$) at different surface pressures spread on citrate phosphate buffer (pH 5.5). The amount of injection was 45 μL at room temperature……..71

Figure 5.4 Stability measurements of the CTB Langmuir monolayer at two different surface pressures (A) 20 and (B) 30 mNm^{-1} by spreading 45 μL of CTB (0.2 $mg.mL^{-1}$) on citrate phosphate buffer (pH 5.5) at room temperature……72

Figure 5.5 UV-vis absorption spectra of the CTB Langmuir monolayer on citrate phosphate buffer (pH 5.5) (A) and plot of absorbance versus surface pressure at 230 and 280 nm wavelengths (B)……………………………73

Figure 5.6 *In situ* fluorescence spectra at air-subphase interface of the CTB (1.7×10^{-5} M) Langmuir monolayer (A) and the plot of maximum emission at 350 nm as a function of increasing surface pressure (B)………………………76

Figure 5.7 The plot of fluorescence intensity vs time of wait of the CTB Langmuir monolayer…………………………………………………………..77

Figure 5.8 Normalized *p*-polarized IRRAS spectra of the CTB Langmuir monolayer: (a) at a surface pressure of 15 mNm^{-1} with different incident angles, (b) comparison of spectra for different surface pressures at an incident angle of 60°, and (c) expanded spectra to show the amide I and II region clearly….79

Chapter 6

Figure 6.1 Structure of Fumonisin B1 (FB1)……………………………….…….85

Figure 6.2 Surface pressure (π)- area (A) and surface potential curve of Fumonisin B1………………………………………………………………...88

Figure 6.3 Simulation of FB1 molecule at the air-water interface to calculate its size…………………………………………………………………90

Figure 6.4 Compression-decompression π-A curves at two different surface pressures (15, 23 mNm^{-1})…………………………………………………..……….92

Figure 6.5 *In situ* UV-vis spectra of FB1 Langmuir monolayer at different surface pressures……………………………………...……………………..94

Figure 6.6 Plot of absorbance vs surface pressure at two different wavelengths viz. 233 and 278 nm………..……………......……………………………..........…94

Figure 6.7 *In situ* fluorescence spectra for the FB1 Langmuir monolayer at different surface pressures (a) and plot of intensity vs surface pressures at 307 nm (b)……………………………………………………………………...95

Figure 6.8 Kibron trough experimental setup with the adjusted green light source to study the effect of light on the FB1 Langmuir monolayer……………….97

Figure 6.9 Surface pressure vs time shows the drop of surface pressure in absence (a) and presence (b) of green LED light. Magnitudes of error bars are calculated as the standard deviation from three experiments…………………..…....98

Figure 6.10 Photoluminescence spectra of FB1 before and after treatment with light.99

Figure 6.11 UV-vis spectra of FB1 before (a) and after (b) the treatment of green light…………………………………………………………………..100

Figure 6.12 Mass Spectra of fumonisin B1: (a) Without irradiation, (b) With irradiation, and (c) Enlarged to show the clear peaks…..................…..…………...102

LIST OF TABLES

Chapter 1

Table 1.1 Difference between chemisorption and physisorption ……………..……..1

Chapter 2

Table 2.1 Data showing the limiting molecular area and collapse surface pressure with different subphase used…......................……..……………………….19

LIST OF SCHEMES

Chapter 3

Scheme 3.1 Reaction showing the split of X-gal in presence of β-galactosidase enzyme…..……………………………………..……………………30

Chapter 4

Scheme 4.1 Mechanism of conjugation of β-galactosidase and CDs in presence of EDC…………………………………………………………………47

Scheme 4.2 Electrochemical setup showing three-electrode system….….…..………...57

Scheme 4.3 Two enzyme system of biosensing…….…..……………………..……….61

Chapter 7

Scheme 7.1 Conjugation of Fumonisin B1 with CDs…….…………………………108

LIST OF ABBREVIATIONS

1-ethyl-3-(3-dimethylaminopropyl) carbodiimide	EDC
Atomic force microscopy	AFM
Cholera toxin B	CTB
Circular dichroism	CD
Enzyme-linked immunosorbent assay	ELISA
Fourier transform infrared spectroscopy	FTIR
Fumonisin B1	FB1
High pressure liquid chromatography	HPLC
Infrared reflection absorption spectroscopy	IRRAS
Intensity of incident light	Io
Langmuir-Blodgett film	LB film
Light emitting diode	LED
Liquid condensed	LC
Liquid expanded	LE
Photodynamic therapy	PDT
Rose Bengal	RB
Surface potential-area	ΔV-A
Surface pressure	π

Surface pressure-area	π-A
Surface tension	γ
Two Dimensional	2-D
Ultraviolet-visible	UV-vis
β-galactosidase	β-gal

Chapter 1

Introduction

1.1 Surface Chemistry and Langmuir Monolayer

Surface chemistry is a biophysical approach used to understand biological functions like: nature of cell membrane and interfacial properties of peptides and proteins. Langmuir monolayer technique is used to analyze the surface chemistry and *in situ* spectroscopy of proteins (enzymatic as well as non-enzymatic). Langmuir monolayer study is also considered as the study of adsorption at air-water interface. There are several types of adsorption processes. Most common type of adsorption are physisorption and chemisorption. The difference between these two adsorptions is shown in **Table 1.1.**

SN		Chemisorption	Physisorption
1	$-\Delta H_{ads}$	Approx. 40-1000 $kJmol^{-1}$	Approx. 10-40 $kJmol^{-1}$
2	Kinetics of activation	Can be activated	Non-activated
3	Number of layers	One monolayer	Monolayers and multilayers
4	Chemical Reactivity	Can cause reactivity changes in the adsorbate	Little change
5	Specificity	Normally dependent on specific adsorbate-surface interactions	Non-specific, needs low temperature to get substantial amounts

Table 1.1 Difference between chemisorption and physisorption

The Langmuir isotherm is the most commonly used model for an adsorption isotherm and describes ideal chemisorption systems[1]. It can be derived on the basis of kinetic, thermodynamic, and/or statistical mechanical models. Despite the limitations of the Langmuir isotherm, it continues to be widely used. This is because it is a simple model which can help to deduce quantitative relationships between the amount of adsorbate on the surface and the pressure in the gas phase above it. In principle, the Langmuir isotherm contains all of the parameters which are needed to do this and provides a good first approximation. The Langmuir isotherm essentially provides a framework for describing the extent and strength of adsorption on a surface, it sets a reasonable basis for a useful method of determining surface kinetics and it can also be used to determine the surface areas of solids which is particularly important in studying catalyst.

1.2 Importance of Surface Chemistry and Spectroscopic Studies to Investigate the Properties of Enzymatic and Non-Enzymatic Molecules

To study biomembranes there are various model systems, of which Langmuir monolayer is one. It is important to discuss these model systems[2-3] before selecting the most appropriate one for the study of enzymes and non-enzyme molecules. The major three model membranes are: i. Bimolecular lipid membranes, ii. Lipid bilayers (vesicles or liposomes), and iii. Langmuir monolayer or supported lipid bilayers. These systems permit the examination of the aggregation of proteins and allow the unique path in the application of physiochemical techniques whose interpretation would be highly difficult with such natural biological membranes. It has been noted that unilamellar or multilamellar bilayer dispersions suffered from the significant limitations like, the limitation in phase state, inability to regulate the lipid lateral-packing density[4-5]. Furthermore, the modules failed to unleash the composition and area exposed to the medium. To overcome these limitations, a lipid Langmuir monolayer at the air-water interface was introduced.

Irvine Langmuir introduced the Langmuir monolayer technique which is essentially a molecular film at the air-water interface.[6] This technique presents a unique methodology that helps to determine the chemical and physical behavior of monolayer of amphiphillic molecules at the phase boundary. In the latest years, the application of the surface chemistry and spectroscopy of Langmuir monolayer and Langmuir-Blodgett (LB) film techniques show a growth in diversity. LB film is a monolayer or multilayer transferred from the air-water interface onto a solid substrate by vertical dipping.[7-8] LB film is also a useful tool in verifying the orientation of the molecules at the air water interface.

Surface pressure – area isotherm, surface potential – area isotherm, infrared reflection absorption spectroscopy, in situ uv-vis and fluorescence spectroscopy, Brewster angle microscopy, sum frequency generation are the specialized techniques of surface chemistry and spectroscopic studies. We have used these techniques to study the enzymatic and non-enzymatic molecules. Most of the experimental works are performed by using different troughs. **Figure 1.1** shows two different Langmuir troughs in our lab. In **Chapter 2**, the interfacial properties of enzyme β-galactosidase are investigated. Previously, interfacial work was related to amphiphilic molecules which are insoluble in water. Proteins (enzymes) can also be considered as amphiphilic molecules as they possess polar and hydrophobic regions. The main reason to study the interfacial property of β-galactosidase was to determine whether the enzyme denatures at an interface and other reason was to investigate how the Langmuir monolayer of the enzyme changes when substrate, X-gal is introduced in the subphase.

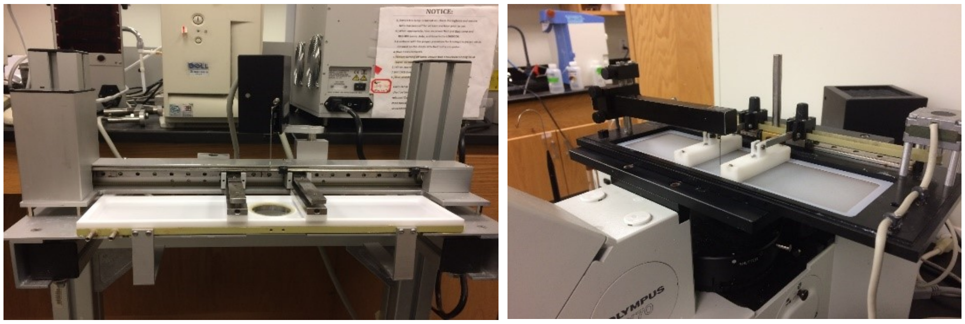

Figure 1.1: Image of two different Langmuir troughs (namely KSV Nima at right and Kibron at left) in our lab

In **Chapter 3**, we used experimental as well as theoretical methods to study the interaction of β-galactosidase and its substrate, X-gal. It was found that the secondary structure of the enzyme changes while interacting with X-gal but the overall structure does not change as the whole structure depends on primary, secondary, tertiary, and quaternary structures.

Chapter 4 focuses on the study of interfacial property of β-galactosidase/Carbon dots conjugate and the use of interfacial properties of β-galactosidase learnt from Chapter 2 and 3 were used to construct a biosensor. It was already proved the enzyme remains active on the monolayer and does not get denatured or aggregated. Further, the conjugation of the enzyme, β-galactosidase with the lab synthesized carbon dots (CDs) showed the appreciable increase in its stability at room temperature. These properties were enough to construct a stable biosensor having high sensitivity.

In **Chapter 5**, the surface chemistry and spectroscopy of pharmaceutically important molecule, cholera toxin B (CTB) was investigated. This choice was based on the fact that this protein was basically not studied detailly from a surface chemistry and spectroscopic perspective. It was found that the 'benign' toxin was highly stable at the interface which opens the prospect of the molecule suitable in microfluidic devices, to study the cell adhesion, and understand the property of transmembrane receptors.

Chapter 6 deals with the investigation of fumonisin B1 (FB1) toxin. Having in mind the importance of this molecule, we first performed the systematic investigation of its interfacial properties. Later, we irradiated the Langmuir monolayer of FB1 with green LED light at 525 nm. It was found that the molecules on the monolayer dissolve on the subphase with the subsequent irradiation of LED light. We compared the interfacial phenomenon with the bulk phase. With the solution and interfacial properties on hand, one could have a new insight regarding the treatment of keratitis.

1.3 States of Monolayer on the Subphase

The air-water interface provides a unique methodology to study matter in two dimensions.[9] The π-A isotherm is a plot of the change in surface pressure (π) with respect to area (A) available to each molecule at the air-water interface. **Figure 1.2** shows an example of a surface pressure-area isotherm for stearic acid.

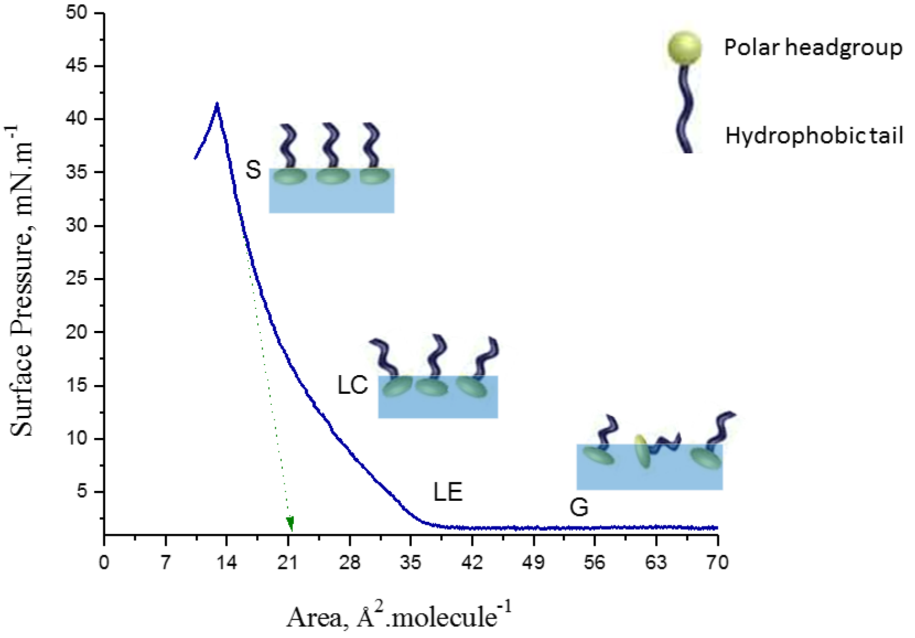

Figure 1.2: Langmuir isotherm of stearic acid (10^{-3} M in $CHCl_3$), 45 μL spread volume.

As the surface pressure increases, the two-dimensional monolayer goes through different phases in which the molecules may exhibit a different orientation or different degree of freedom. When the sample is spread at the interface and the molecules are far apart, the floating film is in a two-dimensional gas phase where the surfactant molecules are not interacting. As the monolayer is compressed, the surface pressure rises and the area per unit molecule decreases, indicating a change in phase to a two-dimensional liquid-expanded state, which is analogous to a three-dimensional liquid.

Further compression of the monolayer is accompanied by a steeper rise in surface pressure as the liquid-expanded phase transforms into a liquid-condensed phase. The condensed phase tends to have short-range molecular interactions. In the higher-pressure region of the liquid condensed phase, the compressibility is very low (solid phase) and the molecular areas correspond closely to the true molecular cross-sectional areas. The configuration of molecules approaches close-packed vertically oriented chains. Upon further compression, the monolayer reaches the collapse surface pressure and the area at the final collapse is the absolute minimum area into which the molecules can be crowded. Collapse of the Langmuir monolayer begins by clasping of the monolayer followed by folding of the buckle into a bilayer in the subphase. The bilayer folds have a semielliptical shape and can transform into flat circular bilayers or vesicles and disconnect from the monolayer. The parameter that is used to characterize the condensed monolayer requires extrapolating the steepest area of the slope to zero surface pressure (π) prior to the collapse. This extrapolated area corresponds to the state of the monolayer in the most closely packed molecular state, or minimum cross-sectional area per molecule at the air-water interface.

Thermodynamically, a monolayer is not a Gibbs phase, but part of an interfacial region. It may be considered to consist of phases in two dimensions analogous to Gibbs in three. The transitions in a general case along an isotherm with the increase in the pressure are:

$$\textbf{Gas} \xrightarrow{\textbf{1st order}} \textbf{Liquid I (expanded)} \longrightarrow \textbf{Intermediate} \xrightarrow{\textbf{2nd order}} \textbf{Solid}.$$

The intermediate phase may be considered to consist of two or more parts, which may later be proved to be phases: (i) Transition, with great compressibility; exhibits hysteresis, but not as yet demonstrated as heterogeneous, which changes more or less gradually to, (ii) Liquid II (condensed), compressibility relatively low. Dervichian considers the intermediate phase as mesomorphous, or an array of two-dimensional crystals, because this phase lies between a solid and a liquid.[10-11] He considers liquid I as the only true liquid. Actually, the liquid I is not isotropic but exhibits a considerable degree of molecular orientation, which increases with pressure. The analogy to a three-dimensional liquid is closer in: (a) L I (expanded) in that it is formed by a first-order change from a gaseous film. (b) L II (condensed), with respect to coefficient of expansion and compressibility. Thus, for L I at low pressures the coefficient of expansion (α) is of the order of ten times that of a three-dimensional liquid, while for compressibility the factor is of the general order of 100. In addition, he considers that the film collapses at specific area which is known as the area of the cross section of the molecules in a plane perpendicular to the long axis.

1.4 Advantages of Langmuir Monolayer Approach

Membranes of plant and animal cells are typically composed of 40-50 % lipids and 50-60 % proteins (**Figure 1.3**). There are wide variations in the types of lipids and proteins as well as in their ratios. The proteins associated with the several diseases are found near the membrane surfaces more specifically, near lipid rafts. Moreover, the behavior of proteins in the bulk solution or aqueous solvents and the membrane surfaces is different. An effective way to investigate the interactions between lipids and the proteins or to study the behavior of proteins near membrane surfaces is the Langmuir monolayer technique.

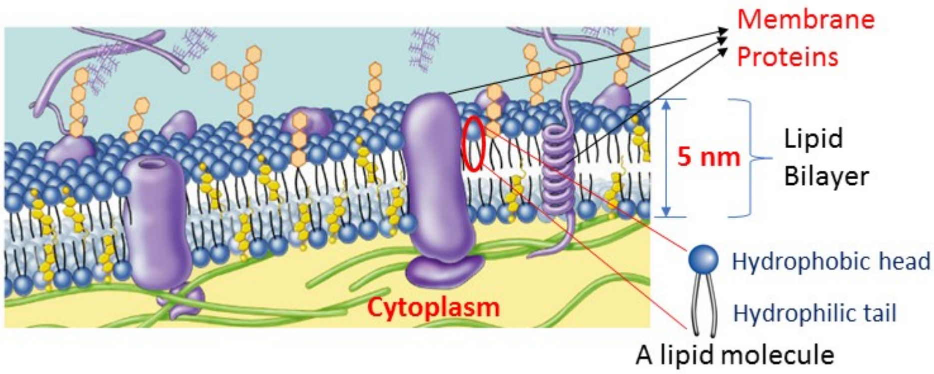

Figure 1.3: Structure of cell membrane showing membrane proteins

An important advantage of studying the lipid-peptide/protein interactions using the Langmuir monolayer approach is that the range of molecular areas known to occur in natural membrane can be investigated systematically while avoiding the mesomorphic changes that often occur in bulk hydrated dispersions, e.g. bilayer vesicles, as the lipid composition is varied. The Langmuir monolayer technique can address the variation of the surface pressure at will. This is an important parameter because it is possible to simulate the surface pressure between 30-35 mN.m^{-1} generally appropriate to model a biological membrane.[12-14] It has been noted in some cases that the phase separation behavior of the initial Langmuir monolayer is more easily understood by comparing both low (10-15 mN.m^{-1}) and higher surface pressures (larger than 20 mN.m^{-1}). Another feature of the Langmuir monolayer model is the fact that the in-plane lipid-lipid interactions can be isolated from the influence of changing trans-bilayer compositional distributions that may occur in bilayer systems, for example when cholesterol composition is varied.[15] For these reasons, Langmuir monolayer investigations of lipid-cholesterol, especially sphingolipid-cholesterol interactions, have proven useful.[16-18]

Chapter 2

Study of β-galactosidase Langmuir Monolayer at Air/X-gal Subphase Interface

2.1 Background

β-galactosidase (EC 3.2.1.23) is an important enzyme which catalyzes the hydrolysis of β-galactosides through the breaking of glycosidic bond.[19] The enzyme is composed of four identical subunits having total 1,024 amino acids, firstly sequenced from *E. coli.*[20] This enzyme is very important in the human body and its deficiency causes lactose intolerance. β-galactosidase has been employed in many food industries to hydrolyze lactose, enhance digestibility, sweetness, solubility and flavor of dairy products.[21] **Figure 2.1** summarizes the importance of β-galactosidase enzyme.[22] As the lack of this enzyme or reduction in enzyme activity in the body causes problem in lactose digestion, there are vast numbers of people worldwide suffering from lactose intolerance. A study has shown that 65% of the world population experiences from various degrees of lactose intolerance[23]. Symptoms of lactose intolerance include diarrhea, nausea, muscular spasm, swelling, borborygmi and chronic flatulence.[23]

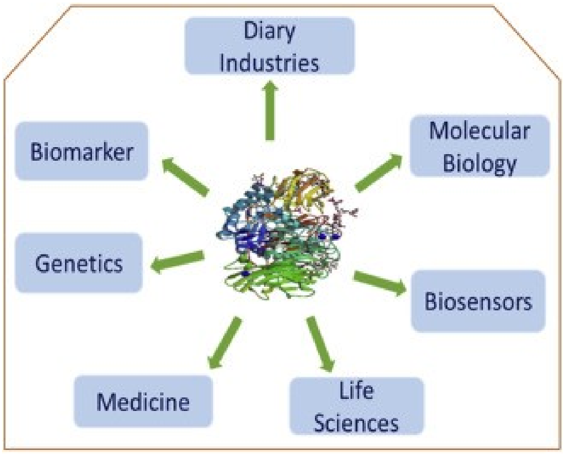

Figure 2.1: Different applications of β-galactosidase enzyme (Adopted from Elsevier).[22]

The results of lactose malabsorption are dermal disease, rheumatological complaints, persistent exhaustion, and lack of growth and development in children.

As β-galactosidase is a multifaceted enzyme, in this chapter, our aim was to study the surface properties of β-galactosidase, as a monolayer at the air-subphase interface and to identify whether it retains its hydrolytic activity in the monolayer form. The reasons for undertaking this work are three-fold: to understand the surface chemistry behavior of this important enzyme in a model systems representing vaguely cell membrane environments[24], to prove the activity of the deposited enzyme in a form of the monolayer for a possible future glycomics sample preparation microfluidics device development[25], and to prove existence of catalytic activity and stability of monolayer for possible future biosensing applications. As β-galactosidase belongs to the class of exoglycosidase enzymes[26], it plays important roles to hydrolyze the β-glycosidic bond formed between a galactose and other organic residue in glycans.[27] As such, it is one of the most important metabolic enzymes. Besides fundamental importance in key biochemical pathways *in-vivo*, β-galactosidases have lot of tangible applications in the lab as a key life science tool in applications such as blue-white screening, in an ELISA assays[28] based on color generation by action on X-gal or similar substrate, electrophoresis, and more recently as a key enzyme for glycans sample preparation and glycans digestion and analysis. The β-galactosidase can hydrolyze several of the β-glycosidic glycan analogs, like 5-bromo-4-chloro-3-indoyl-β-D-galactopyranoside (X-gal) which produce colored, luminescent or fluorescent compounds, and as such is commonly used enzyme in vitro assays and in biosensing applications.[29]

X-gal is an artificial organic compound that consist of galactose linked to a substituted indole and is highly employed in molecular biology.[30] The most commonly used substrate for β-galactosidase is X-gal, resulting in the cleavage of glycosidic linkage to galactose and indigo type dye revealing a strong indigo blue color. The β-galactosidase – X-gal reporting system is commonly utilized in gene expression, as a marker in gene cloning, plasmid construction, structural stabilization of fusion proteins, process monitoring and purifications.[31-36] Nonetheless, the amphiphilic natures of vesicles and cell membrane that exist in vivo and interaction mechanism around the amphiphilic natures is not clear. This chapter studied the interaction of β-galactosidase and X-gal at the air-subphase interface, which can be extensively used to mimic the amphiphilic membranes structure *in vivo*.

Langmuir film technique is considered as an effective way to understand how surface proteins interact with their membrane and subphase environment by studying their air-subphase behavior.[37-39] In this technique, one molecule-thick monolayer of proteins is produced which ultimately guides to study its transformation at the air-water interface from the gaseous phase to condensed phase via liquid condensed phase. Basic information like protein packing and conformation studies can be obtained from measurement of the surface pressure, average molecular area and surface potential, however, detailed information about secondary structures of enzyme can be obtained by employing infrared reflection absorption spectroscopy (IRRAS) and Brewster angle microscopic (BAM) studies gives real image of the monolayer at different surface pressures.[40-41] In Langmuir monolayer, amphiphilic molecules are spread at the air-water interface. In doing so, movable barriers are employed for compression in order to control molecular packing.[42] The study of Langmuir film is basically used to measure the surface pressure as a function of surface area available to surfactant molecules at constant temperature which is so called as surface pressure-area (π-A) isotherm. This measurement gives information about the existence of different phase transitions and the stability of the film of enzymes in the absence and presence of the substrate. The isotherm behavior of the Langmuir film is usually estimated by the physical and chemical properties of amphiphilic molecules and composition of the subphase (such as salt concentration).[43-44]

In this chapter, we explored the surface chemistry properties and activity of β-galactosidase monolayer on hydrolysis of X-gal subphase. We exploited the Langmuir monolayer film technique to assimilate basic surface chemistry properties and to scrutinize the behavior of β–galactosidase at the air-subphase interface at different surface pressures that concur to different states, ranging from the gaseous phase to the liquid compressed phase. In this study we investigated the β-galactosidase Langmuir monolayer in absence and presence of varying concentration of X-gal and the sodium chloride subphase. β-galactosidase was chosen to study the Langmuir monolayer because it is an important enzyme in our metabolism[45], useful for the structural investigation of carbohydrate, determination of lactose (foodstuffs analysis) and as an enzyme label for enzyme immunoassay.[45-46] Furthermore, X-gal was chosen as an ingredient in the subphase because an active enzyme can be detected by using X-gal which gives the intense blue color product after cleavage by the enzyme and is easy to quantify.

After the successful completion of this work, it was found that that the β-galactosidase in the monolayer form remains active and performs hydrolysis of the X-gal in the subphase. We have investigated the β-galactosidase Langmuir monolayer in absence and presence of X-gal in the subphase of varying concentration of X-gal with the sodium chloride solution, it was revealed that that the limiting molecular area as well as the collapse surface pressure kept on decreasing with the increasing concentration of X-gal. Moreover, it was found that β-galactosidase forms a stable monolayer that does not aggregate at the air-subphase interface. The stability of the monolayer at the air-subphase interface was studied by using compression-decompression cycles with and without X-gal at varying concentration and different surface pressures. The infrared reflection absorption spectroscopy (IRRAS) and Brewster angle microscopy (BAM) of β-galactosidase Langmuir monolayer was also investigated for pure 0.1 M NaCl and mixed with X-gal at the air-subphase interface.

2.2 Experimental Section

2.2.1 Chemicals

β-galactosidase enzyme (EC 3.2.1.23) was provided by MP Biomedicals (Solon, OH). The molecular weight of enzyme was 540,000 Da as determined using matrix-assisted laser desorption ionization time of flight (MALDI-TOF) mass spectrometer. Specific activity of the enzyme as provided by company was 700 U/mg by analysis with O-nitrophenyl-β-D-galactopyranoside (ONPG). X-gal (5-bromo-4-chloro-3-indoyl- β-D-galactopyranoside) and sodium chloride (99.5% pure) were also obtained from MP Biomedicals. Water utilized in these experiments was used from Modulab 2020 Water Purification System (Continental Water System Corp., San Antonio, TX) with the resistivity of 18 MΩ cm, surface tension of 71.6 mN/m, and pH of 6.0 at 20.0 ± 0.5 °C.

2.2.2 Equipment

All the Langmuir isotherm measurements were carried out in a clean room (class 1000) where temperature (20.0 ± 0.5°C) and humidity (50% ± 1%) were maintained constant. A Kibron μ-trough (Kibron Inc., Helsinki, Finland) having area of (5.9 cm × 21.1cm) was used in the study of surface pressure-area (π-A) isotherms, surface potential-area isotherms, stability, and compression-decompression cycles. Kelvin probe that consist of a capacitor-like system was utilized to measure surface potential. The vibrating plate was adjusted at 1 mm (approx.) above the surface of Langmuir monolayer and a gold-plated trough acted as a counter electrode. The Wilhelmy method was deployed to assess surface pressure with a 0.51 mm diameter alloy wire probe having sensitivity of ±0.01mN/m.

2.2.3 Langmuir Monolayer Preparation

The solution of β-galactosidase was prepared in pure water (pH 6.0) at the concentration of 3.7×10^{-7} M. NaCl (0.1M) and varying concentration of X-gal were used to prepare the subphase. Initially, X-gal was dissolved in minimal amount of dimethyl formamide (DMF) and further diluted by using pure water. The β-galactosidase was spread uniformly over the air-X-gal/NaCl interface by using a 100 μL syringe (Hamilton Co., Reno, Nevada). The spreading volume of the enzyme solution was 45 μL for the surface chemistry and spectroscopic measurements. After spreading the solution, Langmuir monolayer was allowed to attain the equilibrium state approx. for 20 min. Then, monolayer was compressed with the rate of 3,990 $Å^2$.molecule^{-1}.min^{-1}.

2.2.4 Infrared Reflection Absorption Spectroscopy (IRRAS)

To obtain infrared spectra, Bruker Equinox55 FTIR instrument (Billerica, MA) equipped with the XA-511 accessory for the air-water interface was used at the air-interface subphase. Kibron μ-trough S (Helsinki, Finland) with dimensions of 5.9 × 21.1 cm was employed for the experiment. The measurements were carried out by the use of p-polarized light and a mercury-cadmium-telluride (MCT) liquid-nitrogen-cooled detector. Each spectrum was acquired by the co-addition of 1200 scans at a resolution of 8 cm^{-1}.

2.2.5 Brewster Angle Microscopy (BAM)

KSV Optrel BAM 300 from KSV Instrumentals Ltd., Finland linked to a film balance system (KSV Minitrough, KSV Instrumentals Ltd., Finland) was used for the BAM measurements of Langmuir films at air-subphase interface. A standard laser of a 20 mW He-Ne emitting p-polarized light of 632.8 nm wavelength and a 10 × objective was employed. The angle of incidence was set at 50º at 298.2 K. Triply distilled water having surface tension 71.9 mN/m and resistivity 18 MΩ cm was used in preparing the subphase with NaCl (from Nacalai Tesque; Kyoto, Japan) roasted at 900 K for 24 h to eliminate surface-active organic impurities) and X-gal. A high-grade charge-coupled device (CCD) camera (EHDkamPro02, EHD Imaging GmbH, Germany) was used to record the reflected beam and the BAM images were digitally saved.

2.3 Results and Discussion

2.3.1 Surface Pressure and Surface Potential-Area Isotherms

Interfacial properties and Langmuir monolayer behavior of β-galactosidase on the surface of X-gal/NaCl was investigated by spreading 45 uL of the enzyme having concentration of 3.7×10^{-7} M on the 9.78×10^{-3} M X-gal and 0.1M NaCl subphase solution. These conditions reproducibly displayed the proper formation of two-dimensional enzyme Langmuir monolayer. The main reason of spreading the enzyme on the subphase that contains an active substrate was to investigate and compare the surface phenomenon that would make useful in industrial and medical applications by using the surface property of the enzyme. An initial zero in surface pressure starting at 120,000 Å^2.molecule^{-1} for a spreading amount of 3.7×10^{-7} M of enzyme is ideal correlating the gaseous phase (**Figure 2.2**). The enzyme molecules continue to condense till 45,000 Å^2.molecule^{-1} when the sharp increase in surface pressure can be observed which is referred as liquid expanded phase.

When the maximum compression is reached the phase reached at around 25,000 Å^2/molecule. The liquid condensed film of the enzyme monolayer is observed in the range of 35,000 to 23,000 Å^2.molecule^{-1}.

Basically, surface pressure quantifies the interactions between molecules in close contact (van der Waals interaction) and surface potential evaluates the potential difference or dipole moment difference above and below the Langmuir monolayer film in the same experiment, which is the interaction of molecules at longer distances regarded as dipole-dipole interaction. The surface potential-area isotherms exhibit the molecular interactions that occurs before and during phase change of the monolayer as seen during the compression.[47]

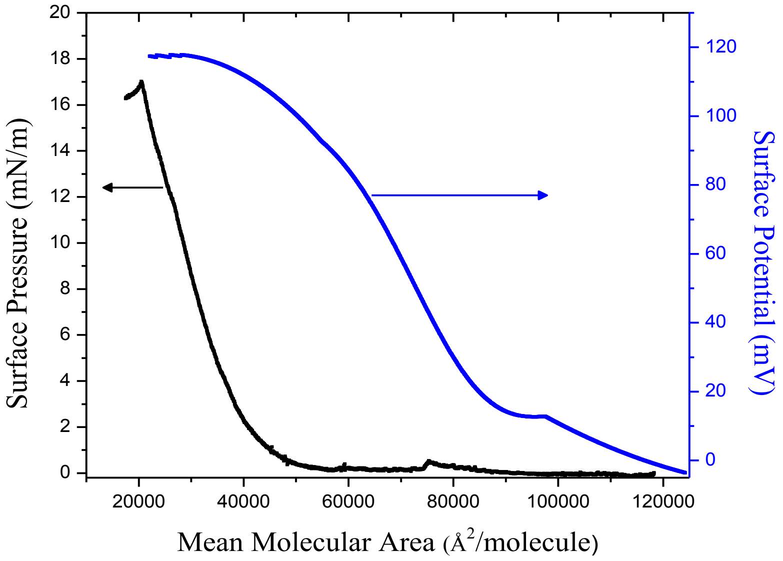

Figure 2.2: Surface pressure and surface potential versus area.molecule^{-1} when the subphase was NaCl (0.1M) and X-gal (9.78× 10^{-3} M).

As per expectation, when compression of the monolayer is started the surface potential-area isotherm shows the increase in the surface potential. This is because of the charges that are present on β-galactosidase. When the monolayer begins to move from a liquid expanded phase to liquid condensed phase there appears the kink on the surface potential curve at about 95,000 Å^2.molecule^{-1} and change in surface potential is observed.

The other small bumps seen in the surface potential curve at very low surface pressure are due to β-galactosidase molecules rapidly moving on the subphase surface under the vibrating electrode. The maximum voltage of 120 mV relates to the compact packing structure of the enzyme molecules. At this value, due to short distance among molecule some of the dipole-dipole interactions gets cancelled out which ultimately results in a steady value in surface potential.

2.3.2 Concentration Effect of X-gal in the Aqueous Subphase

To observe the effect of X-gal on the enzyme Langmuir monolayer, the experiments were conducted by using NaCl aqueous solution and NaCl/X-gal aqueous solutions. **Figure 2.3** shows the π-A isotherms for 0.1 M NaCl and mixed 0.1 M NaCl – (2.45, 4.89, 7.34 and 9.78) × 10^{-3} M of X-gal. As barrier goes on compressing the enzyme monolayer, the surface pressure starts to rise and at lift-off area due to repulsion of the particles that start to order and hence interact as so called two dimensional liquid. For NaCl (0.1 M) subphase the limiting molecular area was 79,300 Å^2.molecule^{-1} and adding definite amount of X-gal in the preparation of the subphase subsequently lowered the limiting molecular area as shown in **Table 2.1**. The limiting molecular area of Langmuir monolayer depicts the minimum cross-sectional area per molecule. This value can alter with subphase conditions. For example: the conformation of an enzyme gets affected due to the changes in pH there by destabilizing certain vital components throughout the molecule. Similarly, the collapse surface pressure for the NaCl (0.1 M) subphase was 43 mN.m^{-1} and starts getting lowered when X-gal is added to the subphase solution.

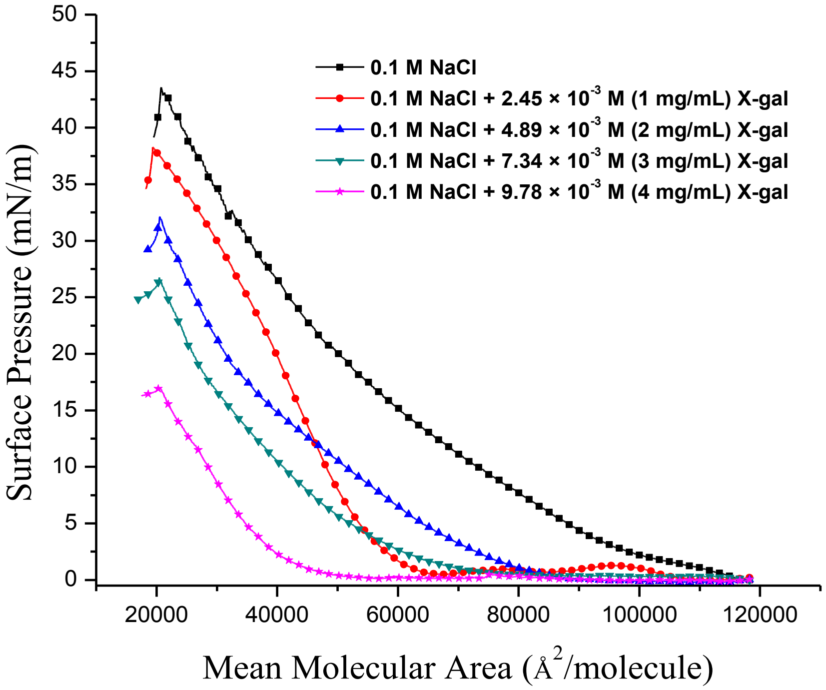

Figure 2.3 Surface pressure versus mean molecular area isotherms for 3.7×10^{-7} M β-galactosidase spread on 0.1M NaCl and (2.45, 4.89, 7.34 and 9.78) × 10^{-3} M of X-gal.

Hence, we concluded that when NaCl (0.1M) is only used as a subphase then the limiting molecular area as well as collapse surface pressure is higher but when X-gal is added then the limiting molecular area as well as the collapse surface pressure also goes on decreasing. This fact can be best described as the increased interaction among the X-gal and β-galactosidase due to concentration effects. This trend goes on when the concentration of X-gal is increased. The notable decrease in the limiting molecular area in case of NaCl (0.1 M)-X-gal aqueous subphase is interpreted as the larger interaction between β-galactosidase and X-gal.

Subphase	**Limiting Molecular Area** (Å ^{2}.molecule^{-1})	**Collapse Surface Pressure** (mN.m^{-1})
0.1M NaCl(only)	79,300	43
0.1M NaCl + 1mg/mL X-gal	58,200	38
0.1M NaCl + 2mg/mL X-gal	52,200	33
0.1M NaCl + 3mg/mL X-gal	44,050	28
0.1M NaCl + 4mg/mL X-gal	41,000	17

Table 2.1: Data showing the limiting molecular area and collapse surface pressure with different subphase used.

2.3.3 Compression-Decompression Cycles

The compression-decompression data reveals the extent of loss of analyte to desorption from the interface into the subphase or/and change in the conformation of the enzyme known as hysteresis[48]**.** The active compression-decompression Langmuir monolayer films at the air/subphase interface gives minute data on molecular dimensions, phase transitions of the film, and its packing properties. Moreover, assessing the compression-decompression cycle gives information relating the stability of the film, attribute thermodynamics and kinetics.[49-50] As β-galactosidase has more negative charges than positive charges on the surface [51] and due to this fact β-galactosidase molecules should repel each other when monolayer is compressed. Our hypothesis was confirmed using the compression and decompression cycles of β-galactosidase. **Figure 2.4** (column A) reveals that the β-galactosidase monolayer was compressed 3 folds. The surface pressure for compression and decompression was chosen as: 5**,** 15**,** and 30 mN.m^{-1}. For the successive 3 compression/decompression cycles that followed, a hysteresis behavior of the isotherm was observed. These cycles reveal that when compressed to 5 mN.m^{-1} there is small hysteresis due to the fact that stable monolayer has not been formed yet. It has been found that only 6% of the initial isotherm has been reduced in comparison of the first and last cycle, whereas 15 and 30 mN.m^{-1} only exhibit hysteresis difference of 4.0 and 3.0%, respectively.

These observed results reveal that β-galactosidase molecules reorganize at the interface while the salt subphase renders the partial insoluble enzyme molecules. Beside the solubility of enzyme in the subphase, other possible explanations might be considered such as: i) the denaturation of enzyme (protein) ii) the alteration in the conformation of the protein with time. The small difference in hysteresis after three compressions at different upper limit in surface pressure (5, 10 and 15 mN.m^{-1}) is therefore integrated as a reorganization of the enzyme Langmuir film.

Similar to the absence of X-gal, three different compression-decompression cycles were examined by taking the higher concentration of X-gal, i.e. 4 mg.mL^{-1} (9.78×10^{-3} M) in the case of presence of X-gal. The maximum surface pressure for compression and decompression was taken at 15 mN.m^{-1} because there was the collapse of monolayer called collapse surface pressure at 17-18 mN.m^{-1}. The surface pressure for compression and decompression was chosen as: 5, 10, and 15 mN.m^{-1}. In this case, there was lesser hysteresis in comparison to the absence of X-gal. It has been found that only 4.0% of the initial isotherm has been lost in comparison of the first and last cycle, whereas 10 and 15 mN.m^{-1} show 3.0 and 2.5%, respectively.

This fact can be best described on the basis of increased interaction between the X-gal and β-galactosidase molecules at the interface to give a soluble galactose and 5-bromo-4-chloro-3-hydroxyindole. The latter dimerizes and oxidizes to give 5,5'-dibromo-4,4'-

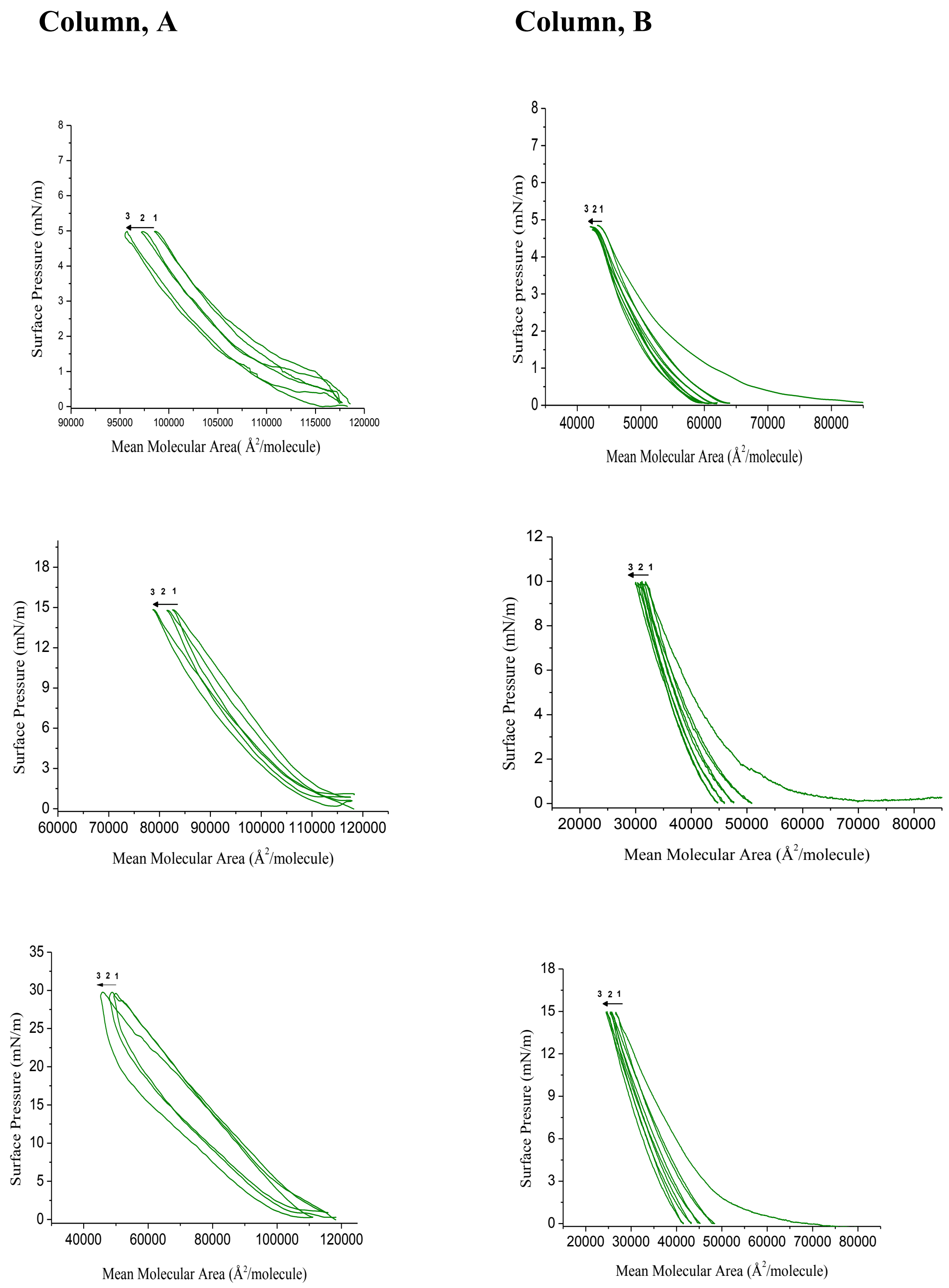

Figure 2.4: Compression-decompression of Langmuir isotherm of β-galactosidase. **Column A:** absence of X-gal in the subphase maintained at the surface pressure of 5, 15 and 30 mN/m. **Column B:** presence of X-gal (4 mg/mL, 9.78 × 10^{-3}M) in the subphase maintained at surface pressure of 5, 10 and 15 mN/m.

-dichloro-indigo, an intense blue colored product.[52]

It has been observed that there is more hysteresis when the subphase is only 0.1M NaCl[47]. This is because the desorption of enzyme on NaCl subphase is greater than the subphase of X-gal + NaCl solution. This fact can be also be attributed to a loss of film forming molecules in the bulk which is also known as the dissolution of the monolayer.[53] Hitherto we showed that Langmuir monolayer of β-galactosidase was more stable when spread on the X-gal+ NaCl subphase than when subphase was NaCl or pure water and the reproducibility of the surface pressure-area isotherms was good despite the difference in the concentration of X-gal. The stability measurements at constant pressure was also performed during the absence and presence of X-gal in the subphase (not shown here) at constant pressure over an extended time period (about 70 min) which verified that the monolayer was more stable in presence of X-gal in the subphase.

2.3.4 Infrared Reflection Absorption Spectroscopy (IRRAS)

The IRRAS experiment of lipid/protein monolayer films *in situ* at the air/subphase interface provides unique conformational and orientational information from the film constituents. This technique is considered important in studies of lipid/protein interaction in a physiologically pertinent environment. Different types of applications like, the elucidation of lipid chain conformation and tilt as well as determination of protein secondary structure are reviewed by using this technique.[54-56] Presented in **Figure 2.5** are the normalized p-polarized IRRAS spectra of the enzyme monolayer that is collected at various surface pressures during compression at an incident angle of 45° in absence and presence of different concentration X-gal. This angle was selected because it showed highest signal-to-noise ratio. Typically, the p-polarized light has the highest signal and therefore the best signal-to-noise ratio at about the Brewster angle. In absence of X-gal, there was no appreciable variation in band position and no disappearance of bands during compression which clearly means that there is no alteration in secondary structure of the β-galactosidase Langmuir monolayer. Band positions in the amide I region (1700-1600 cm^{-1}) is due to C=O (70-80%) stretching vibrations of peptide bonds and it demonstrates that the β-sheet conformation dominates the secondary structure which is in accordance with the previous study. The amide II region (1600-1500 cm^{-1}) shows the α-helical and unordered structures (random coils) content.

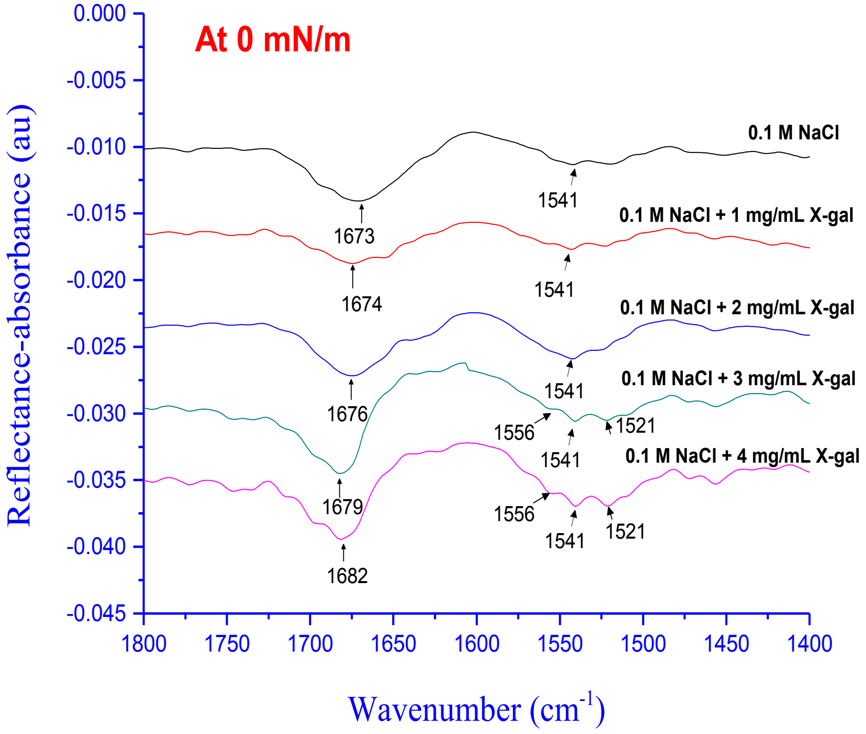

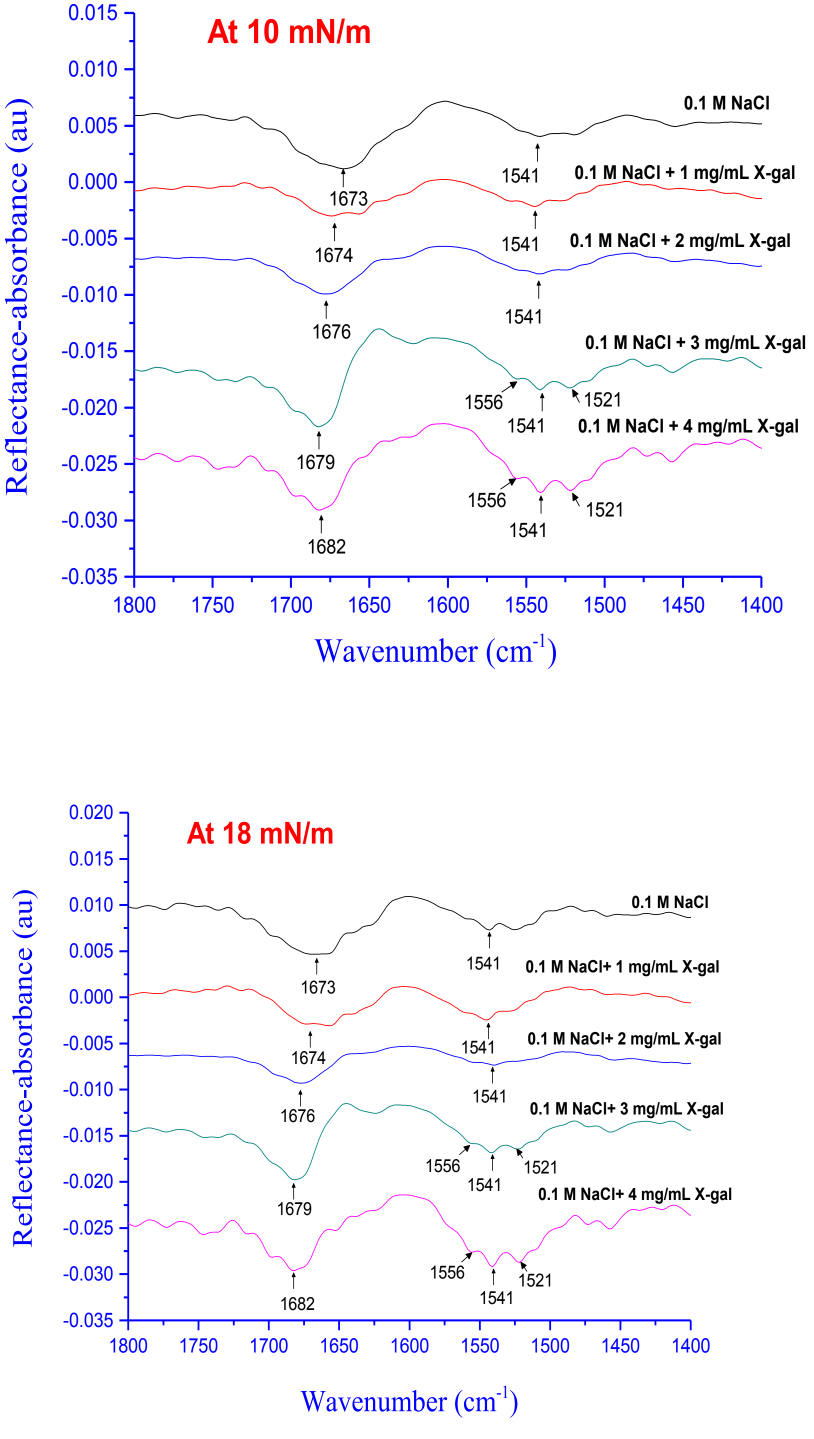

Figure 2.5: Normalized p-polarized IRRAS spectra at the air-subphase interface of the β-galactosidase Langmuir monolayer compared at different surface pressures in absence and presence of X-gal in the subphase at a 45° incident angle.

Being in crystalline structure, the abundance of β-sheet in the IRRAS spectra is expected for this enzyme[57] and in a study, it has been found that the native secondary structure of β-galactosidase comprises of 22% beta-turns, 14% parallel β-sheets, 25% anti-parallel β-sheets, 34% unordered structures (random coils) and only 5% α-helices.[58]

We were more interested in the molecular structure and orientation at the presence of X-gal in the subphase. As seen from the figure, in the region of amide I, the most prominent bands are centered at 1674, 1676, 1679 and 1682 cm^{-1} for change in concentration of X-gal and this represents the shifting of the peak due to the products formed by the cleavage of X-gal in the interface by β-galactosidase as well as the change in secondary structure of the enzyme. This amide I region is directly related to the backbone conformation. The band observed at 1673 cm^{-1} is assigned to α-helices. The bands corresponding to α-helices are higher in intensity at Amide I region as compared to the β-sheet. The likely reason for this observation might be due to the presence of carbonyl groups in α-helices that are lying parallel to the air-subphase interface in collation with the carbonyl groups present in β-sheet. The Amide II region is due to the C-N stretching (20-40%) vibrations in combination with N-H bending (40-60%). The Amide II bands at 1556 and 1541 cm^{-1} correspond to α-helices and band at 1521cm^{-1} corresponds to β-sheets. At different surface pressures we found that the band intensities remained almost constant which reveals that the amide chains are oriented parallel to the air-subphase interface. The C-H stretching peaks are observed in the range of 2800-3000 cm^{-1} and C-O peaks are observed around 1200 and 1300 cm^{-1} (not shown). The signals are very weak and, therefore, difficult to assign. From the data, we came to the conclusion that presence of X-gal in the subphase alters the secondary structure of enzyme and the band positions are shifted with the increase in the amount of X-gal in the subphase. But, this necessarily does not mean that the overall conformation of the enzyme changes because the conformation of enzyme is based on primary, secondary, tertiary and quaternary structure. Being acquainted with the fact that use of D_2O in the subphase helps in the identification of the vibrations of the side chain moieties from the secondary structure of protein, here we have used X-gal and NaCl as subphase because our purpose is to investigate our hypothesis of the conformation and change in orientation of the enzyme monolayer observed at different concentration of X-gal.

2.3.5 Brewster Angle Microscopy (BAM)

The lack of hysteresis and increase in stability of isotherms in presence of X-gal in comparison to the absence of X-gal in the subphase (**Figure 2.4**) was described as the lack of aggregate formation of the enzyme. To confirm this finding and to explore the topography of the monolayer surfaces BAM experiment was performed. This technique is very responsive to interfacial changes due to properties of phase domains in monolayers like surface density, anisotropy, interfacial roughness and thickness.[59-60] As Brewster angle for the air-subphase interface is estimated as 50° (for air-water interface being 53°) and under this condition the image of a pure air-subphase appears black since no light is reflected and addition of enzyme to the interface modifies the local refractive index and hence small amount of light is reflected which gets displayed within the image. **Figure 2.6** shows the micrographs obtained during compression of the β-galactosidase Langmuir monolayer in the subphase in absence and presence of X-gal. **Figure 2.6 A** show the micrographs obtained at the surface pressures of 1, 5 and 15 $mN.m^{-1}$ in absence of X-gal that does not reveal any aggregate or domain formation which comprehends the basis of homogeneity of the micrographs. The BAM micrographs obtained during compression at surface pressures 1, 5 and 15 mN.m^{-1} with 2.45 × 10^{-3} M X-gal in the subphase is shown in **Figure 2.6 B**.

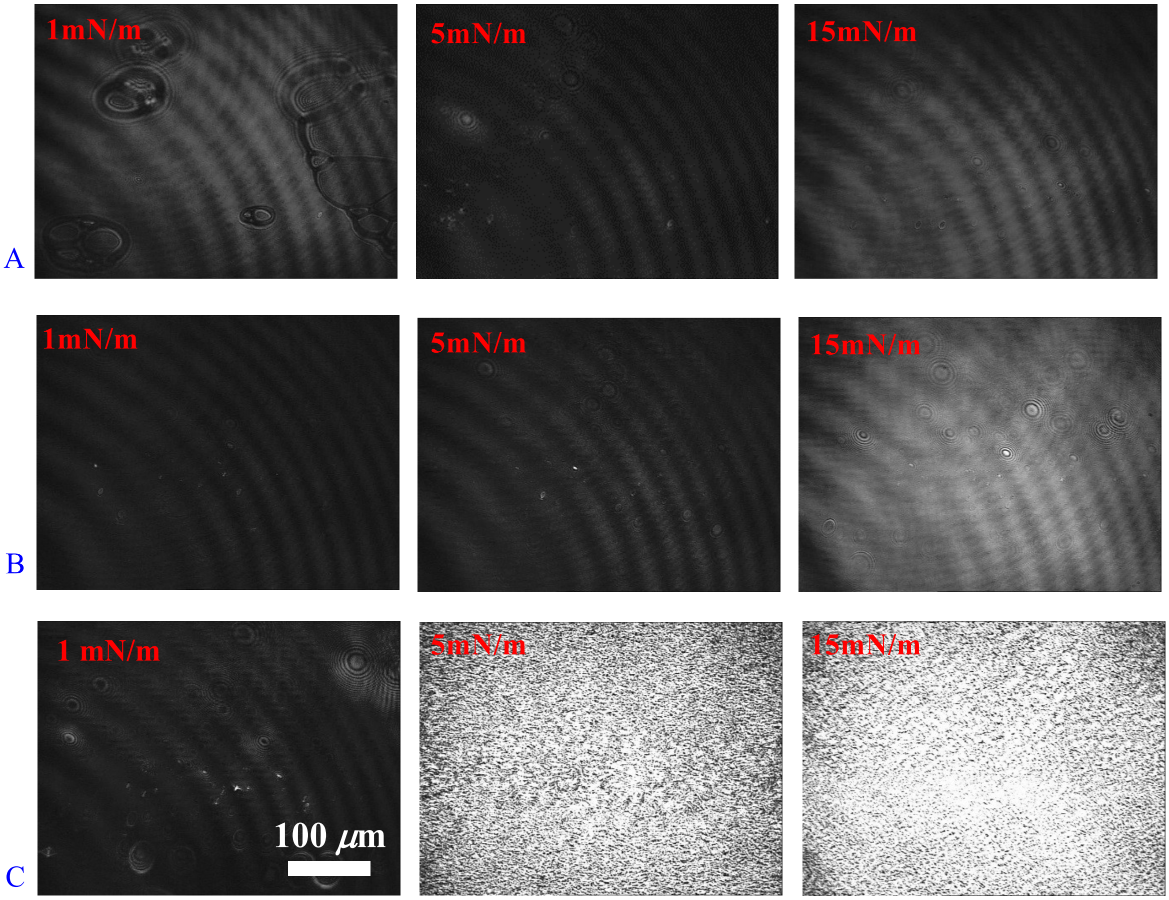

Figure 2.6 Brewster angle micrographs for β-galactosidase spread on the (A) 0.1 M NaCl, (B) 0.1 M NaCl + 2.45 × 10^{-3} M X-gal and (C) 0.1 M NaCl + 9.78 × 10^{-3} M X-gal at different surface pressures during compression. The scale bar represents 100 µm.

The micrographs substantiate the conclusion drawn on the basis of **Figure 2.4** as no aggregate or domain formation is revealed. **Figure 2.6 C** shows the micrographs obtained at surface pressures of 1, 5 and 15 mN.m^{-1} in presence of 9.78 × 10^{-3} M X-gal in the subphase. The BAM micrograph obtained during 1 mN.m^{-1} also does not exhibit any aggregate or domain formation. Additional compression of the monolayer to attain surface pressures 5 and 15 mN.m^{-1} revealed a number of tiny needle-like structures. These tiny structures are due to the 5,5'-dibromo-4,4'-dichloro-indigo which is the dimerized and oxidized form of the 5-bromo-4-chloro-3-hydroxyindole formed due to the cleavage of X-gal which are not soluble in the subphase.

2.4 Summary

After the surface chemistry and spectroscopic study of the β-galactosidase Langmuir monolayer, we found that limiting molecular area and the monolayer collapse surface pressure kept on decreasing with the increasing amount of X-gal in the subphase. On the basis of the results of the BAM imaging, it was concluded that β-galactosidase forms a stable monolayer which do not tend to aggregate at the air-subphase interface. In general, subphase stabilizes the monolayer, and in the case of the β-galactosidase we have demonstrated that the monolayer is more stable with less hysteresis in presence of X-gal than with compared to the absence of X-gal in the subphase. It was demonstrated using the p-polarized infrared absorption reflection spectroscopy (IRRAS) that the enzyme secondary structure is altered due to presence of X-gal in the subphase. The BAM imaging provides visual evidence of the absence of aggregates and domains, thus indicating that the β-galactosidase monolayers have less hysteresis and hence more stable due to the presence of X-gal in the subphase. The presence of the indigo color formation in the subphase indicates that the activity of the enzyme is preserved in the monolayer form, opening a door for the future investigations of possible use of β-galactosidase and other glycolytic enzymes for the glycan sample preparation and biosensors applications.

Chapter 3

Probing of Interaction Between β-Galactosidase and X-gal by Experimental and Theoretical Methods

3.1 Background

Beside the study of surface chemistry and spectroscopy of β-galactosidase Langmuir monolayer in air-water and air-subphase interface, there are lots of things to be assimilated in the study of the monolayer. For example: the interaction of β-galactosidase and X-gal in the interface can be studied. In the past decade, monolayer has been used to illustrate the interfacial interactions of proteins with lipids, and they constitute an excellent experimental setup of protein-monolayer interactions where the effects of protein insertion on the lipids can be accurately quantified.[61] Among different methods, we studied the interaction by using Second Harmonic Generation (SHG), Infrared Reflection Absorption Spectroscopy (IRRAS) and Molecular Dynamics (MD) Simulations.

SHG is a non-linear process in which photons with the same frequency interacting with a nonlinear material are effectively combined to generate new photons with twice the energy, and therefore twice the frequency and half the wavelength of the initial photons. It is a technique used to analyze surfaces, interfaces and to study the interaction of biomolecules at molecular level.[62] SHG is a special case of Sum Frequency Generation (SFG) in which the angular frequencies of two input photons are equal. In a typical SFG setup, two laser beams mix at a surface and generate an output beam with a frequency equal to the sum of the two input frequencies. The concentration of enzyme as low as 10 nM could be easily sensed by the SFG spectroscopy.[63] Since media with inversion symmetry are forbidden from generating second harmonic light, surfaces and interfaces make interesting subjects for study with SHG. Surface sum frequency generation vibrational spectroscopy (SFG-VS) has been widely used as an effective spectroscopic probe for chemical bonding, structure, and molecular interaction of both fundamentally and technologically important interfaces. [64-67] SHG can also be used to study the orientation of molecules on the interface.[68] Buck, M. and M. Himmelhaus have studied many of the common chemical functional groups, such as -CH_3, -OH, -CN, C=O, -CH in the aromatic ring, -NH and even -SiH, with SFG-VS and reviewed in the literature.[65] In this chapter, we present the succinct study of interactions among β-galactosidase enzyme and X-gal at air/ subphase interface. The β-galactosidase enzyme acts as the catalyst in the cleaving process of X-gal (**Scheme 3.1**).

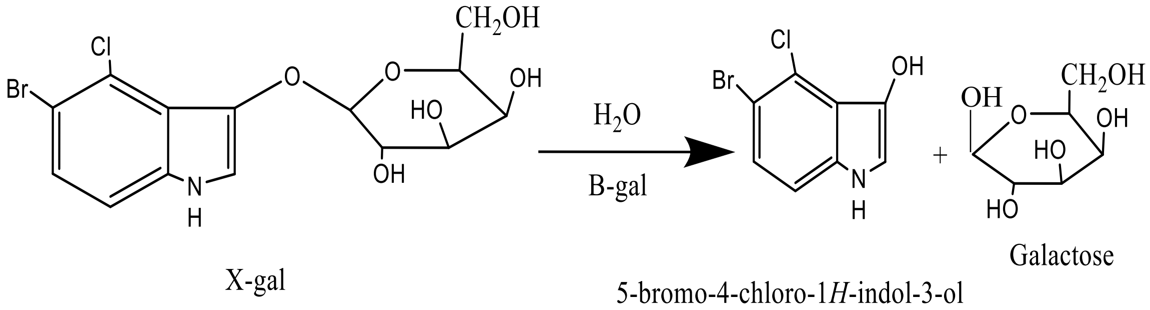

Scheme 3.1: Reaction showing the split of X-gal in presence of β-galactosidase enzyme

3.2 Experimentation

β-galactosidase (EC 3.2.1.23) was obtained from MP Biomedicals (Solon, OH) having the molecular weight of 540,000 Da as determined by matrix-assisted laser desorption ionization time of flight (MALDI-TOF) mass spectrometer. The specific activity of the enzyme is 700 U/mg obtained by analysis with O-nitrophenyl-β-D-galactopyranoside (ONPG). X-gal (5-bromo-4-chloro-3-indoyl- β-D-galactopyranoside) and sodium chloride with a purity of 99.5% were also obtained from MP Biomedicals. Water utilized in these experiments was used from Modulab 2020 Water Purification System (Continental Water System Corp. San Antonio, TX) with the resistivity of 18 MΩ cm, surface tension of 71.6mN/m, and pH of 6.0 at 20.0± 0.5 °C. The solution of β-galactosidase was prepared in pure water (pH 6.0) at the concentration of 3.7×10^{-7} M. NaCl (0.1M) solution and 9.78×10^{-3} M concentration of X-gal was used to prepare the subphase. X-gal was dissolved in minimal amount of dimethyl formamide (DMF) and further diluted by using pure water. The β-galactosidase was spread at the air-X-gal/NaCl interface by using a 100 μL syringe (Hamilton Co., Reno, Nevada) by small droplet deposition uniformly over the subphase surface. The spreading volume of the enzyme solution was 45 μL for spectroscopic measurements. For the SFG results, the spectra were taken using the EKSPLA commercial system (EKSPLA, Inc., resolution about 6 cm^{-1}). The picosecond sum frequency generation (SFG) spectrometer laser system was built by EKSPLA using a copropagating configuration. The visible signal at 532 nm and IR pulses around 2750-3000 cm^{-1} were about 23 ps at 10 Hz. The full range of the IR tunability was 1000-4300 cm^{-1}. The incident angle of the visible beam is 60°(β1), and it is 55°(β2) for the IR beam. The SFG signal is collected within a small range (about 0.3°), depending on the corresponding IR wavelength (from 2750 to 3000 cm^{-1} in our experiment), around 59°(β) at the reflection geometry. In all experiments, each scan was obtained with an increment of 2 cm^{-1} and an average over 100 laser shots per point. The energy of the visible beam was typically about 300 μJ and that of the IR beam about 200 μJ. Such energy cannot damage the liquid sample and also cannot cause any heat effect or other photo chemical reaction.

3.3 Results and Discussion

3.3.1 Sum Frequency Generation Study

Figure 3.1 shows the SFG data for β-galactosidase in absence and presence of X-gal. The spectrum of β-galactosidase at the air/water interface shows a dominating peak at ~ 1660, mainly due to the alpha-helical structures. With the addition of X-gal on the subphase, along with a peak at 1660 cm^{-1} two more peaks show up, one at 1610 cm^{-1} and the other at 1700 cm^{-1}. The 1700 cm^{-1} peak may due to the DMF that is used as solvent. The 1610cm^{-1} peak may be from the X-gal. The presence of the peak at 1660 cm^{-1} in both cases indicates that the overall structure of β-galactosidase does not change with the addition of X-gal in the subphase. This necessarily does not mean that the sensitive secondary structure does not change.

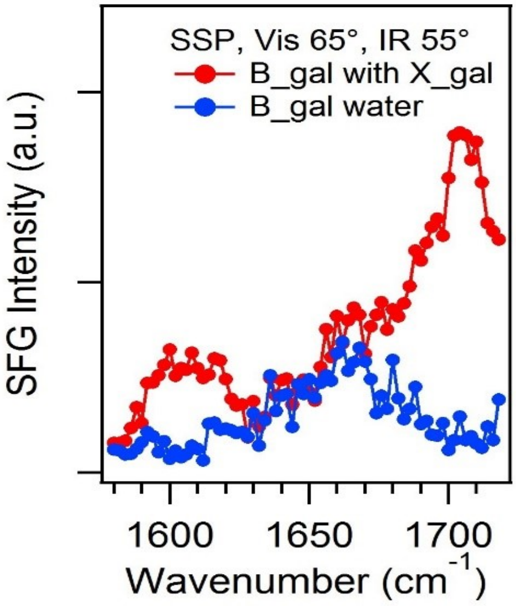

Figure 3.1: SFG spectra for presence and absence of X-gal in the subphase.

3.3.2 Infrared Reflection Absorption Spectroscopy (IRRAS)

Apart from SHG, IRRAS provides the information of change in secondary structure. The IRRAS data provided below show the effect of X-gal on the subphase of β-galactosidase Langmuir monolayer. **Figure 3.2** provides the p-polarized IRRAS spectra at the air-subphase interface when the subphase has only 0.1 M NaCl at an incident angle of 45°. The band observed at 1673 cm^{-1} is due to α-helices (amide I region) whereas the other band between 1600-1500 cm^{-1} are due to β-sheets and random coils.

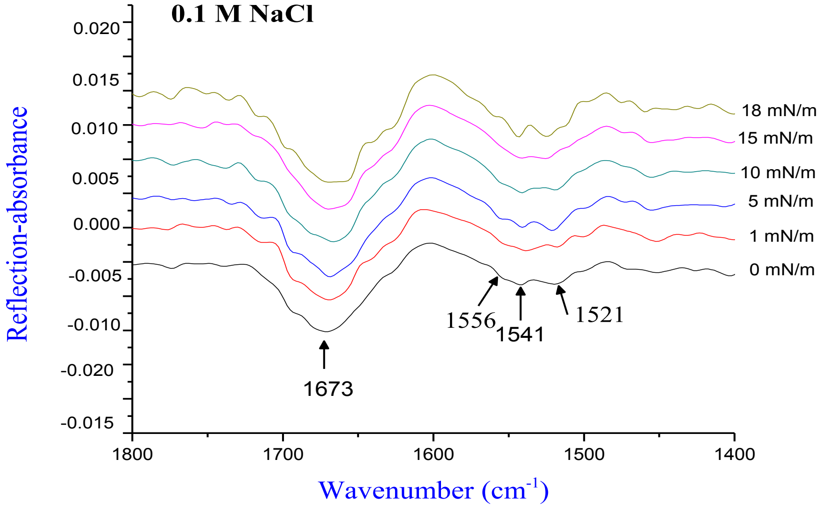

Figure 3.2: p-Polarized IRRAS spectra at the air-subphase interface of the β-galactosidase Langmuir monolayer in absence of X-gal in the subphase at a 45° incident angle.

Figure 3.3 shows the p-polarized IRRAS spectra of β-galactosidase Langmuir monolayer spread over 0.1 M NaCl and varying concentration of X-gal. Upon the increase of X-gal concentration from (2.45 to 9.78) × 10^{-3} M, the α-helix band position keeps on shifting from 1674 to 1682 cm^{-1}. This shifting of band is due to the change in secondary structure of the enzyme due to the interaction with X-gal molecules. But, the amide II region band positions do not change. This means that β-sheets remain unaltered during the process.

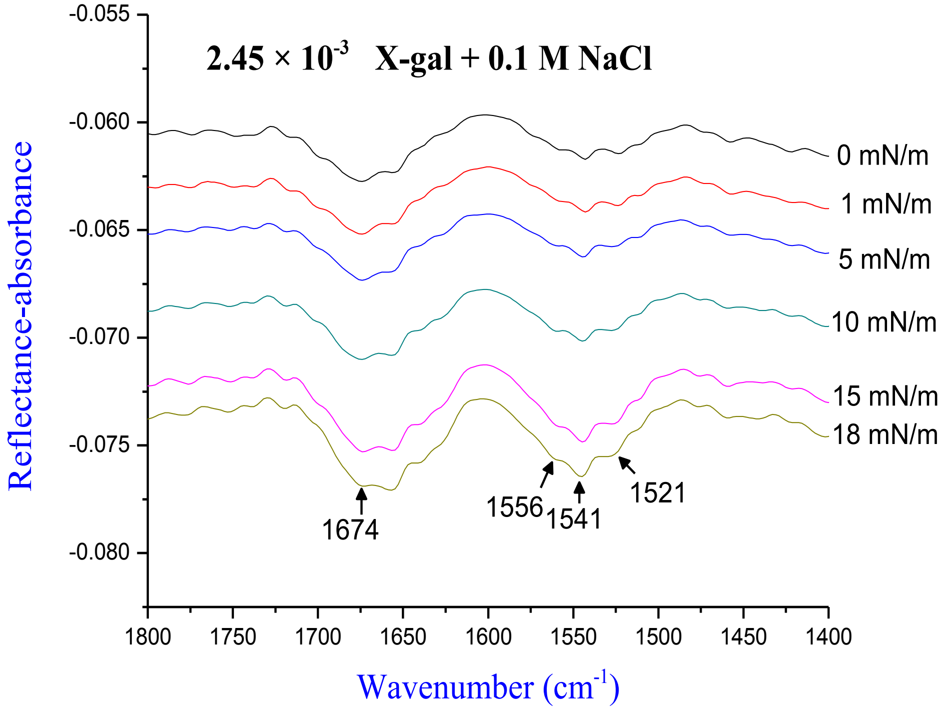
2.45 × 10-3 X-gal + 0.1 M NaCl
Reflectance-absorbance
-0.055
-0.060
-0.065
-0.070
-0.075
-0.080
0 mN/m
1 mN/m
5 mN/m
10 mN/m
15 mN/m
18 mN/m
1674
1556
1541
1521
1800
1750
1700
1650
1600
1550
1500
1450
1400
Wavenumber (cm-1)

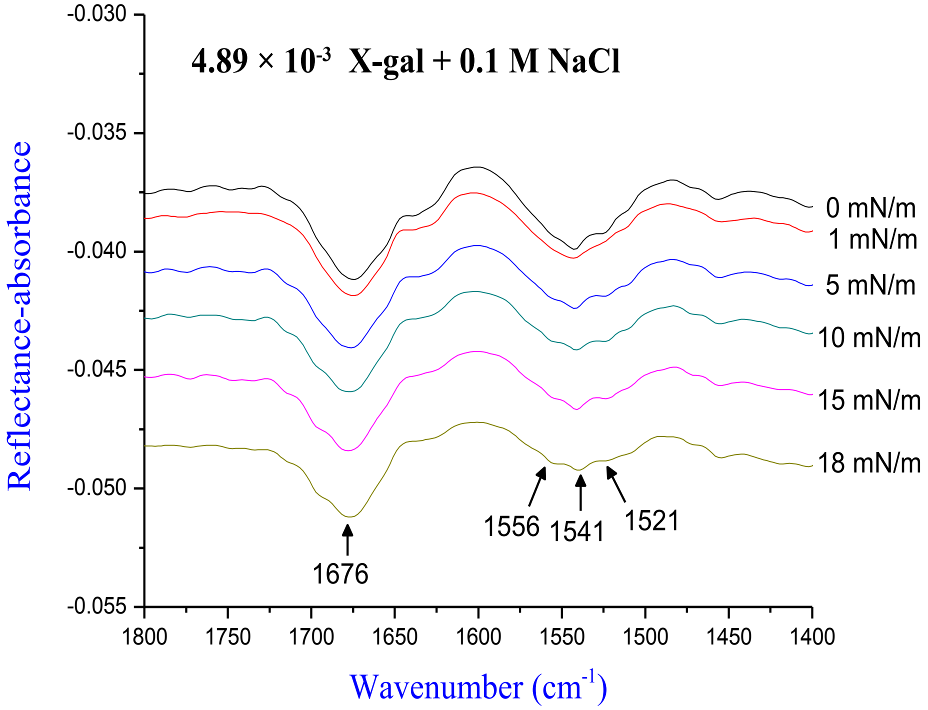
4.89 × 10-3 X-gal + 0.1 M NaCl
Reflectance-absorbance
-0.030
-0.035
-0.040
-0.045
-0.050
-0.055
0 mN/m
1 mN/m
5 mN/m
10 mN/m
15 mN/m
18 mN/m
1676
1556
1541
1521
1800
1750
1700
1650
1600
1550
1500
1450
1400
Wavenumber (cm-1)

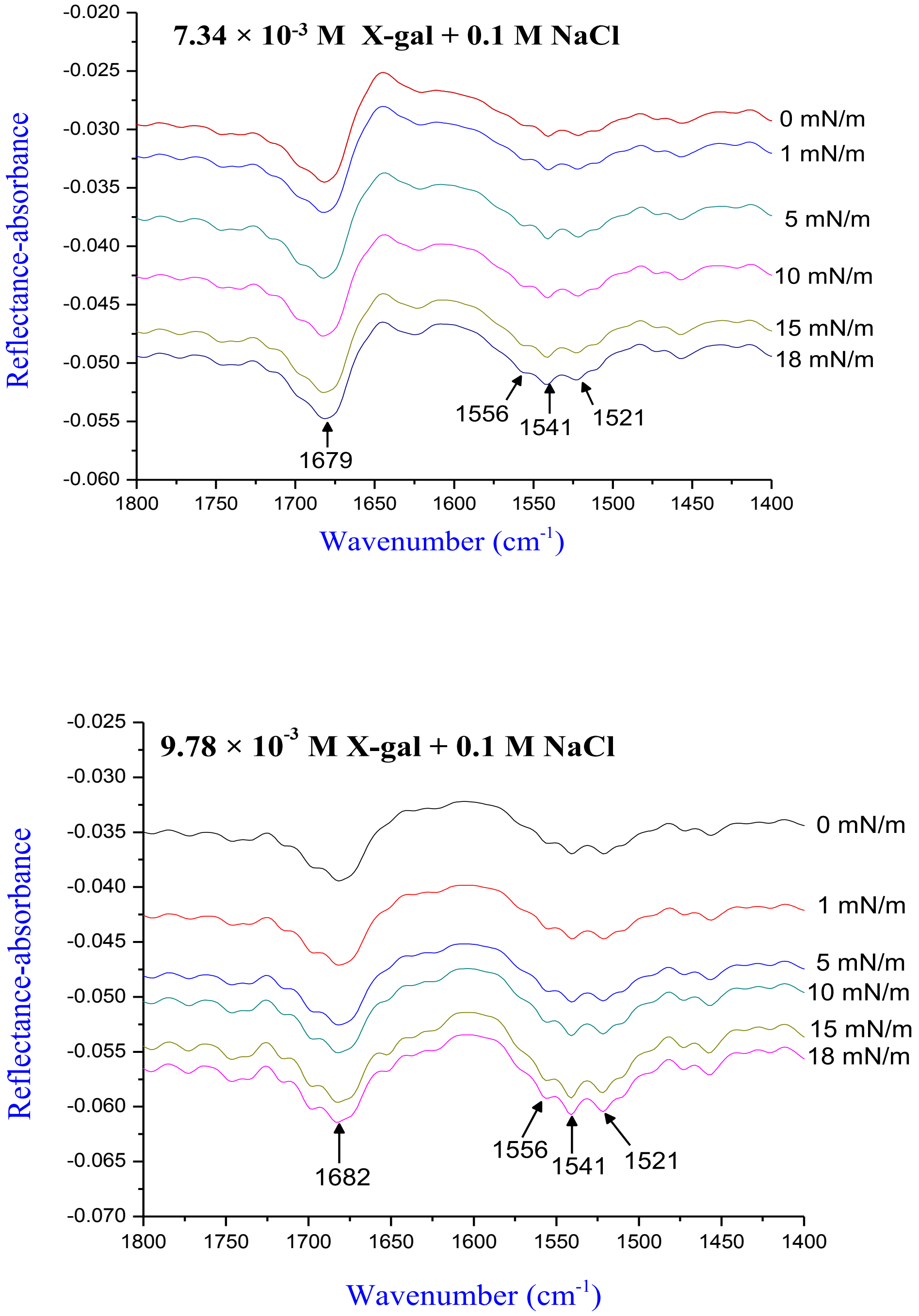

7.34×10^{-3} M X-gal + 0.1 M NaCl

9.78×10^{-3} M X-gal + 0.1 M NaCl

Figure 3.3: p-Polarized IRRAS spectra at the air-subphase interface of the β-galactosidase Langmuir monolayer in presence of X-gal (2.45, 4.89, 7.34 and 9.78) × 10^{-3} M of X-gal in the subphase at a 45° incident angle.

3.4 Computer Simulation to Investigate the Interaction of β-galactosidase and X-gal

The IRRAS data showed that there was change in secondary of the enzyme due to the interaction of X-gal. To confirm this, we investigated this phenomenon by using computer simulation. In this perspective, the study of active sites and protein conformation is most important.

Protein conformational study is necessary to determine the influence of binding of the protein to the lipid matrix on the protein structure and dynamics. β-galactosidase is a member of exoglycosidase family which has four monomers. Each monomer subunit has an active site and is responsible for binding to the substrate. As we have focused to determine the mechanism of interaction among the enzyme and its substrate X-gal, the knowledge about the conformation of the binding subunit is needed. The detail of the conformational drift was obtained by computing the root mean-square deviation (RMSD).

3.4.1 Method

The β-galactosidase structure was obtained from the Protein Data Bank (PDB ID: 1JYN) at a resolution of 1.8 Å.[69] The X-gal complex was modelled using the Gaussian 09 program package and optimized without any geometrical constraint.[70] Additionally, antechamber (an in-built tool in Amber) was used to calculate the RESP charges to construct the topology file.[71-72] Molecular docking was performed using YASARA software[73] to study the best binding pose of X-gal to β-galactosidase active site. Multiple docking procedures were done using different grid size. Out of which, the best pose was selected for the molecular dynamics (MD) procedures, MD simulations of the enzyme were performed using the GROMACS [74-75] program using AMBER03 [76] force field. First, the protein was placed in the cubic box 10 × 10 × 10 nm. This dismissed the unwanted effects that may arise from the applied periodic boundary conditions (PBC). Then the box was filled with TIP3P[77] water molecules. Some of the water molecules were replaced by sodium and chloride ions to neutralize the system (overall charge = -40) and to simulate a physiological ion concentration of 154 mM. Energy minimization of the starting structure was done by steepest descent method for 3000 steps. This step freezes the active site coordinates in order to remove any local strains. A 100 ns MD simulation was performed with constant number of particles (N), pressure (P), and temperature (T) (NPT ensample). The LINCS algorithm was used to constrain the bond lengths of the peptide, while the SETTLE algorithm[78] was used to constrain the bond length and angles of the water molecules. The long-range electrostatic integrations were calculated by the Particle-Mesh Ewald (PME) method.[79] A constant pressure of 1 bar was applied with a coupling constant of 1.0 ps; peptide, water molecules, and ions were coupled separately to a bath at 300 K with a coupling constant of 0.1 pm. The trajectories were computed for each model with a time step of 2 fs, and the data was saved for every 500 steps. The ionizable amino acid residues were set to their normal ionization states at pH 7.0. The tools available in GROMACS were utilized to analyze the MD trajectories. Cluster analysis was done to get the most representative structure, in which the trajectories were analyzed by grouping structurally similar frames [root-mean-square deviation (rmsd), cutoff of 0.30 nm], while the frame with the largest number of neighbors are denoted as a middle structure that represents that particular cluster.

3.4.2 Results and Discussion

In the current work, 100 ns MD simulations were performed on β-galactosidase (**Figure 3.4 a**) with X-gal. The major goal of the study was to elucidate the active site and substrate interaction with the active site of the enzyme. After the simulation was done, a cluster analysis of the resulting trajectories was performed, and the most representative structure was obtained (**Figure 3.4 a and b**). The substrate was attached to the 5 amino acids residues i.e. Glu416, His418, Tyr503, Trp568 and Trp999.

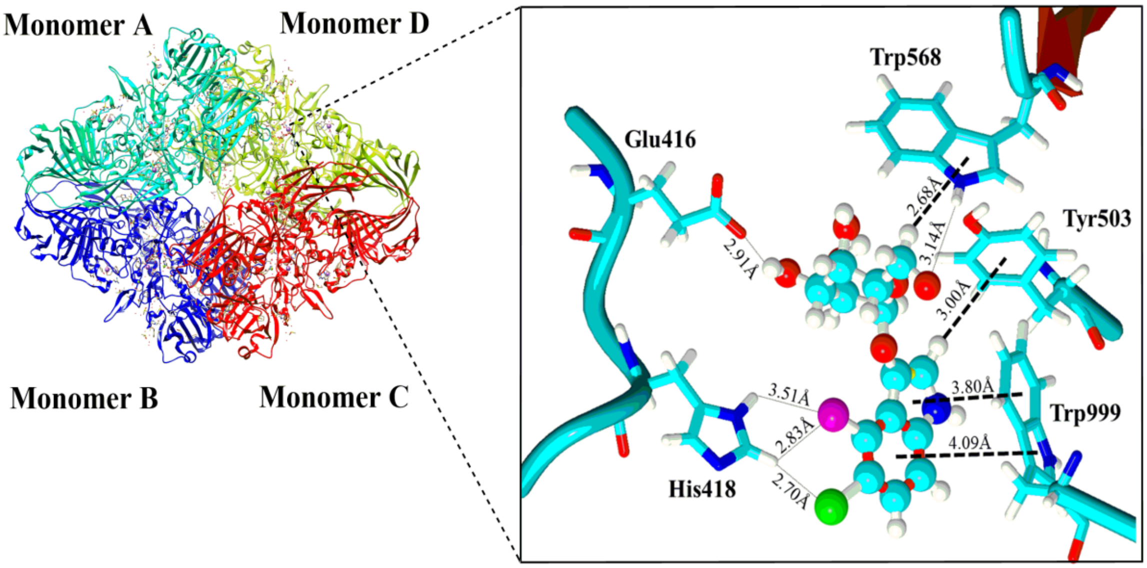

(a) (b)

Figure 3.4: X-ray crystallographic structure of β-galactosidase showing four monomeric units (a), The most representative structure derived from the 100 ns MD simulation on β-galactosidase-X-gal complex with specific interactions of X-gal (shown in ball and stick) at the X-gal binding site (b).

After the substrate binds, conformation changes were observed in the active site. Tyr503 and Trp999 form weak interaction (CH-π and π–π) with the ring of the substrate, whereas Trp568 form π–π interaction with the ring to the X-Gal. Moreover, Glu416 and His418 form a hydrogen bond with the –OH and –Br of the substrate (**Figure 3.5**). In the MD simulations, the binding of X-gal to the active site of β-galactosidase did not change the overall structure of the enzyme. The root-mean-square deviation (RMSD=0.2 nm) values shows that enzyme attained stable conformations all along the simulation time (**Figure 3.6**).

3.4.3 Study of the Active Site

Initially, after the molecular docking the residues which interact with substrate were His418, Tyr503 and Trp999. However, after the MD simulations, conformational changes were observed in the active site. Apart from His418, Tyr503 and Trp999, residue Trp568 and Glu416 also forms the interaction with the active site. As the C-alpha chain of Trp568 and Glu416 was present on the β-pleated sheet of the protein, which is highly flexible, causes to move the residues closer to the substrate forming π-π and H-bond between residues and the substrate. Using MD, we modeled the X-gal interaction and elucidated a mechanism by which X-gal may interact with β-galactosidase.

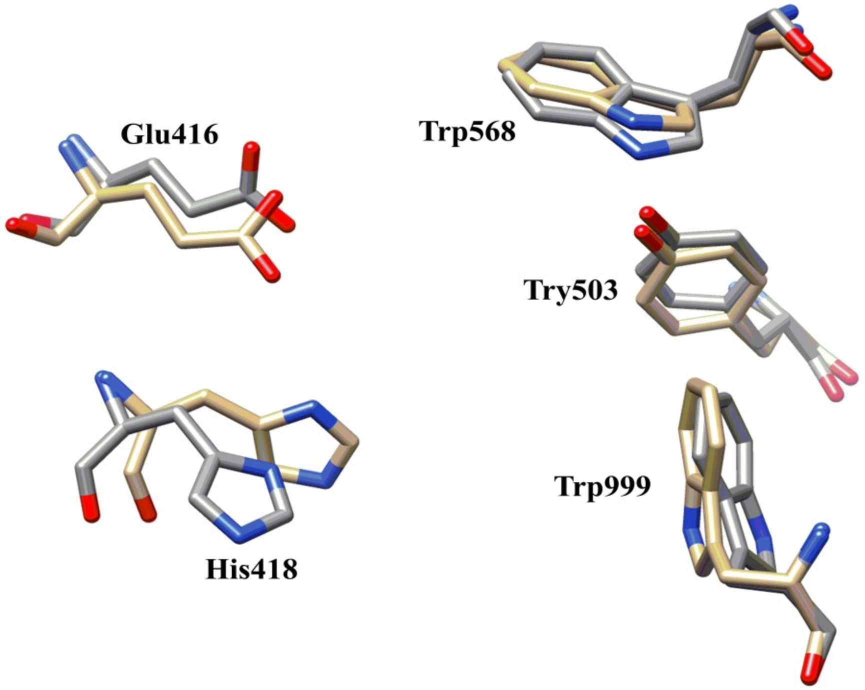

Figure 3.5: Superposition of the conformation of the active site derived from the most representative structure of the complex simulation (yellow color) with the corresponding X-ray structure (grey color).

The interaction of X-gal with these residues introduced significant changes in the secondary structure of β-galactosidase. According to the data, the X-gal-bound structure was different from the free form of the β-galactosidase. The secondary structural analysis of MD simulations also showed that the interaction with X-gal significantly influences the Phe20–Met35 region of the full-length monomeric form of the β-galactosidase.

Altogether, these results suggest that binding of X-gal to β-galactosidase, induces important structural changes that may play a critical role in the catalysis of the glycosidic bond.

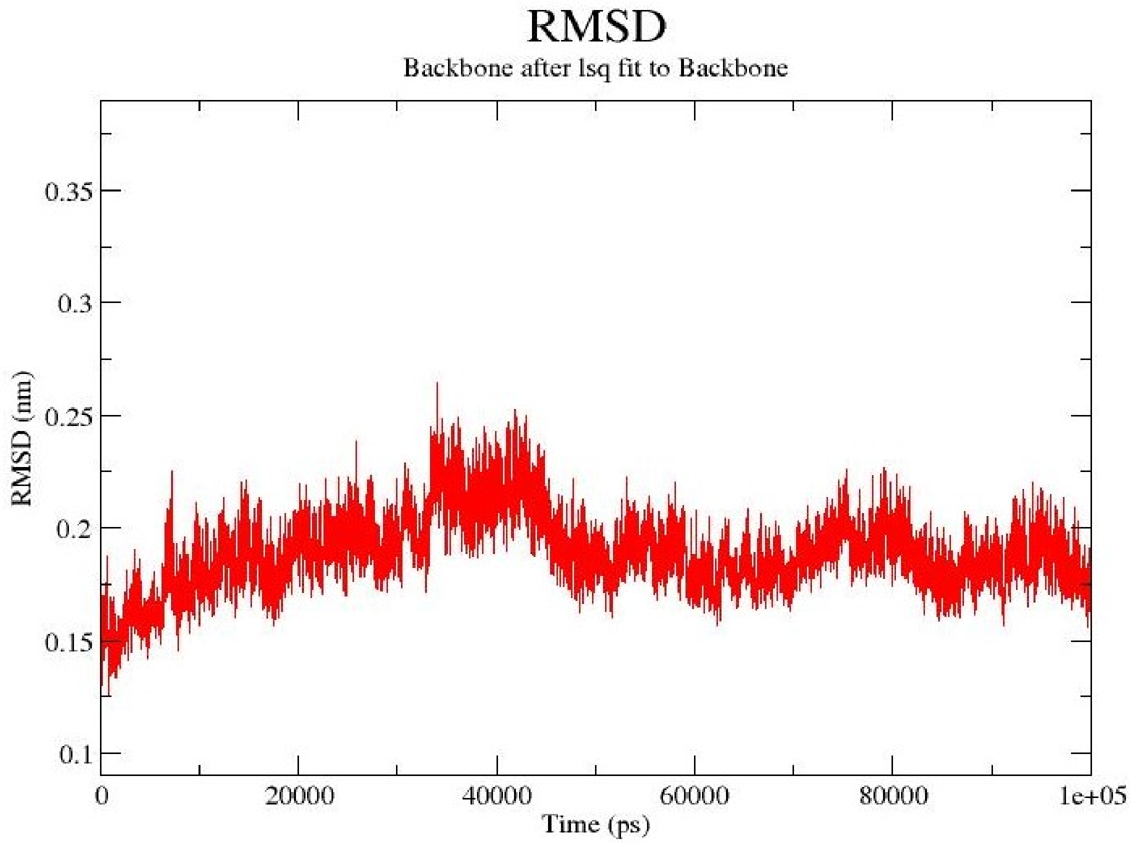

Figure 3.6: Root mean square deviation (RMSD) of amino acid residues. The RMSD is commonly used as an indicator of convergence of the structure towards an equilibrium state.

The RMS fluctuation shown in **Figure 3.7** is the measure of local chain flexibility. In another word, it is the standard deviation of the atom position calculated from the average structure. RMS fluctuation also characterizes changes in structure. It gives an indication which residues are changing position from the start structure. Since there is no appreciable change in the fluctuation (in nm) in the residues, it can be conferred that the overall structure of the enzyme does not change due to the interaction with X-gal.

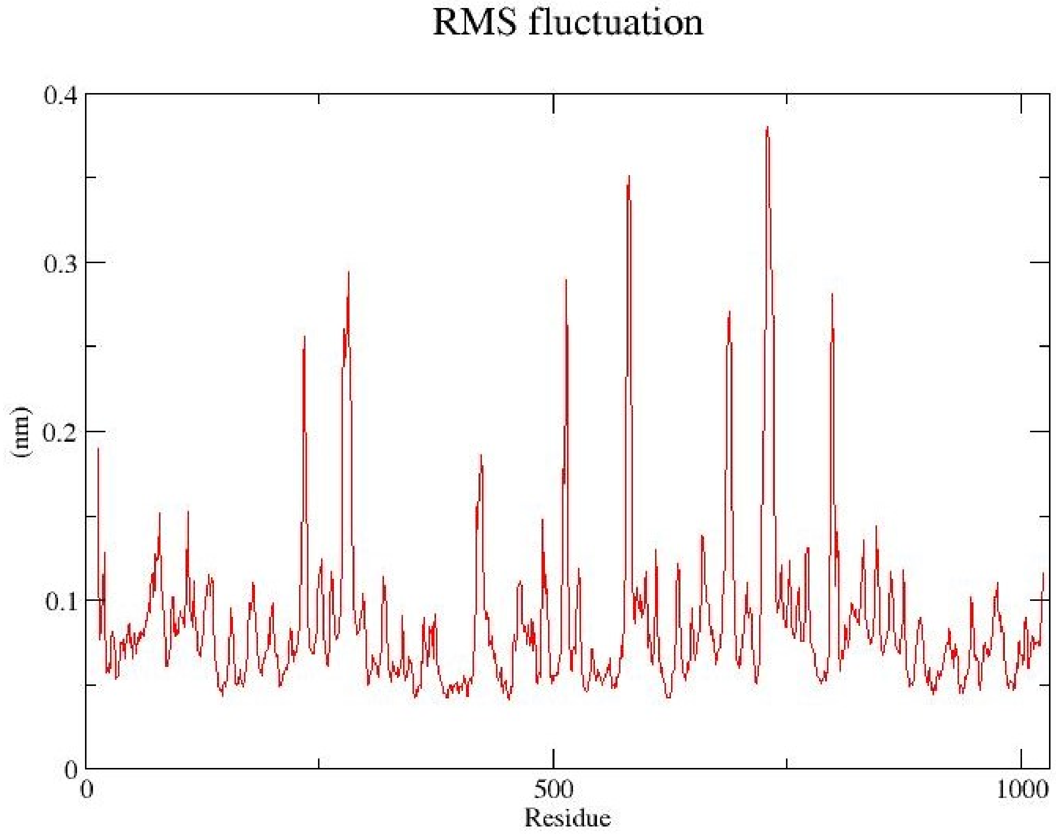

Figure 3.7: RMS fluctuation of residues of enzyme.

3.5 Proposed Mechanism of Interfacial Interaction of β-galactosidase and X-gal

When describing an interaction process, it is vital to realize which bond governs the interaction phenomenon. A number of chemical processes can take place when X-gal is in the contact of active site of β-galactosidase. One of the significant processes is the proton transfer process. In this process, we propose that a proton transfers from β-galactosidase to the X-gal which causes the active site of the enzyme to open up, causing the C-O bond joining 5-bromo-4-chloro-3-indoyl and galactose to weaken. The mechanism for the open up is that the transfer of a proton from an amino acid side chain of the β-galactosidase molecule may destroy hydrogen bonding within the enzyme and cause it to open. This process stretches the X-gal molecule by pulling at each end (**Figure 3.8 b**). In this distorted form, the C-O bond of the X-gal is highly susceptible to attack by a water molecule. **Figure 3.8 c** shows that after this reaction, 5-bromo-4-chloro-3-indolyl and galactose are formed, and the proton transferred back to the β-galactosidase, which causes the active site to return to its original state. The smaller 5-bromo-4-chloro-3-indolyl and galactose molecules leave the active site and the enzyme is ready to go again[80].

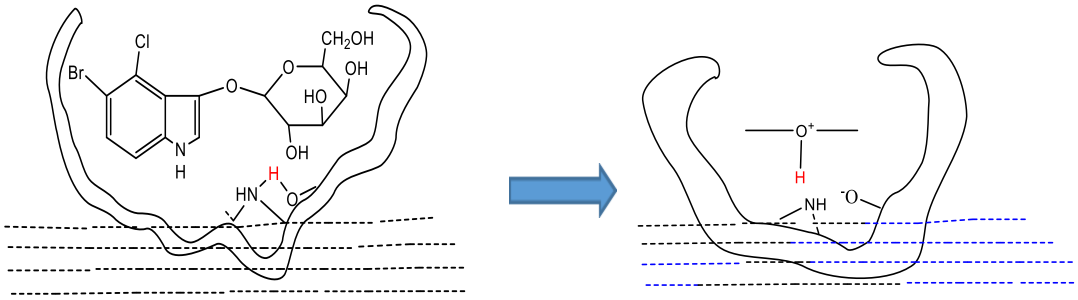

Figure 3.8: (a) Showing the pocket in the enzyme where X-gal fits into it

(b) The transfer of a proton (red) of enzyme to the X-gal by opening C-O bond

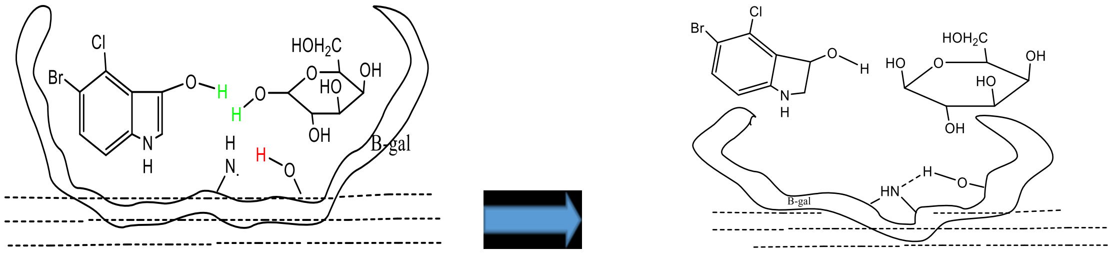

(c) Completion of enzyme catalyzed reaction. Here, the weakened C-O bond in X-gal is susceptible to nucleophilic attack by a water molecule (in green) to produce 5-bromo-4-chloro-3-indolyl and galactose.

3.6 Summary

The interaction of the enzyme, β-galactosidase with its substrate, X-gal was carried out by using both experimental and theoretical methods. The SFG experiment performed in absence of X-gal at air-subphase interface showed an intense dominating peak at ~ 1660 cm^{-1}, mainly due to the α-helical structures. With the addition of X-gal on the subphase, two more peaks at 1610 and 1700 cm^{-1} showed up along with a peak at 1660 cm^{-1}. These additional two peaks are due to the X-gal and DMF, respectively. The presence of the peak at 1660 cm^{-1} in either cases stipulates that the overall structure of β-galactosidase does not change with the addition of X-gal in the subphase. Further, the IRRAS experiment showed that the secondary structure of the enzyme gets changed in presence of X-gal in the subphase. This observation was compared with the theoretical data. It was initially found that conformation of the active site enzyme changes when enzyme binds with substrate, X-gal. But, in MD simulations, the binding of X-gal to the active site of β-galactosidase did not change the overall structure of the enzyme. The root-mean-square deviation (RMSD = 0.2 nm) values showed that enzyme attained stable conformations all along the simulation time.

Chapter 4

Surface Chemistry and Spectroscopic Studies of β-Galactosidase-Carbon Dots Conjugate and it's Use in Biosensing

4.1 Background

Nanotechnology and biosensing have been receiving constant attention since two decades. Nanoparticles have been conjugated to biological systems for numerous applications such as self-assembly, sensing, imaging, and therapy. Development of more reliable and robust biosensors that exhibit high response rate, increased detection limit, and enriched useful lifetime is in high demand. In this perspective, we developed a sensing platform by the conjugation of β-galactosidase, with the lab synthesized gel-like carbon dots (CDs) having high luminescence, photostability, and easy surface functionalization. We found that the conjugated enzyme exhibited higher stability towards the temperature and pH changes in comparison to the native enzyme (**Figure 4.1**). This enriched property of enzyme was distinctly used to develop a stable, reliable, robust biosensor with increased detection limit. Further, we used Langmuir monolayer technique to comprehend the surface property of the conjugated enzyme. It was found that the conjugate was highly stable at air-subphase interface which additionally reinforces the suitability of the use of the conjugated enzyme for the biosensing applications.

From the past, use of different nanoparticles and quantum dots in many applications like catalysis[81-82], imaging[83-84], drug delivery[85-88], and biosensing[89-91] have been common. But their sustainable use has been limited due to their cytotoxicity[92] and other detrimental health effects[93] like pulmonary toxicity, translocation to extrapulmonary sites, and evading phagocytosis. On the other hand, there is increased use of enzymes in food industries[94], pharmaceutics[95] and in energy industry[96] due to their specific catalytic property and selectivity. Nonetheless, enzymes have low operational stability and relatively poor reusability. This drawback is linked with their sensitivity to temperature and pH. Different immobilization techniques have been employed to maintain enzyme stability and reusability.[22, 97] In this case, the use of inorganic and organic supports alters the chemical and physical properties of the enzyme which in turn can lower its activity. Furthermore, the physically adsorbed enzyme through weak hydrogen bonds, van der Waals forces, and electrostatic force have high chance of leaching out easily when the pH of the media gets changed.[98]

The conjugation of nontoxic nanoparticles i.e. carbon dots (CDs) with protein/enzyme molecules, in recent years, to achieve unique properties has attracted many researchers. For example, Liu and co-workers have shown that the conjugation of carbon dots with ricin toxin has enhanced the immunomodulatory activity.[99] Similarly, Pradhan et al. have shown that iron oxide nanoparticles conjugated with glutamine and proline based osmolytes inhibit protein aggregation.[100] Hosseinzadeh et al. showed that the interaction of quantum dots (QDs) and proteins strongly influenced the surface characteristics of the QDs at the protein-QD interface.[101] In this perspective, we conjugated the lab synthesized gel-like carbon dots[102] with the enzyme, β-galactosidase. Surprisingly, we found that the stability of the enzyme was increased appreciably. Like-wise the enzyme activity did not diminish with the relocation of enzyme to the room temperature for more than two months.

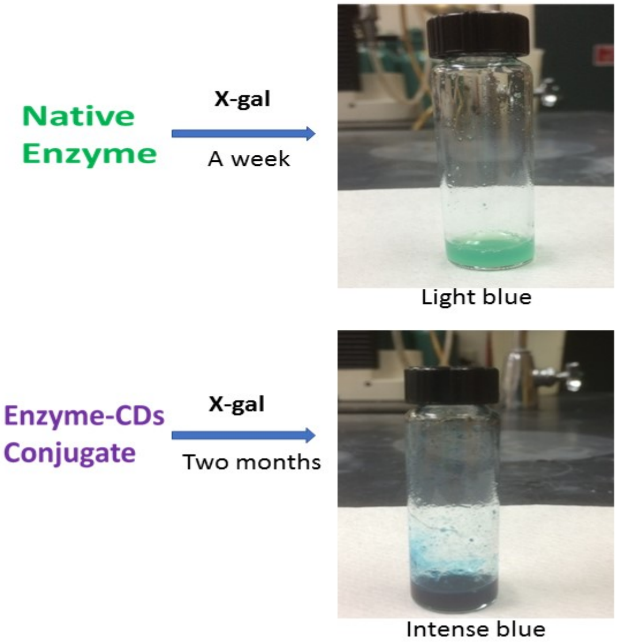

Figure 4.1: The different changes in color after treating the x-gal with the native and conjugated enzyme stored in room temperature after a week and two months, respectively.

4.2 β-galactosidase-CDs Conjugation for Biosensing

Among different kinds of electrochemical biosensor, β-galactosidase biosensor has drawn special attention due to its key role in monitoring lactose levels. There have been great challenges in the development of highly sensitive and advanced glucose biosensor, which includes detailed mechanism describing the behavior of nanoparticles used, enhancement of signal to noise ratio, transduction, and amplification of signals. Although, metal nanoparticles have been widely used for the achievement of lower detection limits, large variations in the analyte detection during batch measurements occurred due to small variations in the density of metal nanoparticles.[103] Numerous nanomaterials have been applied as matrix for the immobilization β-galactosidase in biosensors by several approaches like, cross-linking, physical adsorption, and covalent entrapment.[104] But they are susceptible to the high loss of enzyme during the sensing. Hence, we designed a method of conjugation of β-galactosidase with CDs in presence of EDC to improve the overall sensing capability of the biosensor.

4.3 Experimental

4.3.1 Conjugation of β-galactosidase with CDs

CDs (2mg/mL) was treated with 1-ethyl-3-(dimethyl aminopropyl) carbodiimide-HCl (EDC) and stirred for half an hour. Then freshly prepared β-galactosidase (0.2 mg/mL) was mixed with the existing solution and stirred for 3 hours. The hybrid biocomposite was sonicated and centrifuged at 1500 rpm to remove the loosely bound CDs and β-galactosidase. After sonication and centrifugation, the carefully collected supernatant liquid was analyzed by UV-vis spectroscopy to check whether β-galactosidase has been strongly bound to the CDs. Schematic mechanism for the conjugation process of CDs and β-galactosidase is shown in **scheme 4.1.**

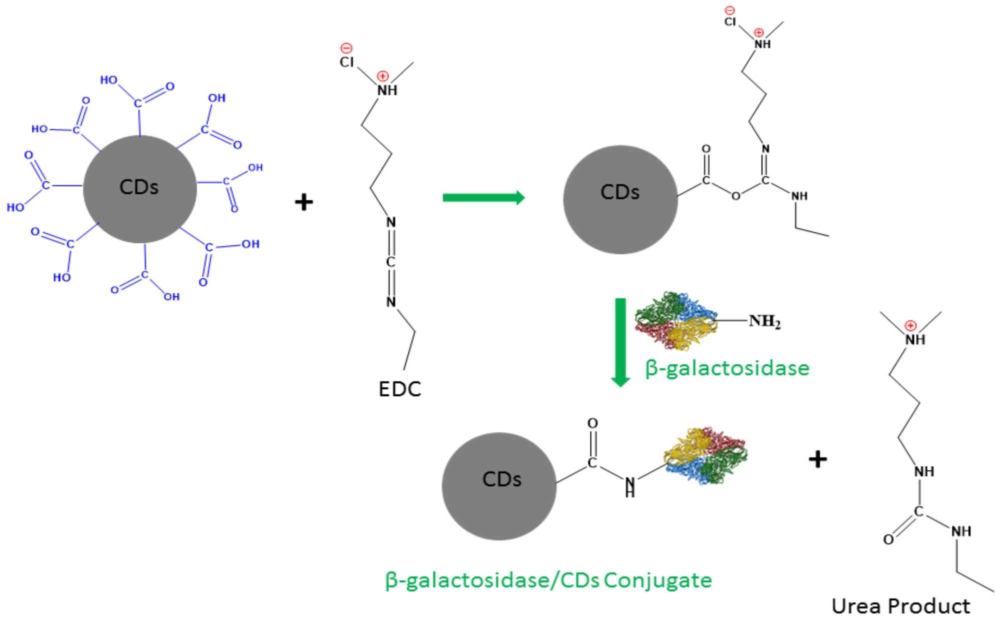

Scheme 4.1: Mechanism of conjugation of β-galactosidase and CDs in presence of EDC

4.3.2 Characterization of the Biocomposite

Characterization of conjugate is very important for its selective use in biosensing. We used the UV-vis, fluorescence, and other *in situ* methods to characterize the enzyme/CDs conjugate.

4.3.2.1 UV-vis Spectra of the Conjugate

The absorption spectra of the β-galactosidase/CDs conjugate is shown in **Figure 4.2.** We observed three different peaks at 282, 290, and 334 nm. The first two peaks are due to π-π* transition and last one due to n-π* transition, respectively. The absorption peak for the enzyme is at 280 nm and for the carbon dots it is at 332 nm.

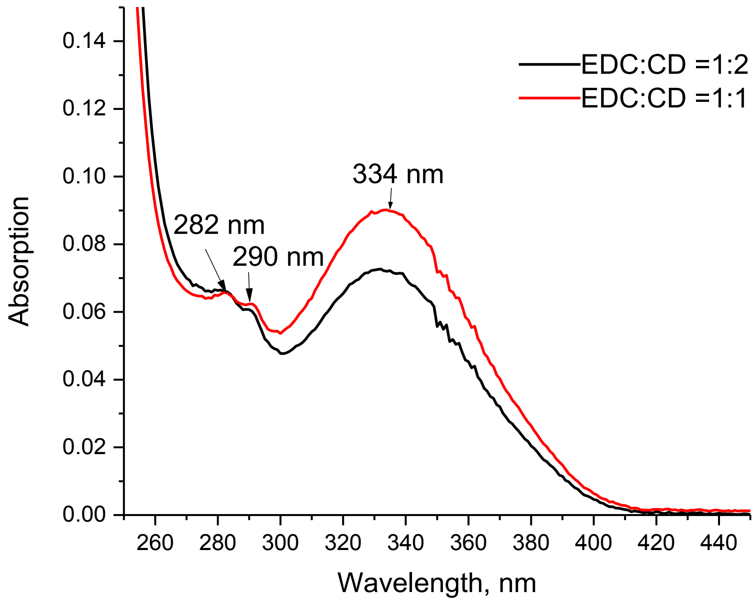

Figure 4.2: Absorption spectra of the conjugate. Here, the concentration of EDC and CDs was same in both cases.

The evolvement of new peak for the conjugate shows the formation of new bond at 290 which is ascribed by the π-π* transition for the new amide bond.

4.3.2.2 Fluorescence Spectra

To confirm the formation of conjugate we took the emission spectra. As we know that the emission of the β-galactosidase is at 350 nm and the photoluminescence of the gel like carbon dot (G-CDs)[102] is at 438 nm. The obtained new peaks are completely different than native enzyme and carbon dots (**Figure 4.3**) corresponds to the formation of the conjugate.

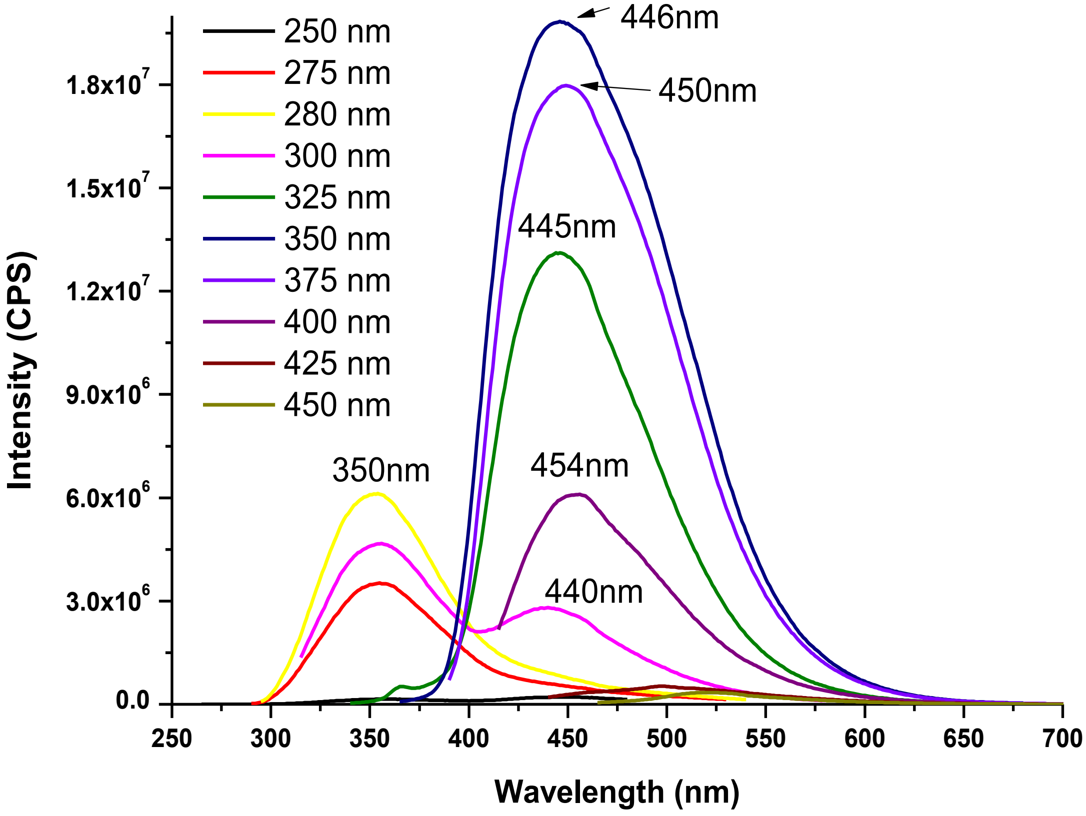

Figure 4.3: Fluorescence spectrum of β-galactosidase-carbon dots conjugate.

4.4 Cytotoxicity Study of the Conjugate on Sea Urchin Embryos

When a biosensor is dipped in the substrate solution to evaluate its concentration, we should be aware that the analyte released, by any chance, is not toxic and does not damage the substrate solution. To evaluate the toxicity of enzyme-CDs conjugate, we used sea urchin embryos as a model system to test static acute toxicity. The rationale for choosing sea urchin embryos is that they are extremely sensitive to toxic chemicals and conductive for experimental observations. Initially, gametes were collected from adult sea urchins with ripe gonads. Fresh eggs were washed three times by cold filtered artificial seawater and mixed with sperm to examine fertilization rates. Eggs with a fertilization rate greater than 95% were only used for the toxicity tests. Toxicity tests were performed in a clean, 24-well cell culture plate. In each well, 100 healthy fertilized eggs were incubated in 2 mL of seawater with conjugate at a concentration of 0, 5, 10, 20, 50, and 100 $\mu g.mL^{-1}$, respectively. The plate of fertilized eggs was incubated at 15°C for 16 h until they reached the mesenchyme blastula-stage embryos.

The results (**Figure 4.4**) show that enzyme conjugate have low cytotoxicity to fertilized sea urchin eggs and embryos. In the presence of 10 $\mu g.mL^{-1}$ conjugate, more than 95% of sea urchin embryos retain a normal morphology after 16 hrs of incubation time. Even at the high concentration of conjugate tested, i.e., 50 $\mu g.mL^{-1}$, more than 90% of embryos remain normal, indicating low cytotoxicity of conjugate to the cells. This shows that if by any mistake, the conjugate gets leaked into the substrate solution it won’t have any alarming effects.

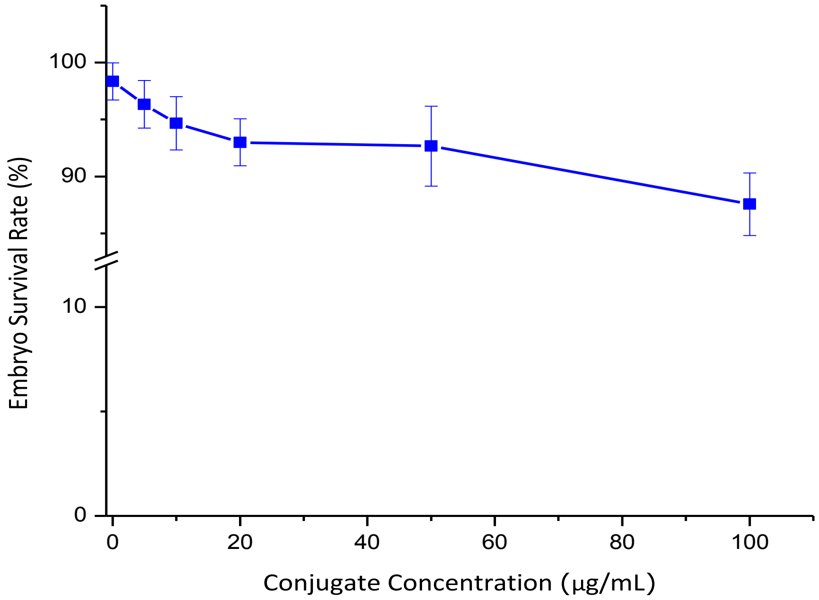

Figure 4.4: Cytotoxicity study of the conjugate.

4.5 Surface Chemistry and Spectroscopic Studies of the Conjugate

4.5.1 Surface Pressure and Surface Potential

We were also interested to know the surface chemistry of the conjugate as its surface property determines its adsorption behavior on the surface of an electrode. Surface chemistry and spectroscopic studies can also be used to reveal the interaction of the analytes at the air-subphase interface and the bulk solution. **Figure 4.5** shows that the conjugate forms good π-A as well as the surface potential isotherm on the 0.1 M NaCl subphase. The limiting molecular area was determined to be 35,000 $Å^2$.$molecule^{-1}$ which describes the cross-sectional area per molecule of the conjugate. The surface potential explains the dipole moment of the analyte below and above the air-subphase interface. Initially, there is sudden increase in surface potential. This is due to the sudden movement of molecules during compression. The crest and troughs seen in the surface potential is due to the rapid movement of conjugate molecules to attain a specific orientation. Finally, there is sudden drop in the surface potential at collapse surface pressure. This is due to the cancellation of dipole moment as conjugate molecules come very near to each other.

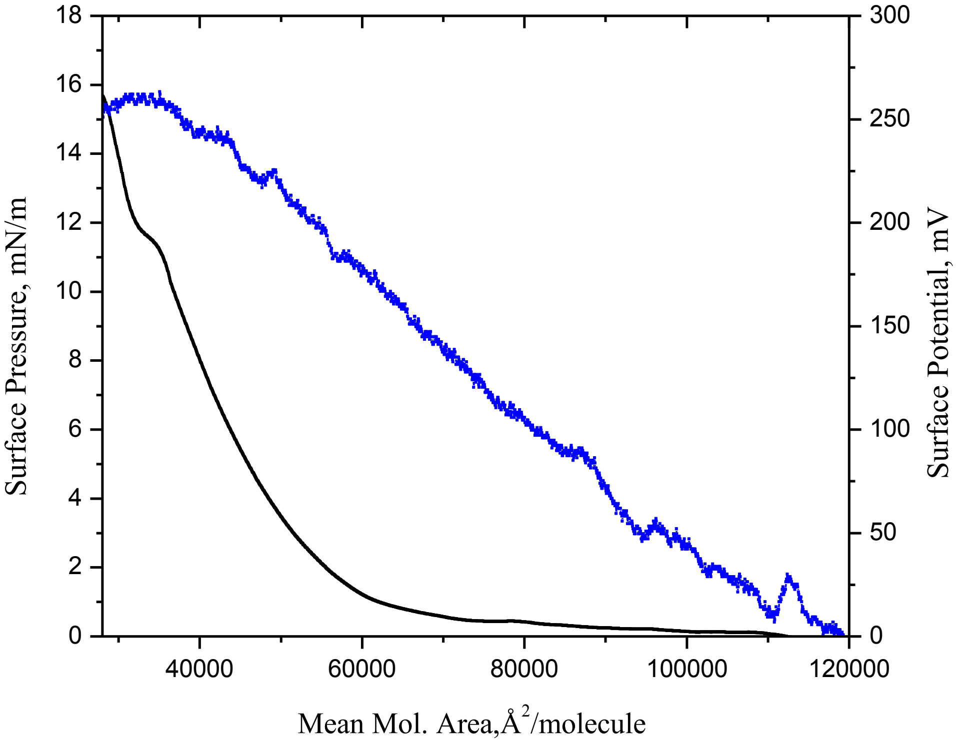

Figure 4.5: Surface pressure and surface potential isotherm of β-galactosidase-CDs Langmuir monolayer.

4.5.2 Effect of Concentration of X-gal on β-galactosidase-CDs Conjugate Langmuir Monolayer

X-gal being the substrate of β-galactosidase enzyme, certainly should have some effects on the Langmuir monolayer of the β-galactosidase-CDs conjugate. **Figure 4.6** provides detailed impact of the different concentration of X-gal on the β-galactosidase-CDs conjugate Langmuir monolayer. We can see that increase in the concentration of X-gal on the subphase increases the limiting molecular area. This fact can be explained with relation to the interaction of conjugate with the X-gal. However, we observed significant increase in the limiting molecular area when 4 mg. mL^{-1} of X-gal was present in the subphase. This may be due the solubilization of conjugate molecules in the subphase because of low ionic strength.

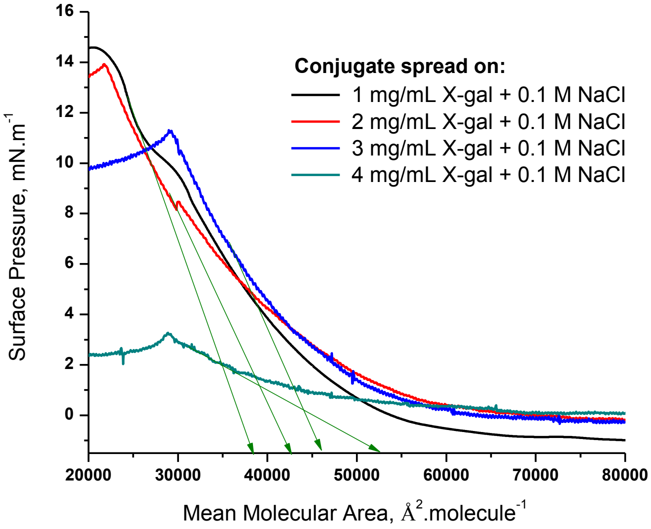

Figure 4.6: Langmuir isotherms of β-galactosidase-CDs conjugate with different concentrations of X-gal and 0.1 M NaCl subphase. The conjugate spread volume was 45 µL at room temperature.

4.5.3 In situ UV-vis Spectrum of the Langmuir Monolayer

Having known that the formation of conjugate was successful through the techniques like UV-vis, fluorescence, we were interested to know the extent of the conjugate that remains on the interface. This is because it directly relates to the stability of the analyte (conjugate) on the interface of electrode while constructing the biosensor. As shown in the **Figure 4.7**, the band peak at 232 nm can be designated as the combined higher-energy maxima of tyrosine and tryptophan residues obtained from the protein molecule[105]. In this case, the peaks from the induced effect CDs on the conjugate in monolayer was not predominant as like the absorbance obtained for the solution. This can be explained in such a way that the free residual amount of CDs were desorbed in the subphase as the CDs are highly hydrophilic. Furthermore, CDs bonded with enzyme in conjugate monolayer also remained immersed on the subphase as only hydrophobic component of the analyte remains projected in the air in air-subphase interface.[106]

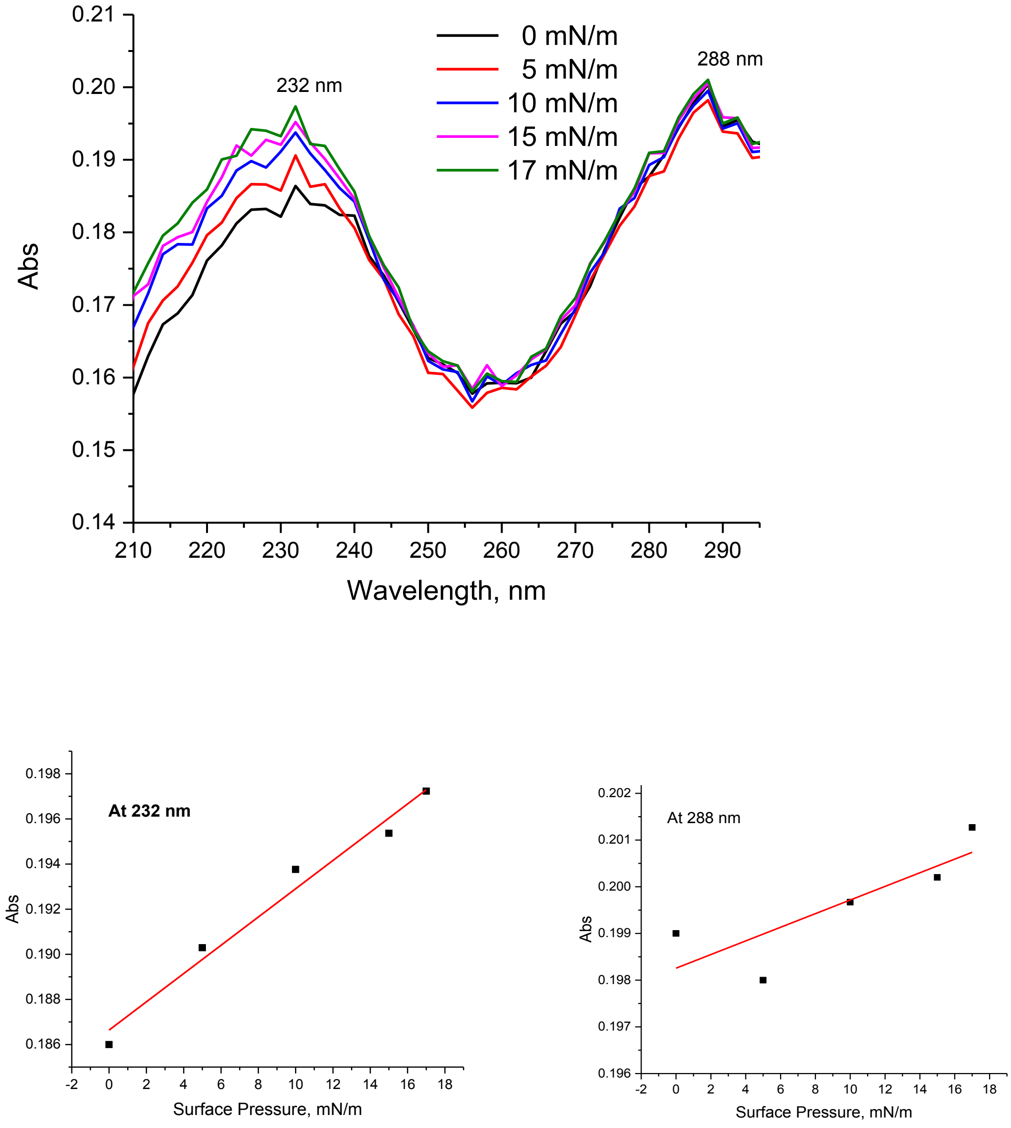

Figure 4.7: In-situ UV-vis spectra of the conjugate (0.1 mg/mL) on the subphase of 0.1 M NaCl.

We plotted the absorbances data obtained for different surface pressure. In doing so a linear relationship was established (**Figure 4.7**). This observation reinforces the interpretation that the conjugate of CDs and the β-galactosidase remains at the air-subphase interface facilitating for the development of a biosensor.

4.6 Monitoring Reaction of the Conjugate and Lactose

While treating the different concentration of lactose with the conjugate of β-galactosidase/CDs we observed the quenching in the intensity of the emission peaks as shown in the **Figure 4.8**. We observed this quenching phenomenon even after the false (F) addition of lactose.

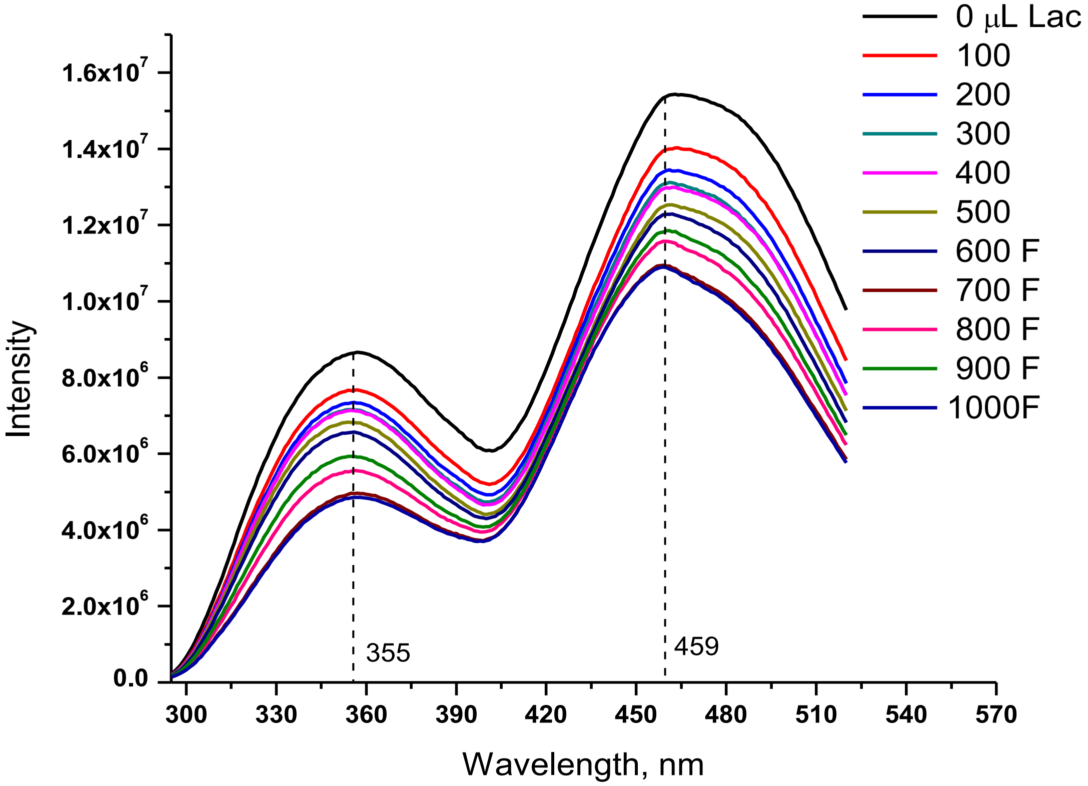

Figure 4.8: Fluorescence spectra of the conjugate with different concentration of lactose.

The quenching of peak usually occurs when the enzyme sites are blocked. We were skeptical whether, it will impact on the electrochemical behavior of the designed biosensor.

4.7 Development of a Biosensing Platform

The β-galactosidase-CDs conjugate was immobilized by the use of PEG on the glassy carbon electrode. It seemed that the higher effective surface area of CDs provides more sites for enzyme immobilization. In this chapter, we were focused on the quantification of lactose present in a sample by using an enzyme-CDs conjugate biosensor.

Lactose, a disaccharide sugar, is found in milk and is formed from galactose and glucose. Lactose makes up around 4.5~5.0% of milk (by weight). Traditionally, the lactose concentration in milk is determined by the use of lactase. Lactose is split into glucose and galactose by lactase. Glucose reacts with a phenolic compound through an enzymatic reaction, with peroxidase, and forms a pink colored complex. The absorbance of the complex is read at 505 nm, and the value is directly proportional to the concentration of lactose in the sample.

To avoid the drawbacks of traditional methods and enrich the stability of the enzyme, we conjugated the enzyme with CDs and constructed a working electrode (glassy carbon electrode) by immobilizing the conjugate along with PEG and activated carbon. The three-electrode system is shown in **Scheme 4.2**. The reference electrode allows us to measure the potential of the working electrode without passing current through it while counter (auxiliary) electrode allows the current to pass.

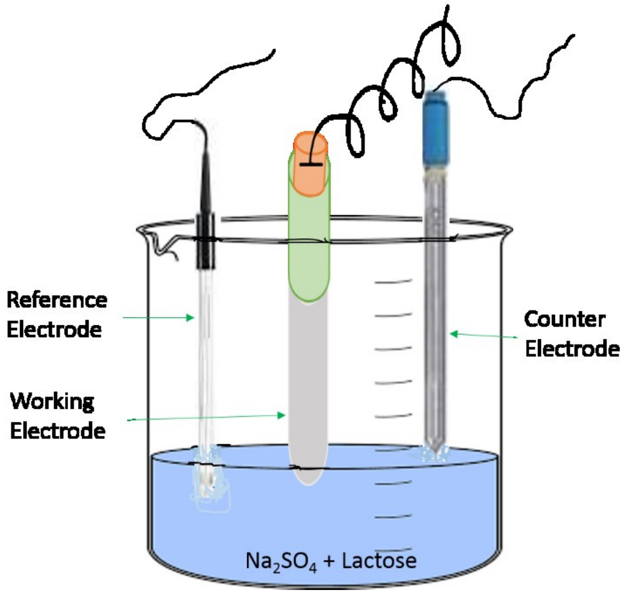

Scheme 4.2: Electrochemical setup showing three-electrode system.

In another word, counter electrode is used to close the current circuit in the electrochemical cell. It is usually made of an inert material (e.g. Pt, Au, graphite, glassy carbon) and usually it does not participate in the electrochemical reaction. If oxidation occurs at the working electrode, reduction using the same magnitude of current is sustained at the counter electrode and hence there is no current flow between working and reference electrode (high input impedance) enabling us to follow changes in working electrode potential accurately. This is not usually possible in a two-electrode system although we can get crude values by using certain types of electrodes which can act simultaneously as working and reference electrode.

4.7.1 Cyclic Voltammetry Study

Cyclic voltammetry is the most versatile technique employed for getting qualitative information about electrochemical reactions.[107] It renders the rapid identification of redox potentials distinctive to the electroactive species under investigation, providing considerable information about the thermodynamics of a redox process, kinetics of heterogeneous electron-transfer reactions, and analysis of coupled electrochemical reactions or adsorption processes.

In cyclic voltammogram, usually, the anodic peak (oxidation peak) appears due to oxidation when scan from lower to higher potential. The cathodic peak (reduction peak) appears due to reduction, when scan from higher to lower potential.

As we immobilized the enzyme-CDs conjugate directly to the glassy carbon electrode (working electrode), this makes our system a third-generation biosensor. We swept a voltage (for example – 1.0 V to + 0.1 V) at a scan rate, 0.1V/s for a selected range, but we did not see a prominent peak i.e., the reduction potential does not exist within that range (**Figure 4.9**). This means that there is no redox reaction occurring. This proves that β-galactosidase enzyme does not have redox center as like the glucose oxidase. The observed curves exhibit the interaction of conjugate and lactose which later leads to the cleavage of lactose to glucose and galactose.

Adding redox active label (Fe^{3+}/Fe^{2+}) allow to monitor the electrode interfacial activity. So as the lactose binds to the enzyme, the electrochemical environment of electrode surface changes as we see from the current. **Figure 4.10** illustrates the voltammetric behavior of the conjugate electrode system in hexacyanoferrate solution (1 mM $[Fe(CN)_6]^{3-}/[Fe(CN)_6]^{4-}$ in 0.1 M PBS, pH 7).

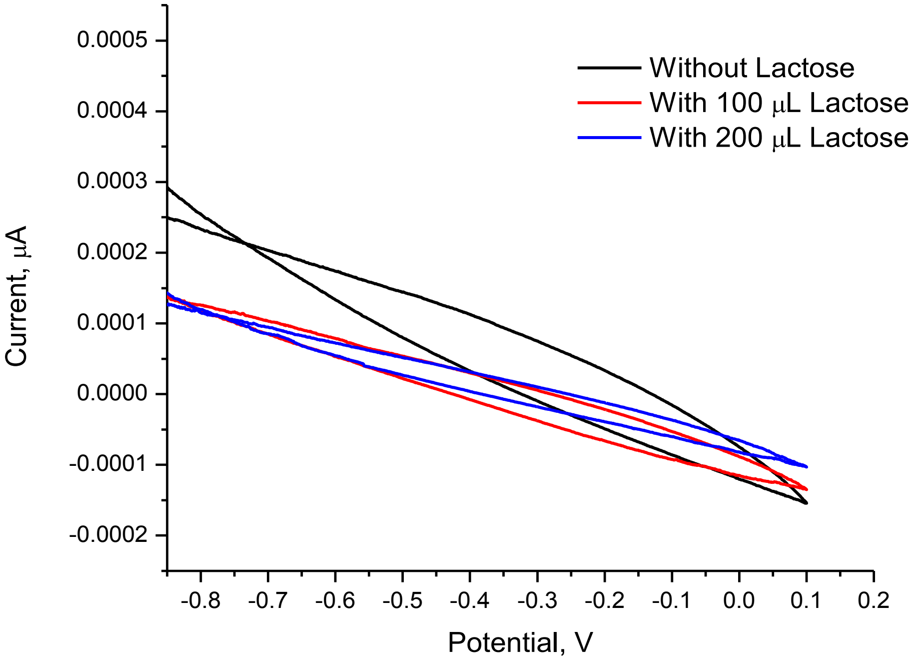

Figure 4.9: Cyclic voltammogram of conjugate on glassy carbon electrode with Ag/AgCl standard electrode in absence and presence of lactose.

It showed a well-defined faradaic response. We found that current keeps on increasing with the increased concentration of lactose into the Fe^{3+} / Fe^{2+} system (**Figure 4.11**). This information elucidates that a redox system is necessary in β-galactosidase-CDs conjugate electrode system to determine the effective concentration of lactose in the sample. **Scheme 4.3** provides the detail in which glucose oxidase, an enzyme with redox center, is used to determine the lactose concentration. This is alternative method for the use of Fe^{3+} / Fe^{2+} system. The detection limit for the biosensor was 2.9×10^{-4} M. The sensitivity of the biosensor was evaluated based on the standard deviation of the plot of current vs concentration of lactose. It was found to be 0.81 μA $mmol^{-1}$ cm^{-2}.

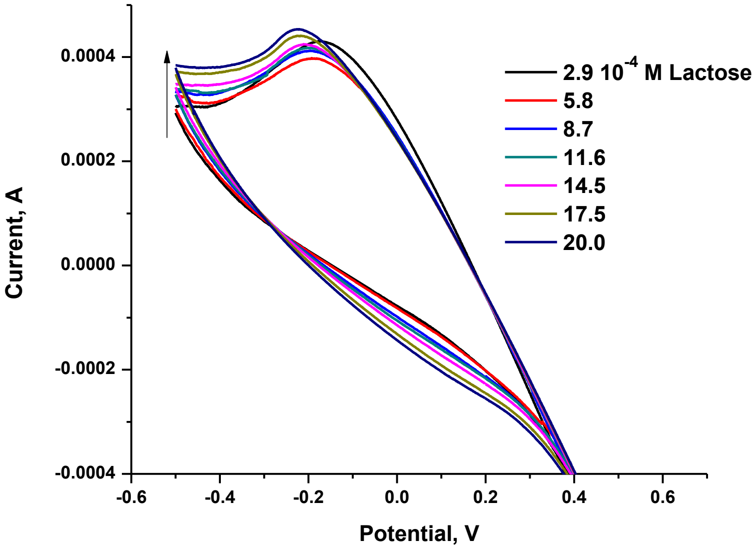

Figure 4.10: Cyclic voltammogram of glassy carbon electrode (adsorbed with β-galactosidase/Carbon Dots conjugate) with different concentration of lactose in Fe^{2+} solution.

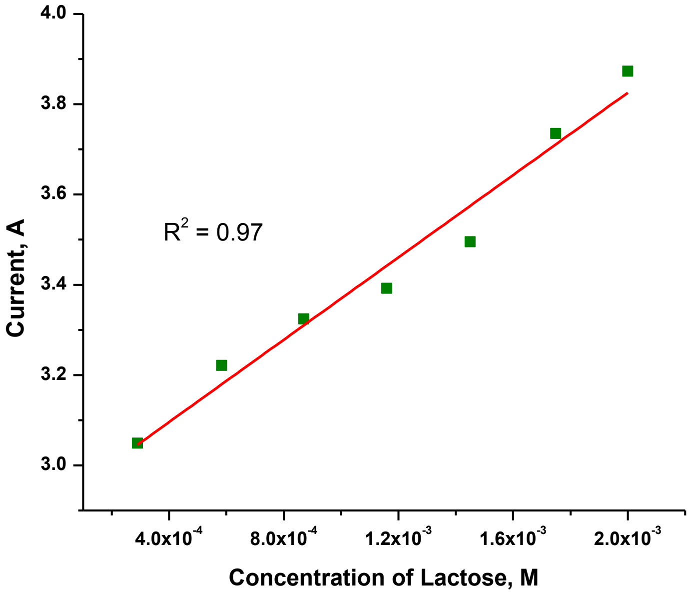

Figure 4.11: Plot of concentration of lactose versus current.

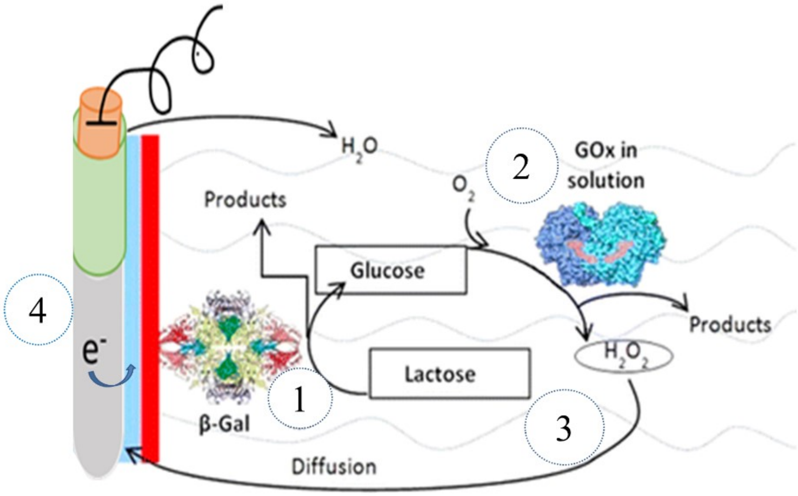

Scheme 4.3: Two enzyme system of biosensing.

4.8 Summary

In conclusion, the Langmuir monolayer isotherm of β-galactosidase-CDs conjugate was studied using the surface chemistry and spectroscopy at the air-subphase interphase. The study of β-galactosidase-CDs conjugate Langmuir monolayer reveals that there is decrease in collapsed surface pressure with the increase in amount of X-gal in the subphase. Also, it was found that the monolayer is stable. Further, the bulk phase study of the conjugate revealed that it was highly stable, and activity lasted for at least two months. But, the native enzyme retains its activity only for few days at room temperature. This property of conjugate was employed in the development of biosensor. The study of the reaction of conjugate and lactose via the fluorescence spectroscopy and cyclic voltammetry showed that there occurs interaction between the conjugate and lactose sufficient to break the lactose into glucose and galactose. The detection limit of the developed biosensor was 2.9×10^{-4} M whereas sensitivity was 0.81 μA $mmol^{-1}$ cm^{-2}. Above all the stability of the biosensor was more than two months.

Chapter 5

Surface Chemistry and Spectroscopic Studies of Cholera Toxin B Langmuir Monolayer

5.1 Background

Cholera toxin (CT) is a protein complex secreted by bacterium *Vibrio choleraes.*[108] This oligomer protein complex of AB_5 family consists of 6 subunits. It is commonly referred as a choleragen and often abbreviated as CTX, Ctx or CT. It is the main virulence factor which causes an acute dehydration effect in Cholera disease. Among 6 subunits, a single copy of cholera toxin A unit (CTA) is enzymatically active monomer subunit consisting of two chains connected by a disulfide bond and is the toxic part of the toxin. The other 5 copies of cholera toxin B (CTB) forms pentamer ring (**Figure 5.1**), and is the nontoxic homopentamer subunit.[109] The molecular weight (MW) of each unit is 11.6 kDa. It is also responsible for the recognition and binding to its membrane bound receptor ganglioside GM1 followed by cell penetration.[110]

Figure 5.1: CTB (top view; Protein Data Bank ID: 1XTC) with CTA subunit removed

There are many research applications of CTB as this subunit is non-toxic ligand to GM1 gangliosides glycans. One of the very common applications of CTB is the use as a neuronal tracer when the CTB-conjugated with fluorescent probes is used either as an imaging or as a quantification tool.[111] It is generally involved in the cell trafficking and signaling machineries.[112] Recently, CTB has been conjugated with quantum dots and non-toxic carbon dots for *in vitro* and *in vivo* imaging applications.[113-114] Furthermore, as GM1 gangliosides are commonly found in the cell wall lipid rafts, the CTB is extensively used as a tool to study lipid rafts morphology and distribution. Because of the ability of CTB to penetrate cells through rapid and high binding affinity to the GM1 gangliosides and nontoxic in nature , it has been extensively used as a tool for retrograde neuronal tracing as there are many cell surface gangliosides on the peripheral neural system.[111, 115] In the therapeutic world, the recombinant CTB is currently used as an add on component to "Ducoral®" oral cholera vaccine.[116-117] In addition to being used as a component of the vaccine, CTB has many potential pharmaceutical applications, such as an immunomodulatory and anti-inflammatory agent[118] and as a drug delivery system for transmucosal delivery.[119-120] Furthermore, CTB can be conjugated to liposomes and modified protocells for targeted delivery of antigens and drugs to motor neurons.[121-122] CTB conjugated with saporin has been used to establish a rodent model for motor neuron death in disease.[123] As increased amount of membrane surface GM1 gangliosides are found in Alzheimer's disease patients,[124-125] CTB may be used in a future as a diagnostic tool for detection of GM1 in amyloid plaques bound to Aβ.[126]

CTB, being a molecule of multiple applications, its structure, function and action mechanism are well studied.[127-129] Various studies have also been conducted about the application and properties of CTB.[130-131] However, the driving force of CTB going to the interface to bind GM1 is not clear. Although the interaction and binding affinity between GM1 and CTB has been roughly studied by various techniques (such as flow cytometry, surface plasmon resonance, lipid bilayers attached on solid surface),[61, 132-137] it is difficult for these methods to mimic the dynamic amphiphilic membrane structure *in vivo*. Langmuir monolayer, a quintessential two dimensional (2-D) surface chemistry approach, can be one of the best techniques to study these dynamic amphiphilic membranes.[40, 106] The structure of cell membranes comprises phospholipids bilayers, which can be divided into three regions as following:[138] i) the interior core of the membrane, which has a hydrophobic character; ii) the hydrophilic headgroups of the lipids; iii) the lipid-water interfacial layer which exhibits similar dielectric permittivity to air-water interface.[139-140] Unfortunately, surface chemistry of monolayer of CTB has not been investigated to the best of our knowledge. In addition, few publications have reported the reason why CTB forms pentamer. Therefore, significant research about the behavior of CTB at the air-water interface must be conducted.

This chapter presents the results of surface chemistry study of CTB at the air-subphase interface, which can be considerably utilized to resemble the amphiphilic membranes structure *in vivo*. Here, we investigated properties of CTB monolayers using Langmuir technique as this technique is viewed as a powerful technique to comprehend how surface proteins communicate with their membrane and subphase environment by studying their air-subphase behavior.[38] Besides, this facile method has been used in reducing interfacial tension, and controlling wetting properties by employing monolayers of chemical surfactant[141] which devises the ease of restraining the intermolecular interactions and disposition of the analyte by the use of controllable variables like, subphase composition, monolayer analyte, surface pressure, and surface potential. This study will make clear about the amphiphilic natures of vesicles and cell membrane in cohesion with CTB that prevail *in vivo* and interaction mechanism around the amphiphilic natures. More specifically, this study will be helpful in apprehending the less understood mechanism of how the bacterial toxins such as CTB cross the plasma membrane of targeted cell because, at first, these toxins bind with the lipids and proteins of cell membrane. Moreover, this approach will be beneficial to study the property of transmembrane receptors, cell adhesion, and its implications for possible future biosensing applications and microfluidic device development.

5.2 Materials and Methods

5.2.1 Chemicals

Cholera Toxin B (CTB) was obtained from Sigma Aldrich having the molecular weight of 11.2 kDa that was determined using matrix-assisted laser desorption ionization time-of-flight (MALDI-TOF) mass spectrometer. The water that was utilized in the experiments was used from PURELAB® Ultra, Elga Lab Water (Veola Water Solutions and Technologies, UK) with the resistivity of 18 MΩ cm, surface tension of 71.6 mNm^{-1}, and pH of 6.0 at 20.0 ± 0.5 °C.

5.2.2 Equipment

Every experiment was conducted in a clean room (class 1000) at which temperature (20.0 ± 0.5 °C) and humidity (50% ± 1%) were maintained constant. In the study of surface pressure area (π−A) isotherms, surface potential-area isotherms, stability, and compression−decompression cycles, a Kibron μ-trough (Kibron Inc., Helsinki, Finland) having area of 124.5 cm^2 (5.9 cm × 21.1 cm) was used. Kelvin probe that consists of a capacitor-like system was utilized to measure surface potential. The vibrating plate was adjusted at 1 mm (approx.) above the surface of Langmuir monolayer and a gold-plated trough acted as a counter electrode. The Wilhelmy method was deployed to assess surface pressure with a 0.51 mm diameter alloy wire probe having sensitivity of ± 0.01 mNm^{-1}. For the *in situ* UV-vis and fluorescence study, we used KSV mini-trough (KSV Instrument Ltd., Helsinki, Finland) having area of 225 cm^2 (7.5 cm × 30 cm).

5.2.3 Langmuir Monolayer Preparations

The CTB solution was prepared in pure water (pH 6.0) at the concentration of 1.78×10^{-5} M. 20 mM citrate phosphate buffer (pH 5.5) solution was used to prepare the subphase. The CTB was spread uniformly over the air-subphase interface by using a 100 μL syringe (Hamilton Co., Reno, Nevada). The spreading volume of the toxin solution was 45 μL for the surface chemistry and spectroscopic measurements. After spreading the solution, Langmuir monolayer was allowed to attain the equilibrium state approximately for 15-20 min. Then, monolayer was compressed with the rate of 270 $Å^2.molecule^{-1}\cdot min^{-1}$. This compression rate was used such that the compression completes in around 10 min to maintain the consistency in the experiments. The experiments were repeated three times, and good reproducibility was achieved. The reason why we employed the Kibron μ-trough for the surface pressure/potential and compression/decompression experiments and KSV trough for *in situ* UV-vis and fluorescence experiments is that KSV trough provides plenty of space to frequently relocate the UV-vis and fluorescence machine parts in comparison to the Kibron trough.

5.2.4 UV-vis Spectroscopy

The *in situ* UV-vis absorption spectra of the Langmuir monolayer were taken with the help of HP spectrometer model 8452 A, fixed on a rail nearby to the KSV trough (KSV Instrument Ltd., Helsinki, Finland). The KSV trough has dimensions of 7.5 cm × 30 cm which is appropriate for reaching towards the quartz window located at the center of the trough.

5.2.5 Fluorescence Spectroscopy

The *in situ* fluorescence spectra of CTB Langmuir monolayer was measured with the help of optical fiber detector on the top of the KSV trough, which was coupled to the Spex Fluorolog fluorespectrometer (Horiba, Jovin Yvon, Edison, NJ). The optical fiber used in the experiment had an area of 0.25 cm^2 and was rested approx. 1 mm above the surface of the subphase. The instrument works such a way that the excitation light gets transmitted through the optical fiber from the light source to the monolayer and the emitted light from the monolayer gets dispatched back to the detector through the optical fiber. Further, Fluorolog-3 (slit width 5 nm) at the excitation and emission was used to measure the amount of CTB casted up into the subphase with definite time interval.

5.2.6 Infrared Reflection Absorption Spectroscopy (IRRAS)

Bruker Equinox 55 FTIR instrument (Billerica, MA) equipped with the XA-511 accessory for the air-water interface was used at the air-subphase interface to obtain infrared spectra. Kibron μ-trough S (Helsinki, Finland) with dimensions of 5.9 × 21.1 cm was employed for the experiment. The measurements were carried out by the use of *p*-polarized light and a mercury-cadmium-telluride (MCT) liquid-nitrogen-cooled detector. Each spectrum was acquired by the coaddition of 1200 scans at a resolution of 8 cm^{-1}.

5.3 Results and Discussions

5.3.1 Surface Pressure and Surface Potential-Area Isotherms

To study the interfacial behavior of CTB Langmuir monolayer at optimized conditions, the toxin was spread at the air-subphase interface. Stable monolayer was obtained by depositing 45 μL of CTB (1.7×10^{-5} M) on the subphase of 20 mM citrate phosphate buffer that demonstrated, reproducibly, entirely essential phases of an appropriate shaping of a two-dimensional (2-D) Langmuir monolayer as shown in **Figure 5.2**. Though the toxin has relatively lower molecular weight (11.2 kDa), concentration of 0.2 mg/mL solution was sufficient to produce stable monolayer. From the figure, an initial zero surface pressure at 2,600 $Å^2$ .molecule^{-1} corresponds to the gaseous phase at which the molecules at the CTB film have little to no intermolecular interactions.

The compression of barriers resulted in the increase of surface pressure as portrayed by the decrease in area per molecule. This shows the liquid phase of the monolayer starting at 2450 $Å^2$.molecule^{-1} and ending at 900 $Å^2$.molecule^{-1} where molecules are less free to move as their orientation grows uniform. Further compression of the monolayer resulted the cease of movement of molecules known as solid/condense phase analogous to the three-dimensional (3-D) liquid that continued until 580 $Å^2$.molecule^{-1}. The limiting molecular area which describes the minimum cross-sectional area per molecule was found to be 2,200 $Å^2$.molecule^{-1}. This experimental value was close to the theoretical value (2350 $Å^2$.molecule^{-1}) obtained by a computer program for modeling, simulation, and docking, YASARA.[142]

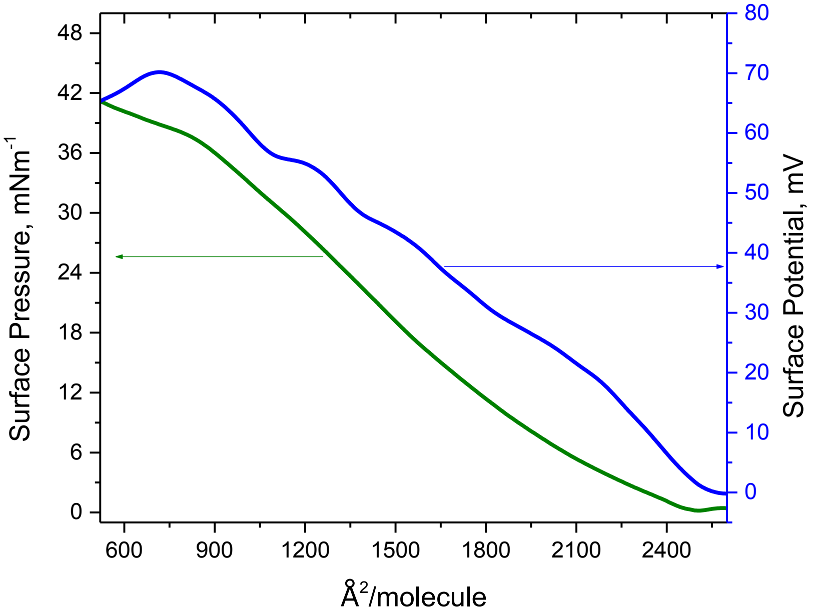

Figure 5.2: Langmuir monolayer of CTB (0.2 mg/mL) obtained after spreading on the 20 mM citrate phosphate buffer subphase (pH 5.5).

The change in phase boundary potential produced by an interfacial film is defined as the interfacial potential of surface potential (SP). It gives the idea of the dipole moment or potential of the monolayer above and beneath the monolayer, molecular interactions that occurs prior to and following to the phase change. In surface potential data of the **Figure 5.2**, there is immediate increase in SP at the gaseous phase which is due to the change in dipole moment by compression indicating that surface dipole forces and orientation of subphase molecules causes a net interfacial orientation. This also suggests that water molecules at the interface aligned with the pendant hydrogen pointing outward together with Na^+ ions from buffer outnumbered rest of the water molecules with negative oxygen end exposed.[143] In the liquid condensed phase, the SP has increased which denotes that the molecules are presumed to take almost vertical orientation as the effective (normal) dipole moment has its utmost value. The small bumps seen in the SP curve are due to the movement of CTB molecules to gain specific orientation on the subphase surface under the vibrating electrode. After attaining the solid/condensed phase at 900 Å^2.molecule^{-1}, we observed the decrease in SP. This is best described as the cancellation of dipole-dipole moment due to the short distance (surface pressure-area isotherm). From this information, it is helpful in knowing the role of electrostatically charged CTB molecules in biological process.

5.3.2 Compression-Decompression Cycles and Stability Curves

It is utmost essential that the monolayer should be stable long enough to perform *in situ* experimentation. From the compression-decompression data we figured out that CTB Langmuir monolayer can be classified as almost reversible collapse because it prolongs the monolayer from cycle to cycle with minimal loss of CTB molecules from the monolayer during each cycle which can be further justified due to the presence of less hysteresis which additionally confirms the high stability of the monolayer. Three compression-decompression cycles were scrutinized at surface pressures 20, 25, 30, and 35 mNm^{-1} (**Figure 5.3**).

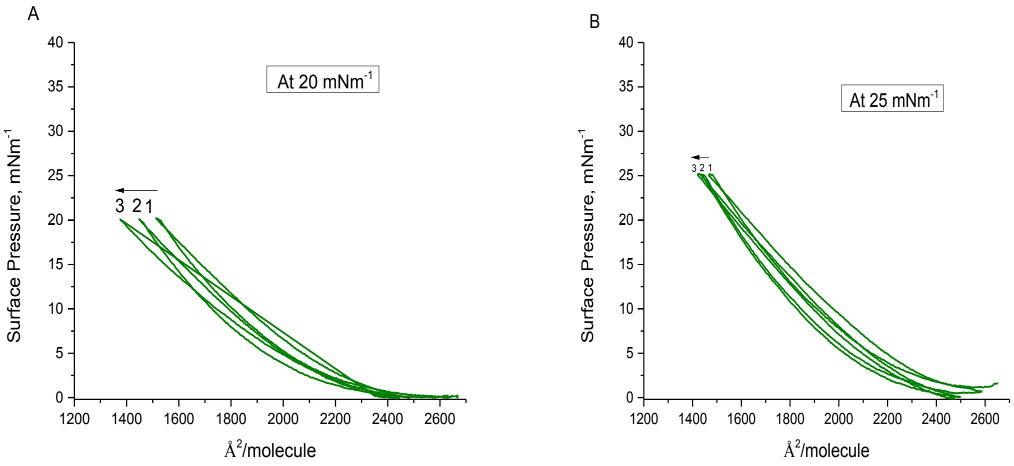

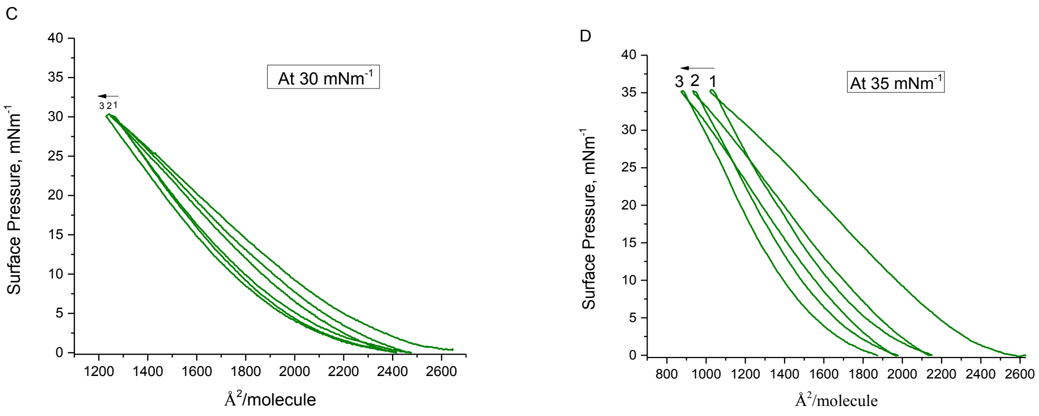

Figure 5.3: Compression-decompression Langmuir monolayer curves of CTB (0.2 mg.mL^{-1}) at different surface pressures spread on citrate phosphate buffer (pH 5.5). The amount of injection was 45 µL at room temperature.

From the figure, we found that the hysteresis, extent of analyte being lost to subphase from the interface slightly increases from 3.5% to 5.7% on going from 20 to 35 mN.m^{-1}. This result reveals that the CTB molecules at the interface were not soluble in subphase due to the rigidity of the Langmuir monolayer, and aggregates and domain formation were negligible. Since, compression-decompression takes appreciable time to complete the cycles, so it can also be used as a criterion to check stability of the monolayer. To confirm the stability of CTB Langmuir monolayer, experiments were performed at two different surface pressures viz. 20 and 30 mN.m^{-1} (**Figure 5.4**). It was found that the monolayer was stable up to 28000 s (7.78 hrs). This stability was achieved at surface pressure 20 mN.m^{-1}. When the surface pressure was adjusted to 30 mNm^{-1}, the stability was suppressed. The main reason for Langmuir monolayer to be less stable at higher pressures is the inability of the monolayer to sustain the analyte at that compressed state. The high stability of the Langmuir monolayer of CTB shows that the amphiphilic nature of CTB is the driving force to push it to the amphiphilic air-subphase interface. To double check whether CTB aggregate at the air-water interface, various surface spectroscopic methods have been used to examine the Langmuir monolayer of CTB and results are shown below.

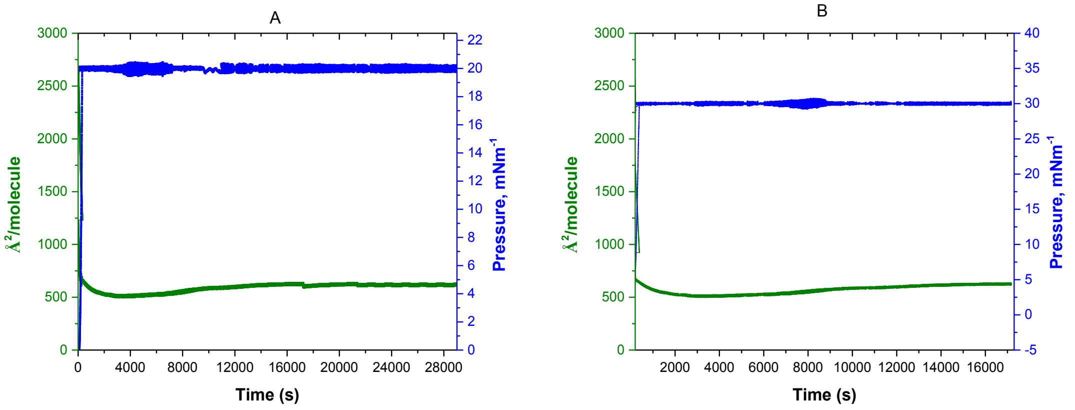

Figure 5.4: Stability measurements of the CTB Langmuir monolayer at two different surface pressures (A) 20 and (B) 30 mNm^{-1} by spreading 45 µL of CTB (0.2 mg.mL^{-1}) on citrate phosphate buffer (pH 5.5) at room temperature.

5.3.3 UV-vis Absorption Spectroscopy

From stability curves, we knew about the stability of CTB Langmuir monolayer. We were further interested to confirm it by perceiving the extent of analyte on the interface. Hence, the UV-vis spectra of the CTB Langmuir monolayer at different surface pressure were measured. The absorption maxima peaks were obtained at 230, 280, and 307 nm as shown in the **Figure 5.5**. The band at 230 nm can be designated to the overlapped higher energy maxima of tyrosine and tryptophan residues obtained from CTB molecule. Also, the band at 280 nm can also be attributed to combination of the absorption band of tryptophan and tyrosine residues, which are actually the external residues of the CTB molecules which remain exposed to the subphase solution. No specific assignment could be given to the peaks at 307 nm.

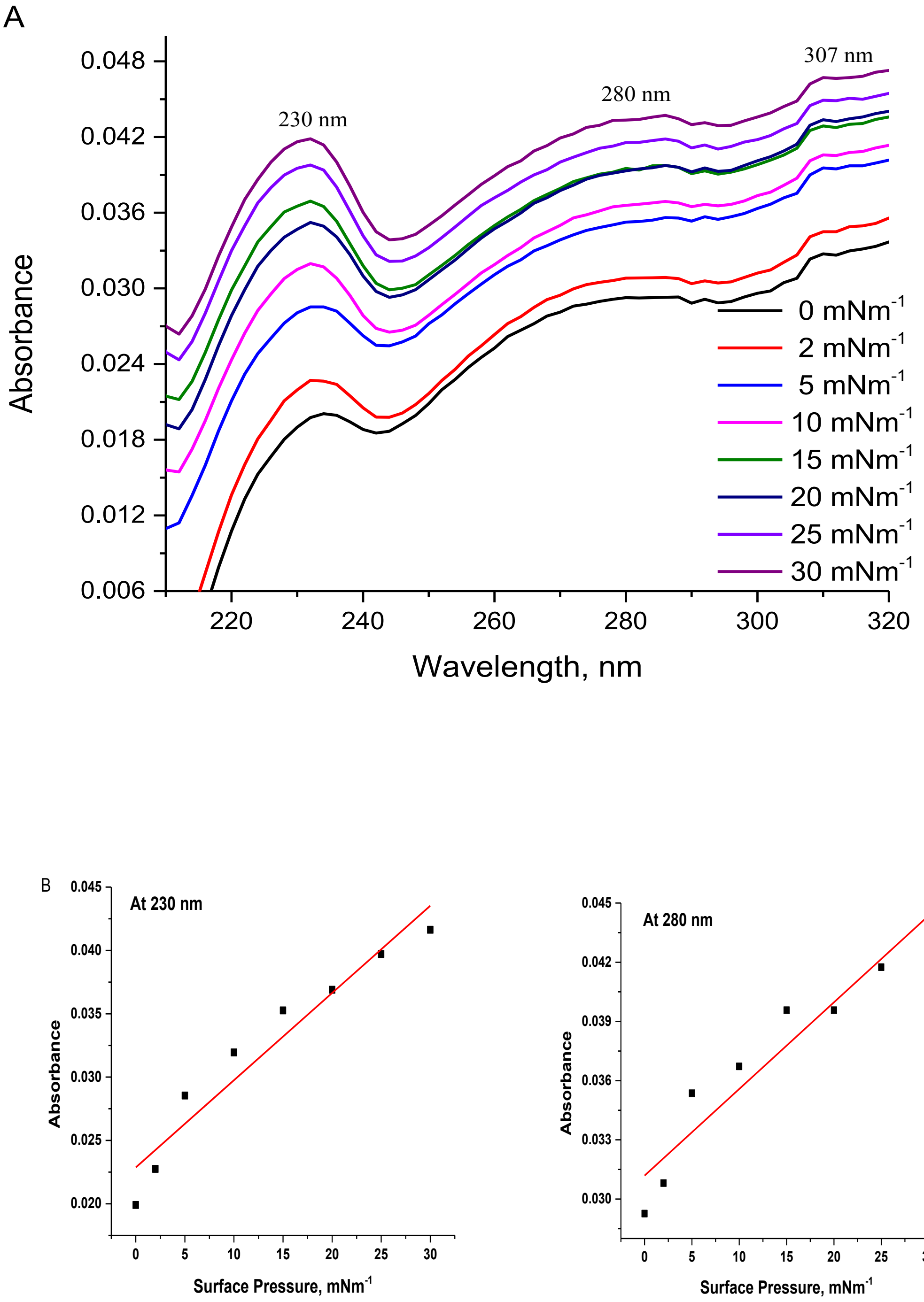

Figure 5.5: UV-vis absorption spectra of the CTB Langmuir monolayer on citrate phosphate buffer (pH 5.5) (A) and plot of absorbance versus surface pressure at 230 and 280 nm wavelengths (B).

On plotting the absorbances and surface pressures, a linear relationship was established at two different wavelengths, viz., 230 and 280 nm, respectively. The slope was approximately same for two different plots. This observation reinforces the interpretation that the protein was retained at the interface. The increase in surface pressure leads to the increase in the absorbance at the band maximum. This is because, while increasing surface pressure due to the compression of the monolayer it ultimately increases the number of molecules per unit area. The absorbance obtained at 0 mNm^{-1} is due to the presence of CTB Langmuir monolayer. This also highly signifies the stability of the monolayer because if the monolayer was unstable, we would not get increase in absorbance intensity but rather would have ended at a plateau as CTB molecules are compelled to discharge into the subphase.

5.3.4 Fluorescence of Langmuir Monolayer

From the *in situ* UV-vis experiments, it was clear that the CTB Langmuir monolayer was appreciably stable. The higher peaks at 230 and 280 nm relates the increase in tyrosine and tryptophan absorbance while CTB monolayer is achieving rigidity at higher surface pressure. As tryptophan has higher absorbance intensity than tyrosine, *in situ* fluorescence spectroscopy (**Figure 5.6**) was also predominated by the tryptophan emission at 350 nm.[144] The figure shows that the dominancy of tryptophan emission was achieved from the gaseous phase to the solid/condensed phase which actually corresponds with the observation achieved from absorbance data at similar surface pressures.

Furthermore, we were surprised to see the negligible impact of blue-shift as seen in DPPC[145] and β-galactosidase.[146] Blue shift occurs altering the absorbance maxima and emission maxima but we achieved the absorbance and emission at 280 and 350 nm, respectively which suggests that the CTB molecules were minimally affected by the subphase molecules.

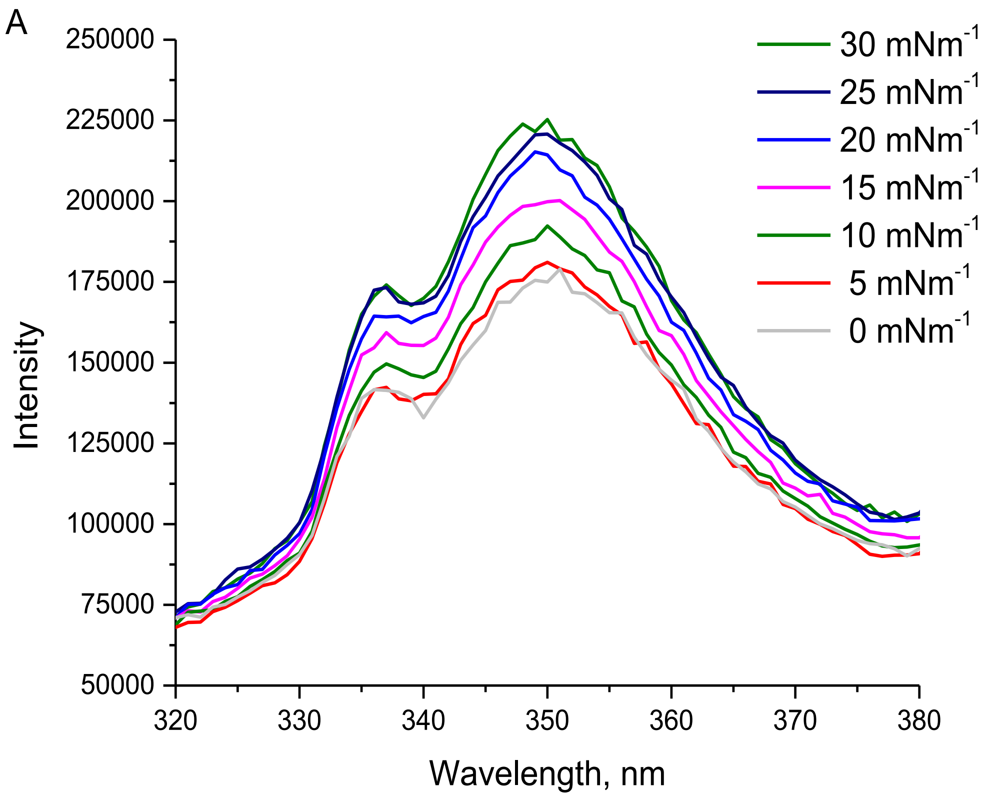

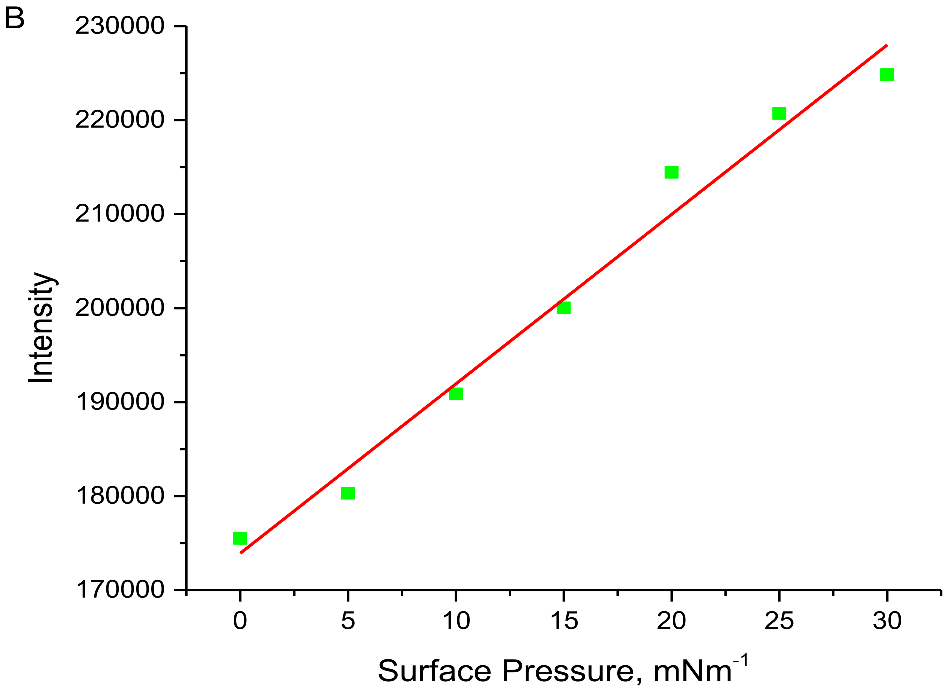

Figure 5.6: *In situ* fluorescence spectra at air-subphase interface of the CTB (1.7×10^{-5} M) Langmuir monolayer (A) and the plot of maximum emission at 350 nm as a function of increasing surface pressure (B).

We were also appealed about the possibility of loss of analyte from the monolayer after the completion of maximum compression. So, we measured fluorescence intensity of the solution directly withdrawn from the subphase after two hours of waiting time in every 15 min intervals up to three hrs (**Figure 5.7**). We observed that there was slight decrease in intensity which might be associated to: i) the solubilization of protein, ii) the aggregation of protein, and iii) the impact of wait time on the intensity of light. From the stability curve, we can outstrip the first point. On performing UV-vis at air/subphase interface for the CTB monolayer the increase in absorption maxima after several rounds of experiment also justifies our hypothesis that the decrease in intensity is not due to the solubilization of protein. The decrease in intensity observed could be due to the slight aggregation of CTB at the monolayer or due to impact of waiting time on the intensity of light.

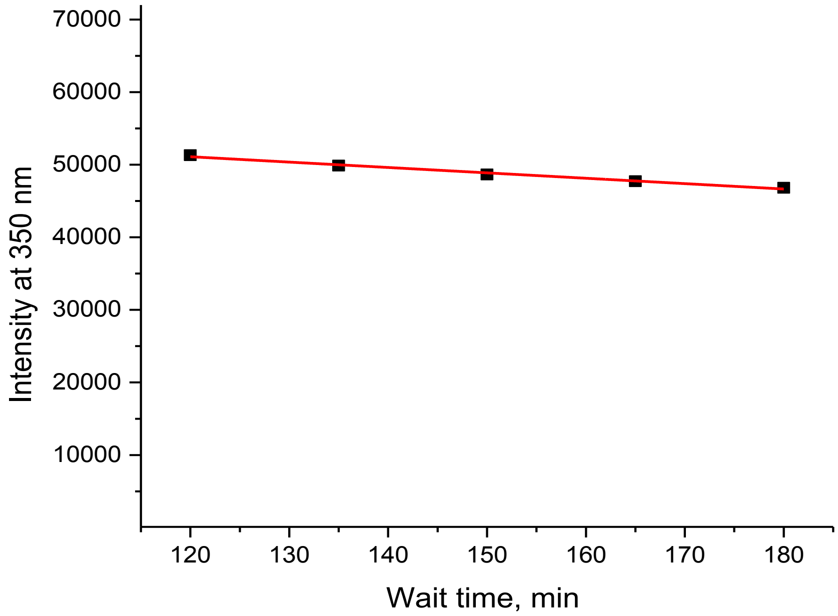

Figure 5.7: The plot of fluorescence intensity vs time of wait of the CTB Langmuir monolayer.

5.3.5 Infrared Reflection Absorption Spectroscopy (IRRAS)

Knowing that fact that there was slight decrease in intensity while performing fluorescence spectroscopy (of solution) obtained by withdrawing little amount of subphase from the trough, we had a doubt that it might be due to the modest aggregation of CTB molecules. To confirm this, we performed IRRAS experiment. The surface selection rule for IRRAS measurement technique is that when the angle of incidence is higher than Brewster's angle of the substrate, the surface parallel (*p*) component of a transition moment yields positive peak and vice-versa.[147] The Brewster's angle for air-water interface is 53° and for the air-subphase that we have used should have lower Brewster's angle (approx. 50°). **Figure 5.8 (a)** shows the normalized *p*-polarized IRRAS spectra of the CTB

Langmuir monolayer at a surface pressure of 15 mNm^{-1} with different incident angles which is in accordance with the surface selection rule. **Figure 5.8 (b) and (c)** exhibits the *p*-polarized IRRAS spectra of CTB for different surface pressures at an incident angle of 60°. We chose this angle as it showed high signal to noise ratio. While examining amide I region (1700-1600 cm^{-1}), amide II region (1600-1500 cm^{-1}) and even amide III region (1400-1300 cm^{-1}), we found that none of the bands were shifting while increasing surface pressure. The peak at 1651 cm^{-1} resembles α-helix (amide I) predominantly due to the C=O (symmetric) and C−N stretching of amide group whereas the peak at 1627 cm^{-1} and 1685 cm^{-1} is due to antiparallel β-sheet.[148] The peak at 1700 cm^{-1} specifies β-turn and antiparallel β-sheet basically due to the absorption from turn and transition dipole coupling in anti-parallel β-sheet.

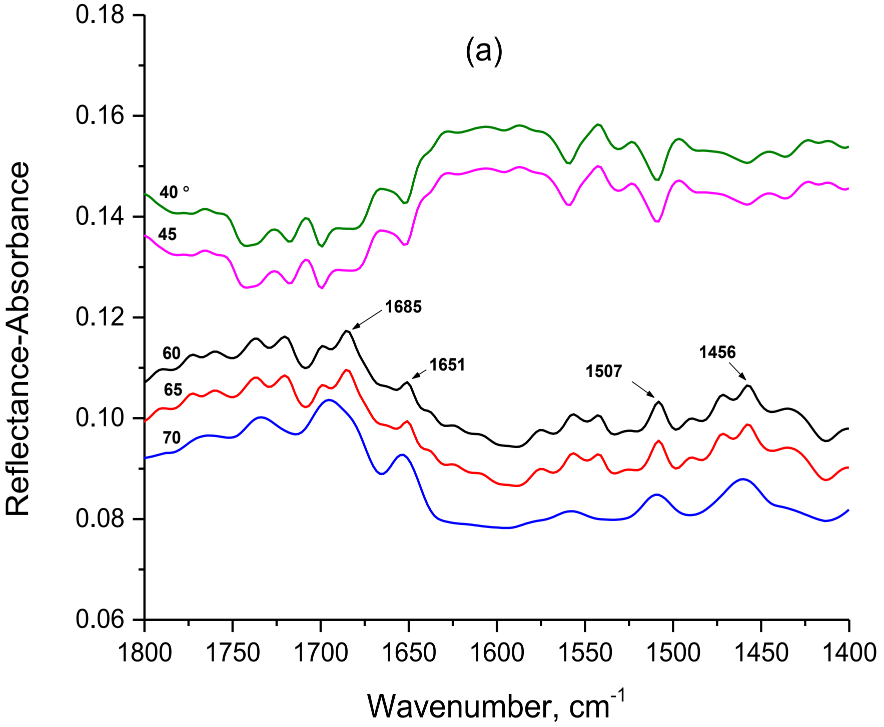

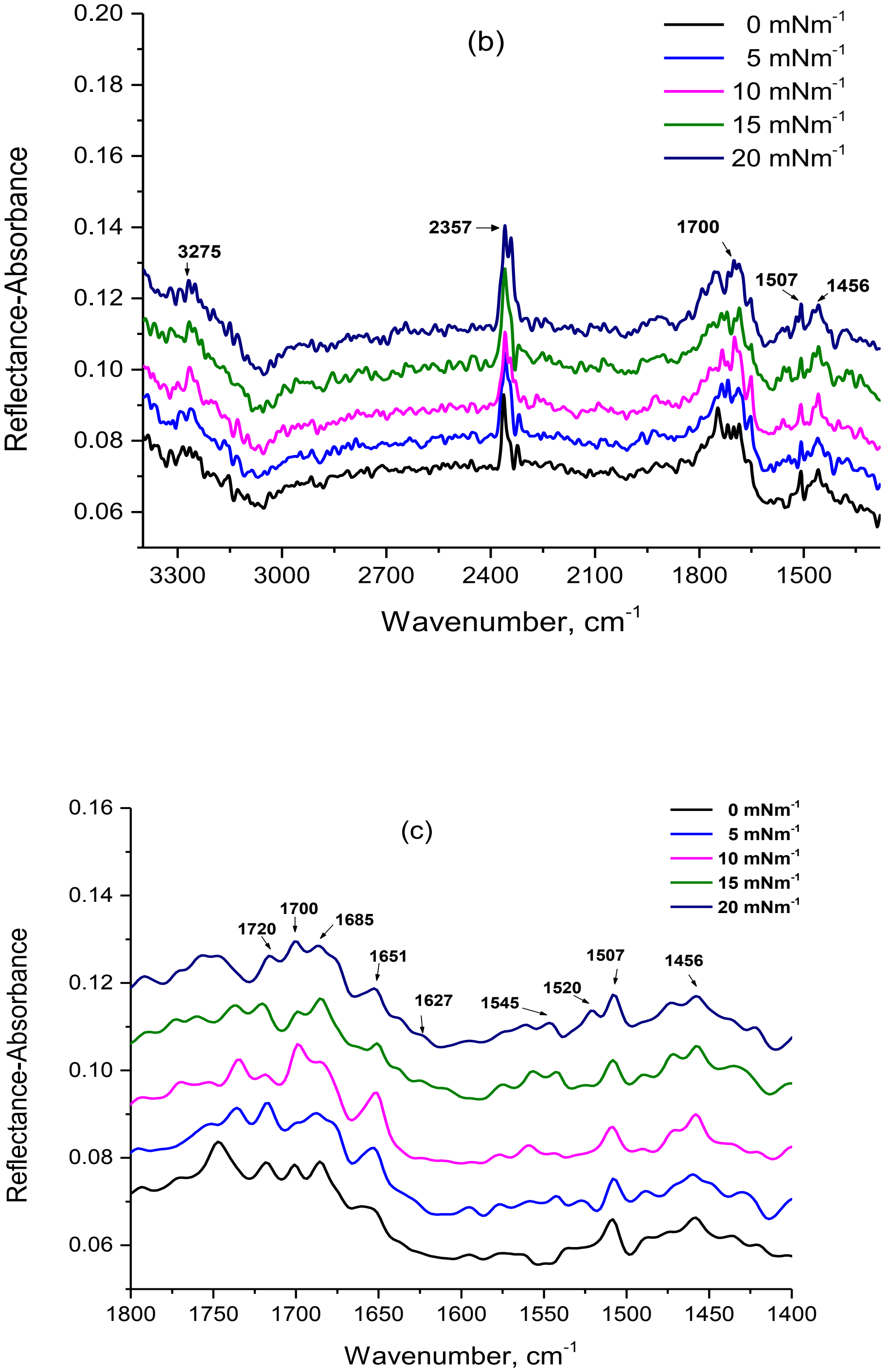

Figure 5.8: Normalized *p*-polarized IRRAS spectra of the CTB Langmuir monolayer: (a) at a surface pressure of 15 mNm^{-1} with different incident angles, (b) comparison of spectra for different surface pressures at an incident angle of 60°, and (c) expanded spectra to show the amide I and II region clearly.

The band observed at 1545 cm^{-1} is due to α-helix (amide II) which arises via the N−H bending (60%) and C−N stretching (40%). The C−H stretching peaks are found in the range of 2800-3000 cm^{-1} and C−O peaks are observed around 1200 and 1300 cm^{-1} whereas the band at 1720 cm^{-1} is due to C=O stretching vibration.[149] The peaks from 3400-3250 cm^{-1} resemble the N−H stretch due to primary and secondary amines. The band at 2357 cm^{-1} is due to CO_2, typically this is significant if the air-subphase is not covered or if covered there is not sufficient nitrogen flow to reduce CO_2 peak. The band at 1456 cm^{-1} could not be assigned. As expected, the band positions at amide I region exhibited the dominancy of β-sheet in the secondary structure of CTB due to the crystalline structure of the molecule.[129] Having seen that no bands are changing appreciably, it was evident that there was no denaturation or aggregation of the CTB molecules on the subphase of citrate phosphate buffer. Furthermore, intensities of bands remaining almost constant at various surface pressures indicate that the amide chains are oriented parallel to the air-subphase interface. Hence, it confirms that the slight decrease in fluorescence intensity was due to the waiting time impact i.e., the intensity of the fluorescence light may decrease during the experiment, which results in decrease in fluorescence intensity.

5.4 Summary

In this chapter, we studied the interfacial property of CTB and found that CTB reproducibly forms a highly stable Langmuir monolayer. We also revealed that there was insignificant impact of blue-shift during the *in situ* spectroscopic studies of CTB molecule which suggests that the analyte was not affected by subphase molecules at all. Besides this, CTB remained active on the monolayer and no aggregation was observed which fits this molecule in diverse pharmaceutical applications because exploring of biological reactions at surfaces is necessary after the development biomaterials for medicals implants like, blood-serum contact devices, and intraocular instruments. In this perspective, the biocompatibility of an analyte is directly related to the surface properties of the substance. For instance, whenever a toxin meets the blood then rapid adsorption of proteins occurs on its surface known as nonspecific protein adsorption. This adsorbed protein on the surface determines the platelets adhesion, that enacts a prime capacity in thrombogenesis and to prevent this various surface modification should be performed. Hence, the investigation of CTB surface property will help in identifying myriad surface modification techniques. In addition, it makes easier in assimilating the surface chemistry behavior of this 'benign' toxin in development of a biosensor, microfluidic devices, to study cell adhesion, to understand the property of transmembrane receptors, and acts as a model system representing cell membrane environments. Based on the results of surface chemistry and spectroscopic studies in this chapter, the lipid-subphase interfacial layer which is similar to the air-water interface is indicated to play an important role to drive the CTB to cell membrane. On the other hand, the role of lipid-subphase interfacial layer in the aggregation of CTB to form pentamer ring can be neglected.

Chapter 6

Surface Chemistry and Spectroscopic Study of Fumonisin B1 and Impact of Green (525 nm) Irradiation on its Langmuir Monolayer

6.1 Background

Fungal keratitis is a sight-threatening ocular disease caused by the incursion of fungi.[150] Fungal infections of the cornea can be caused by filamentous or yeast-like fungi.[151] Among different filamentous fungi *Fusarium* species are most widely linked with keratitis.[152] These species produce toxins called fumonisins. Fumonisins are a group of mycotoxins produced by fusarium species.[153] These are taxonomically challenging mycotoxins which consist of a linear carbon backbone substituted at various positions with hydroxyl, methyl and tricarboxylic acid groups.[154] In contrast to the most familiar mycotoxins, which are soluble in organic solvents, fumonisins are mostly hydrophilic. Due to these characteristics, it makes them difficult to study. These fumonisins are mostly responsible for esophageal cancer and keratitis.[155] The International Agency for Research on Cancer (IARC) has assessed the cancer probability of fumonisins to humans and classified them as group 2B.[156] Fumonisins are usually extracted in aqueous methanol or aqueous acetonitrile.[157,158] Among different fumonisins, we are interested in Fumonisin B1 (FB1), shown in **Figure 6.1**, as this molecule is the most prevalent of the fumonisins in naturally contaminated corn and is usually present as 70% of the total fumonisins detected.[159]

From past, there has been a serious challenge in the proper treatment of fungal keratitis due to the sensitivity of the visionary organ. Several methods like keratoplasty[160], corneal cross-linking[161], antifungal medication[162-163] have experienced different setbacks.[152, 164] In this perspective, the photodynamic therapy has been regarded as the most safest method in the treatment of keratitis.[165-166] In our previous study, we first treated the cornea with Rose Bengal, a photosensitizer and later green light was applied to degrade the actual fungus. We found that green light alone has no effect on the fungus.[167-168] As green light is part of the visible spectrum and part of all indoor illumination fixtures (incandescent, fluorescent, LED, etc.) produce green light, patients wouldn't have corneal perforation due to fumonisin: simply opening one's eyes would allow "green-light" to reach the cornea! Inspite of this, our Langmuir monolayer work showed that the toxin produced by fungus (FB1) gets somehow mortified due to the application of green LED light continuously within certain intervals. This ultimately opens new avenues in the treatment of fungal keratitis.

Furthermore, the study of interaction between invading fungi and host cells is important in the study of fungal keratitis.[169] Adherence is the main mechanism by which this interaction occurs. Fungal infections begin with adhesion of pathogenic fungal cells to the damaged cornea. This adhesion is mediated by adhesins present on the surface of the fungi. Fungal pathogens have a variety of adhesins that can interact with native cell proteins and glycoproteins.[170] Surface chemistry study is powerful tool to mimic the interaction of analyte with the cell membrane.[106] Further, surface chemistry study approach via Langmuir monolayer technique facilitates the study of cell adhesion and its implications. This is very important as most mammalian cells are adherent. Saying so, the surface chemistry study of FB1 (**Figure 6.1**) will provide sufficient information about the interaction of this toxin with the host cell. We chose FB1 among the family of toxins, known as fumonisins as it is the most prevalent member of this family.

This chapter not only deals with the surface chemistry and spectroscopic study of the FB1 Langmuir monolayer to interpret process of interaction of the toxin with the cell membrane but also, provides the impact of green LED (525 nm) on the FB1 Langmuir monolayer. We are aware of the fact that LEDs do not produce energy at a single wavelength (as lasers do). The green LED we selected emits light over a certain bandwidth, the 525 nm LED emission curve show the LED 20% energy values being between 500 to 550 nm. To the best of our knowledge, the impact of light on the FB1 Langmuir monolayer remains unknown till now. Further, to our astonishment, the aqueous methanol solution of FB1 also showed the changes in the band positions of absorption, emission, and mass spectra which suggests that the toxin structure partly gets degraded with the continuous application of green LED light. We hope that this investigation will help in the perusal of customary treatment of fungal keratitis.

In this chapter, our main aim was to study the surface chemistry and spectroscopic property of FB1 molecule and observe the impact on structure of FB1 by treating the Langmuir monolayer of FB1 with green LED light. From the surface chemistry and spectroscopic study, we found that FB1 molecule forms self-assembled Langmuir monolayer sufficient to mimic its interaction with the corneal tissues. The irradiation of green LED light on the FB1 Langmuir monolayer showed that the rate of desorption of the analyte increases as compared to the absence of light. This reveals that FB1 molecules lose their tendency to stay as Langmuir monolayer due to the change in its conformation. To further confirm this observation, the FB1 solution was treated with LED light and its UV-vis, fluorescence, and mass spectra showed the change in band positions which reinforces our Langmuir monolayer observation.

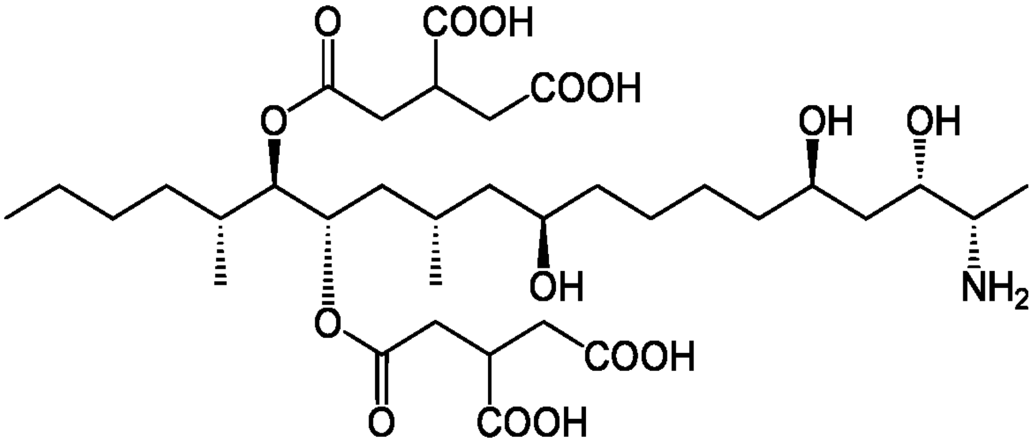

Figure 6.1: Structure of Fumonisin B1 (FB1).

6.2 Experimental

6.2.1 Materials and Reagents

Fumonisin B$_1$ extracted from *Fusarium moniliforme* > 98% (HPLC) was obtained from Sigma-Aldrich, Co., St. Louis, MO, USA. The water that was utilized in the experiments was obtained from PURELAB Ultra, Elga Lab Water (Veola Water Solutions and Technologies, U.K.) with a resistivity of 18 MΩ cm, a surface tension of 71.6 $mN \cdot m^{-1}$, and a pH of 7.4. Methanol required to dissolve FB1 was received from M.P. Biomedicals LLC, Santa Ana, CA, United States.

6.2.2 Equipment

All experiments were carried out in a Clean Room (class 1000) in which the temperature (20.0 ± 0.5 °C) and humidity (50% ± 1%) were maintained constantly. In the study of surface pressure−area (π−A) isotherms, and compression−decompression cycles, a Kibron μ-trough (Kibron Inc., Helsinki, Finland) having area of 124.5 cm^2 (5.9 × 21.1 cm) was used. The Wilhelmy method was employed to assess the surface pressure with a

0.51 mm diameter alloy wire probe having a sensitivity of ±0.01 mN·m^{-1}. For the *in situ* UV-vis experiment, we used a KSV mini-trough (KSV Instrument Ltd., Helsinki, Finland) having an area of 225 cm^2 (7.5 × 30 cm).

6.3 Methods

6.3.1 Surface Pressure-Area Isotherms Preparation

The aqueous methanol (1:5, w/v) dissolved FB1 was diluted with pure water to achieve a concentration of 2.8 × 10^{-4} M (0.2 mg.mL^{-1}) and pH 7.4. The pH of 7.4 was chosen to equilibrize the pH of human corneal stroma[171]. The FB1 was uniformly spread over the air-water interface by the use of a 100 μL syringe (Hamilton Co., Reno, Nevada). The spreading volume of the toxin solution was 45 μL for the surface chemistry and spectroscopic measurements. After the solution was spread, the Langmuir monolayer was allowed to accomplish the equilibrium state for approximately 12−15 min. Then, the Langmuir monolayer was compressed at a rate of 12 Å^2·molecule^{-1}·min^{-1} such that the compression process is complete in around 10 min to maintain the consistency in the experiments. The experiments were rehearsed for three times, and good reproducibility was achieved. The reason behind employing the Kibron μ-trough for the surface pressure and compression/decompression experiments; and the KSV trough for *in situ* UV−vis experiments is that the KSV trough provides plenty of space to continually relocate the UV−vis machine parts as compared to the Kibron trough.

6.3.2 UV-vis Absorption Spectroscopy

The UV−visible absorption spectra of the FB1 Langmuir monolayer at the air-water interface was measured by a UV−visible diode array spectrophotometer (Hewlett-Packard, model 8452A, Palo Alto, CA) on the top of a KSV mini Langmuir trough (KSV

Instruments Ltd., Finland). A quartz window is fitted in the middle of the trough to facilitate the beam to pass through the Langmuir monolayer and the water subphase. The spectra were obtained initially at 0 and 1 mN.m^{-1} and at every 5 mN.m^{-1} surface pressures increment onwards under dark environment up to 20 mN.m^{-1}.

6.3.3 Fluorescence Spectroscopy

The *in situ* fluorescence spectra of the FB1 Langmuir monolayer was measured with the help of an optical fiber detector stationed on the top of the KSV trough. The optical fiber was coupled to the Spex Fluorolog (Horiba, Jovin Yvon, Edison, NJ). The optical fiber used in the experiment had an area of 0.25 cm^2 and rested approximately 1 mm above the air-water interface. Initially, the excitation light gets transmitted through the optical fiber from the light source to the Langmuir monolayer and at the same time the emitted light from the monolayer gets dispatched back to the detector through the optical fiber. This is how the data gets collected.

6.3.4 Compression-Decompression Cycles

To study the hysteresis of the film formed, the Langmuir monolayer of FB1 was first compressed from 0 to 15 or 23 mNm^{-1} and decompressed subsequently to 0 mN/m with a speed of 12 Å^2.molecule^{-1}.min^{-1}. This compression-decompression procedure was then repeated three times to reproduce the data.

6.3.5 Solution Work

Ultraviolet-visible spectroscopy measurements were obtained on an Agilent Cary 100 spectrophotometer (Santa Clara, CA, USA). The fluorescence spectra of the FB1 solution with and without treatment of light was measured with the help of the Spex Fluorolog (Horiba, Jovin Yvon, Edison, NJ) having the slit width of 5 nm for excitation and emission. The mass spectra were obtained from Bruker BioFlex IV Maldi-TOF mass spectrometer.

6.4 Results and Discussion

6.4.1 Surface Chemistry Study

6.4.1.1 Surface Pressure vs Area Isotherm

Fumonisin B1 when spread on the water subphase showed that it has capability to form a stable Langmuir monolayer. **Figure 6.2** exhibits the surface pressure (π) versus mean molecular area (A) and surface tension curve for the monolayer.

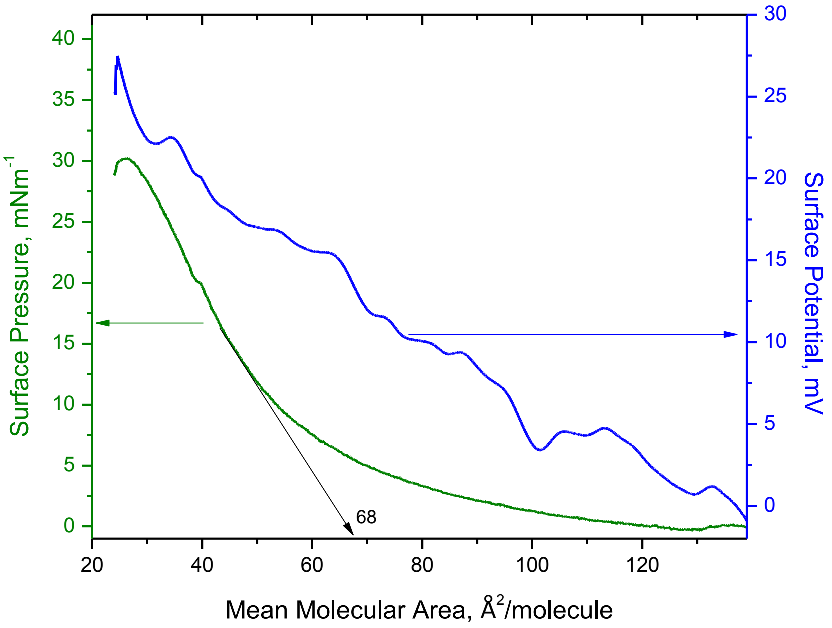

Figure 6.2: Surface pressure (π)- area (A) and surface potential curve of Fumonisin B1.

It is well known fact that the air-water interface possesses an excess free energy emanating from the difference in environment between the surface molecules and those in the bulk. The spontaneous formation of Langmuir monolayer when FB1 is placed on a liquid surface affects the surface tension. This surface tension can be viewed as a negative pressure due to the attractive interactions of the water molecules at the interface, which will be lowered by accumulation of the fumonisins at the air-water interface. The presence of a monomolecular film on a liquid surface invariably results in a reduction of the free energy of the system due to the creation of interactions between the hydrophilic polar group and the water surface molecules, thus reducing the surface tension. The resulting effect of the reduction of the surface tension leads to an expansion of an air-water interface in the presence of surfactants. The π-A isotherm measurement is the initial step to investigate the new materials spread on the subphase which provides insights of existence of different phase transitions, packing, and the stability of Langmuir monolayer which ultimately acts as a model for studies of the interaction of the toxin, FB1 with the cell membrane of cornea.

A surface potential measurement was carried out simultaneously with the surface pressure measurement to know the dipole moment or potential of the monolayer above and beneath the monolayer. This measurement indicates a molecular interactions that might be related to phase change. Moreover, it is helpful to know the role of electrostatically charged FB1 molecules in the biological process. In the figure, there is an immediate increase in surface potential in the gaseous phase, which is due to the change in dipole moment due to compression, stipulating that surface dipole forces and the orientation of water (subphase) molecules convicts a net interfacial orientation. The small bumps seen in the surface potential curve are due to the movement of FB1 molecules to gain a specific orientation on the subphase surface under the vibrating electrode. After attaining the condensed phase, we observed a decrease in the surface potential. This is due to the cancellation of the dipole–dipole moment due to the short distance.

In the π-A isotherm, the limiting molecular area of fumonisin B1 Langmuir monolayer is 68 Å^2.molecule^{-1} as shown in **Figure 6.2** that describes the minimum cross-sectional area per molecule. This value corresponds to the size of the FB1 molecule at air-water interface to be 4.6 Å which is pretty close to the theoretical value of 5 Å as shown in **Figure 6.3** obtained by a computer program for modeling, simulation, and docking; YASARA[142].

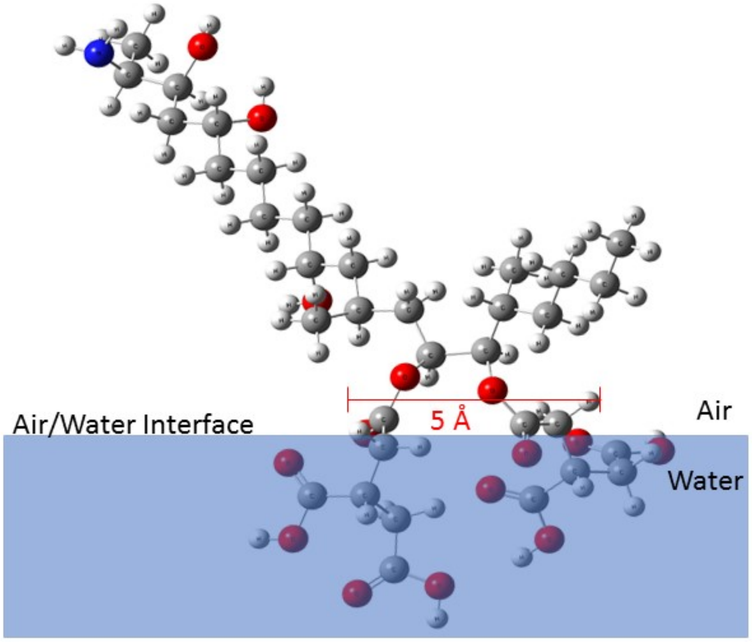

Figure 6.3: Simulation of FB1 molecule at the air-water interface to calculate its size.

6.4.1.2 Compression-Decompression of FB1 Langmuir Monolayer

The examination of the resistance of the FB1 Langmuir monolayer to external mechanical force at the air-water interface was performed by using compression−decompression cycles. **Figure 6.4** shows the three compression−decompression cycles of the FB1 Langmuir monolayer at the air−water interface at two different surface pressures viz. 15 and 23 mN.m^{-1}.

As FB1 is a most polar molecule in comparison to other fumoinsins[172], our hypothesis was that some sort of hysteresis phenomena could be noticed for the FB1 Langmuir monolayer as opposite charges of polar molecule attract and alike charges repel. As per our hypothesis, for the successive three compression/decompression cycles that followed, it was found that a hysteresis behavior of the isotherm was witnessed. These cycles divulge that when compressed to 15 mN.m^{-1}, there is small hysteresis due to the fact that a compact monolayer has not been formed yet. It has been found that only 8.0% of the initial isotherm has been reduced in comparison of the first and last cycle, whereas 23 mN/m only exhibit hysteresis difference of 11.0%. These results show that FB1 molecules reorganize at the interface while the water subphase contributes to this process. Beside the solubility of FB1 in the subphase, other possible explanations might be the alteration in the orientation and conformation of the toxin with time. This observation compression-decompression fortifies that the FB1, a toxin molecule remains somehow active as Langmuir monolayer which underpins the interaction of toxin and cell membrane model.

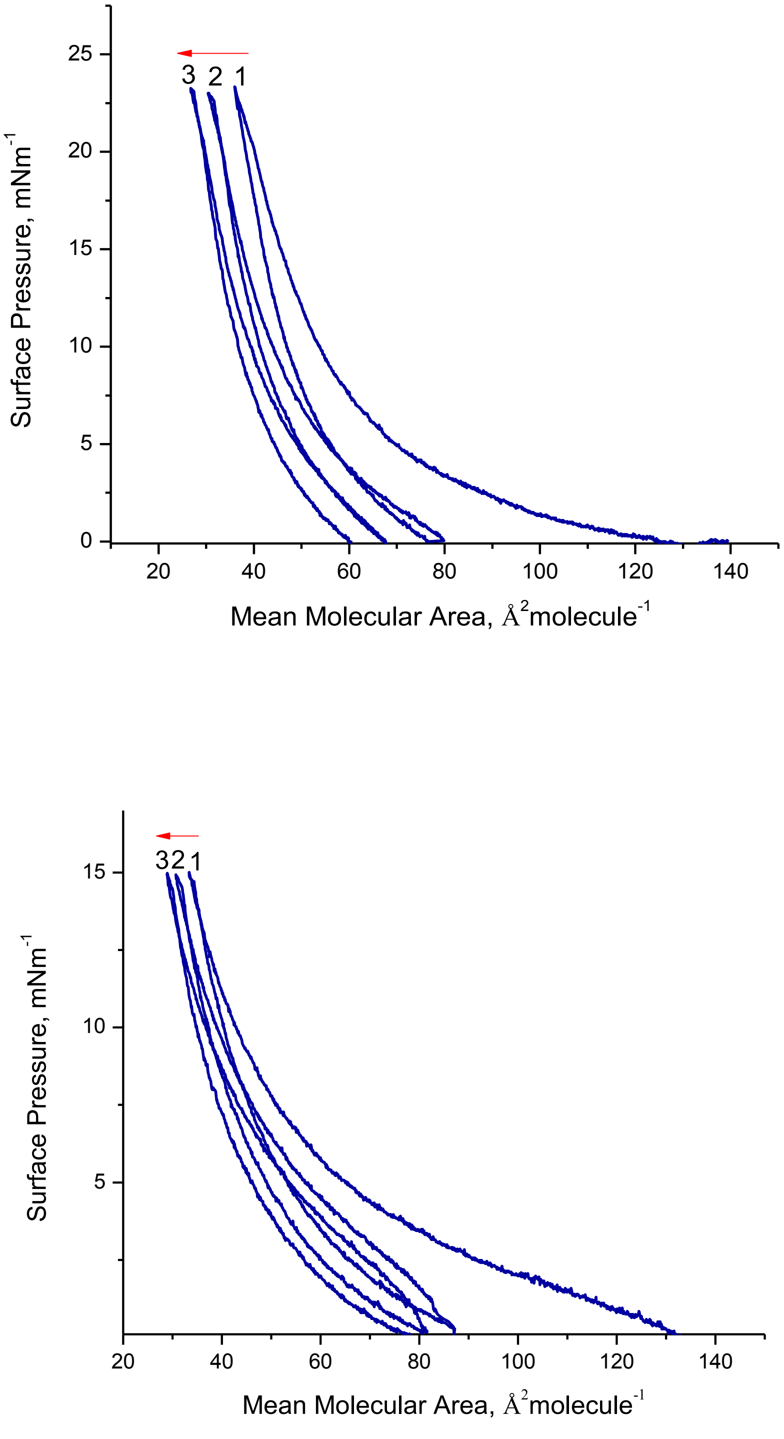

Figure 6.4: Compression-decompression π-A curves at two different surface pressures (15, 23 mNm^{-1}).

6.4.1.3 In situ UV-vis Absorption Spectroscopy of Langmuir Monolayer

From the compression-decompression data, we found that the isotherm at higher surface pressure promulgates the hysteresis behavior. This hysteresis behavior could be minimized and the stability could be increased by the addition of an electrolyte into the subphase.[105, 173] But we wanted to create the similar *in vivo* conditions as of the cell membrane to fit our model. So, we decided to perform *in situ* UV-vis absorption experiment without addition of extra electrolyte. The absorption spectra at different surface pressures were recorded for the FB1 Langmuir monolayer as shown in **Figure 6.5**. Two different bands at 233 and 278 nm were observed. The maximum band at 233 nm corresponds to the n-π* transition of the carboxylic group which are abundantly present in the FB1 molecule. The band peak at 278 nm could not be assigned. This could possibly be due to the formation of intermolecular hydrogen bonding among the oxygen molecule of FB1 and hydrogen molecule of the water subphase. With the compression of the monolayer to higher surface pressures, the intensity of the absorbance increased proportionally. While plotting the surface pressure vs absorbance at 233 and 278 nm, we found that absorbance increases proportionally with the surface pressure within the experimental error as shown in **Figure 6.6**. The slopes of the curves were also almost equal to each other. This observation confirms that the formation of homogenous FB1 Langmuir monolayer at the air-water interface before the monolayer attains the collapse surface pressure. Moreover, it also gives idea of the stability of the monolayer. If monolayer was unstable, the absorbance would not increase steadily rather reach a plateau as molecules are forced to submerge into the water subphase.[47]

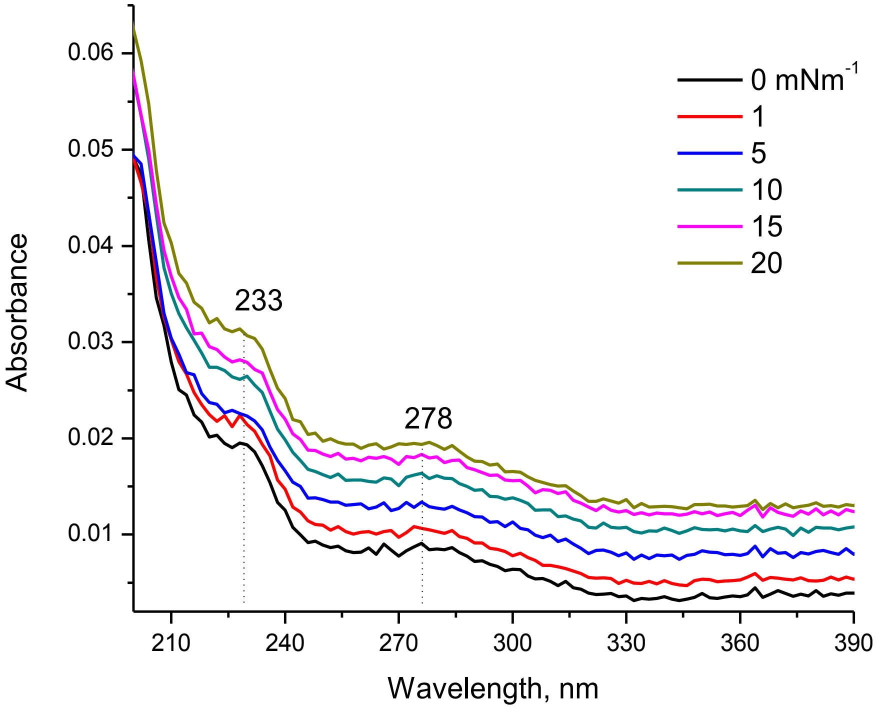

Figure 6.5: *In situ* UV-vis spectra of FB1 Langmuir monolayer at different surface pressures.

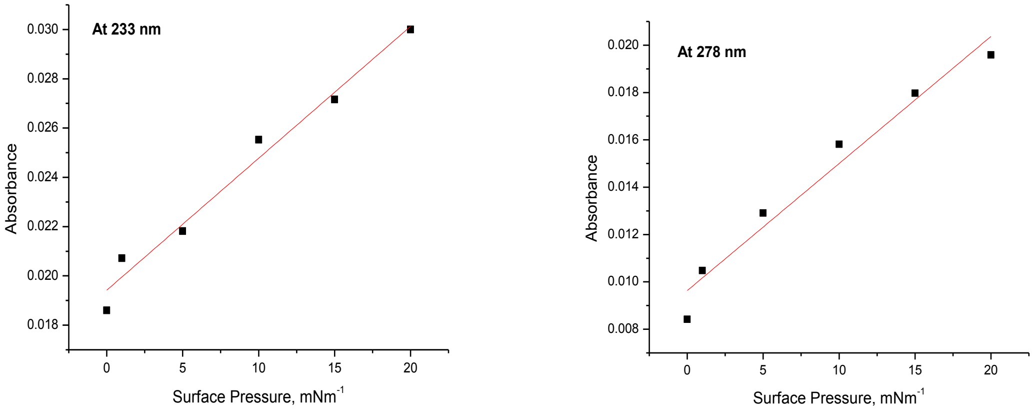

Figure 6.6: Plot of absorbance vs surface pressure at two different wavelengths viz. 233 and 278 nm.

6.4.1.4 In situ Fluorescence Spectroscopy of Langmuir Monolayer

From *in situ* UV-vis spectroscopy, the homogeneity and the stability of the FB1 Langmuir monolayer was also observed.

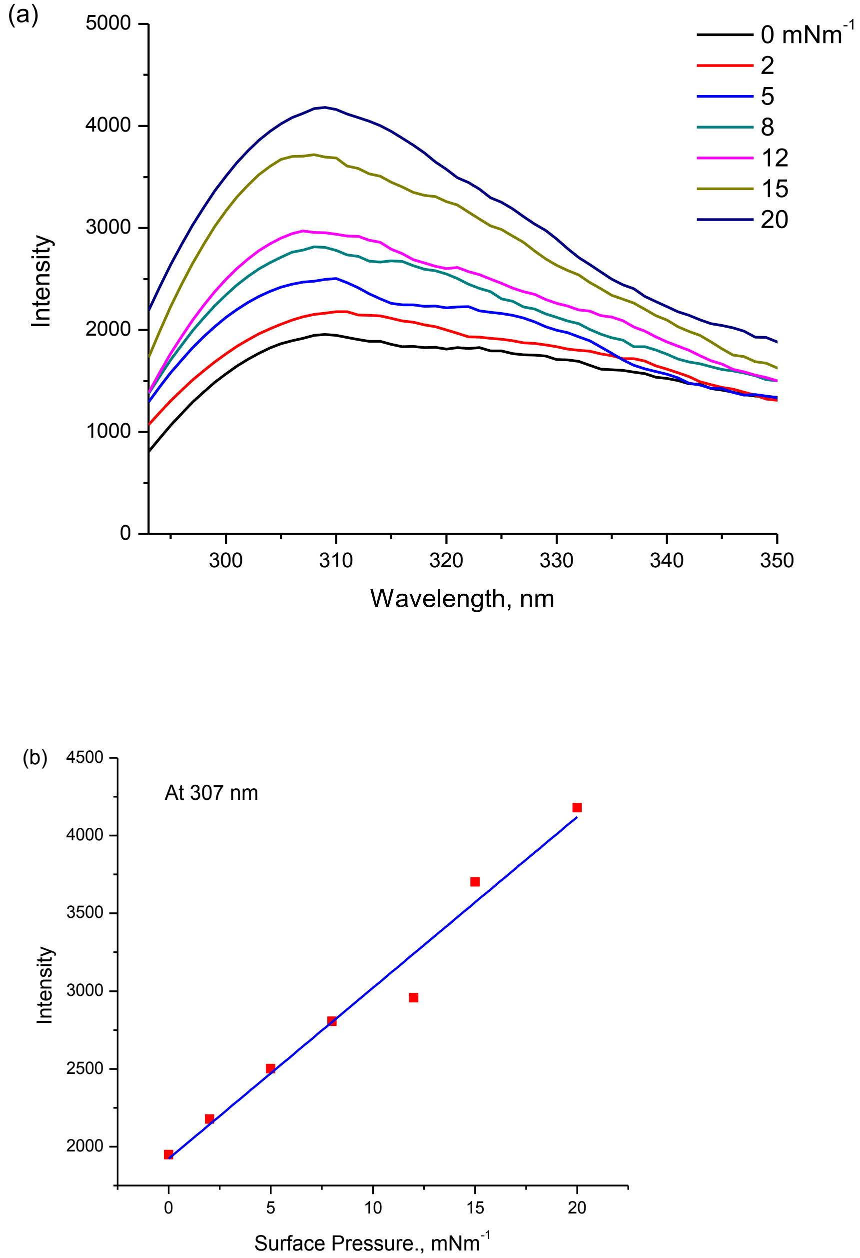

Figure 6.7: *In situ* fluorescence spectra for the FB1 Langmuir monolayer at different surface pressures (a) and plot of intensity vs surface pressures at 307 nm (b).

To confirm this finding, we performed the *in situ* fluorescence spectroscopy of the monolayer as shown in **Figure 6.7 a**. Further, we obtained a linear relationship (**Figure 6.7 b**) by plotting intensity versus surface pressure at 307 nm. This investigation ruled out the hypothesis of loss of analyte in the water during the formation of the Langmuir monolayer.

6.5 The Effect of LED Light on the FB1 Langmuir Monolayer

To study the impact of green light on the Langmuir monolayer of FB1 molecules, an experimental setup was build up as shown in **Figure 6.8**. For this study, the monolayer was compressed to 25 mN.m^{-1} and was kept still without further compression. The green LED light (525 nm) placed approximately 2 mm above the monolayer irradiated the Langmuir monolayer continuously for 5 min and the decrease in surface pressure was recorded with respect to time. **Figure 6.9** shows the difference in the decrease of the surface pressure in absence and presence of green light. It was found that almost 37% decrease in surface pressure was observed while comparing the absence and presence of green LED light. This decrease in surface pressure clearly demonstrates that the toxin is highly solubilized into the water subphase while irradiating with the green LED light. The sinking of toxin into the subphase can be either due to change in structure and/ or configuration which can be explained as the result of degradation of the toxin.

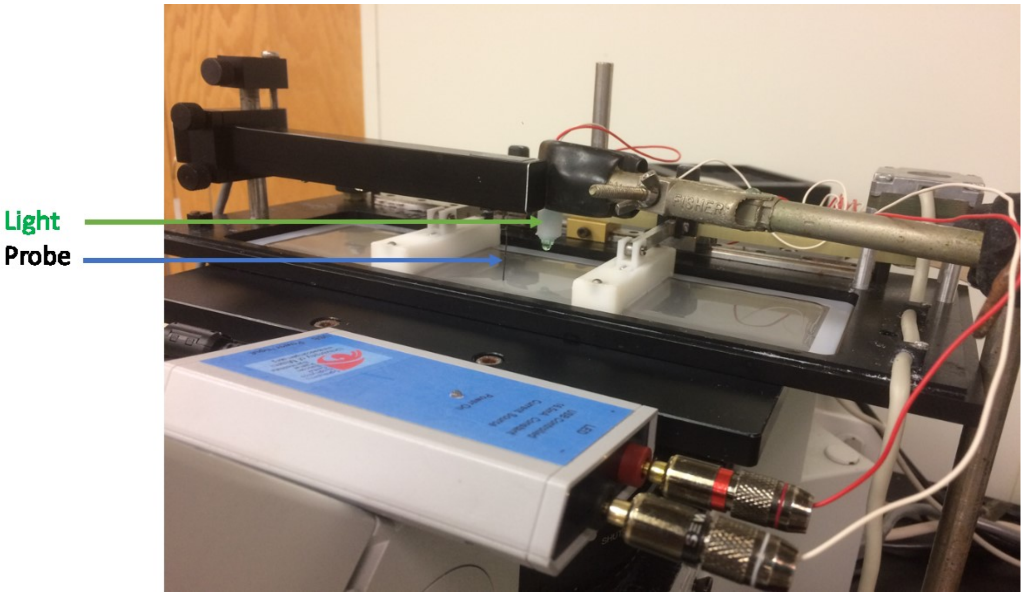

Figure 6.8: Kibron trough experimental setup with the adjusted green light source to study the effect of light on the FB1 Langmuir monolayer.

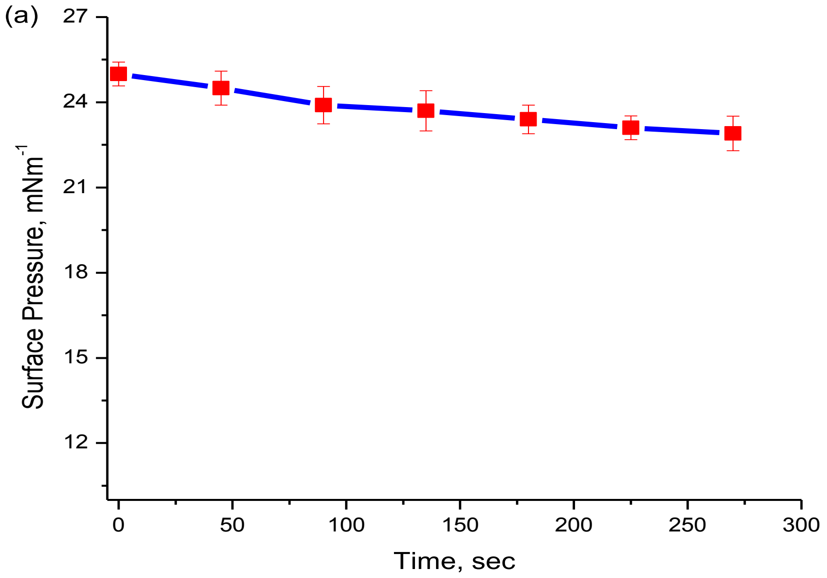

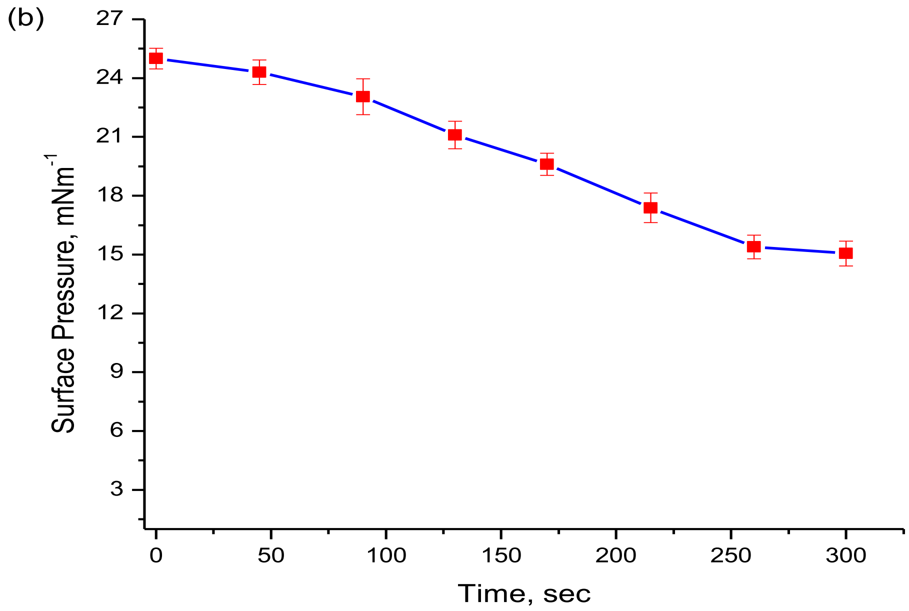

Figure 6.9: Surface pressure vs time shows the drop of surface pressure in absence (a) and presence (b) of green LED light. Magnitudes of error bars are calculated as the standard deviation from three experiments.

6.6 Comparative Study of the Effect of 525 nm LED Light on the FB1 in Solution Phase

After observing the degradation of FB1 Langmuir monolayer under the green LED light irradiation it was important to compare this result to FB1 in solution. For this, we carried out the experiment in which fluorescence spectrum was recorded. In this method, FB1 was irradiated with green light for 20 seconds in the intervals of 5 min for a total of 70 mins. **Figure 6.10** shows the photoluminescence spectra of FB1 before and after the treatment to the green LED light. We can clearly see that there is significant decrease on the photoluminescence of FB1 after irradiation with green light. We also observed a shift of the maximum peak from 370 to 359 nm. The intensity maxima decreased by 38% after 70 min. In the meantime, we can also see that there is evolvement of another new peak centered at 343 nm. This clearly shows that the green LED light has degraded the FB1 molecu

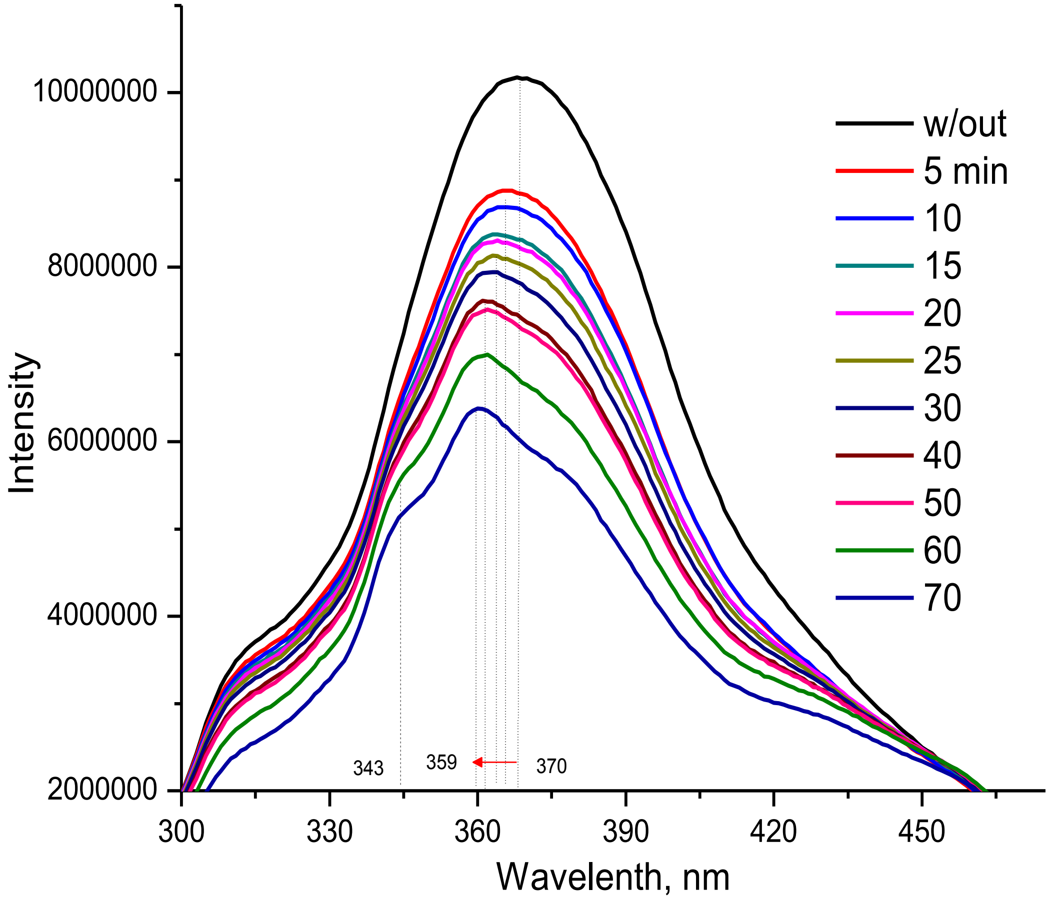

Figure 6.10: Photoluminescence spectra of FB1 (2.8×10^{-4} M) in aq. methanol (1:5; v/v) before and after irradiation with green LED light (optical path length 1 cm).

To further confirm the degradation of FB1 due to the irradiation, we conducted UV-vis experiment. **Figure 6.11** shows the absorbance spectra of FB1 before and after the treatment with light. The FB1 molecule usually on normal state has absorption at 278 nm[174] but after passing light the absorption bands have changed. This data clearly shows the change in absorbance maxima which further fortifies the hypothesis that green LED light degrades the FB1 molecule. Here, it is to be noted that FB1 was dissolved in aqueous methanol ($CH_3OH:H_2O$ = 1:5 v/v), so the solvent effect has been pronounced in the spectra.

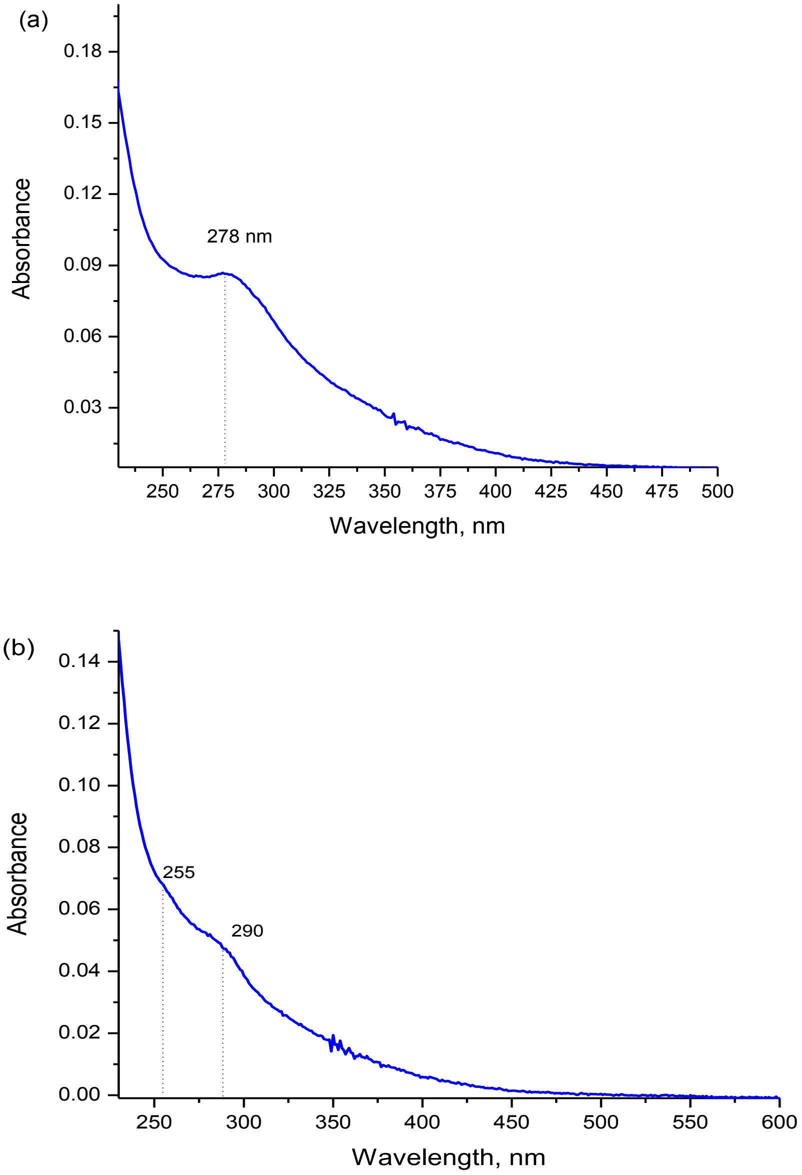

Figure 6.11: UV-vis spectra of aq. methanol solution (1:5; v/v) of FB1 (2.8×10^{-4} M) before (a) and after (b) the treatment of green light. (optical path length 1 cm).

Figure 6.12 shows mass spectrum in absence and presence of the irradiated sample. We can clearly see a maximum peak at 722.39 (+1) m/z peak which is due to the FB1 molecule whose molecular weight is 721. 83 m/z. After treatment of light, we can see the change in the spectrum with the formation of other peaks. This shows that the native structure of FB1 changes to some extent due to the application of green LED light.

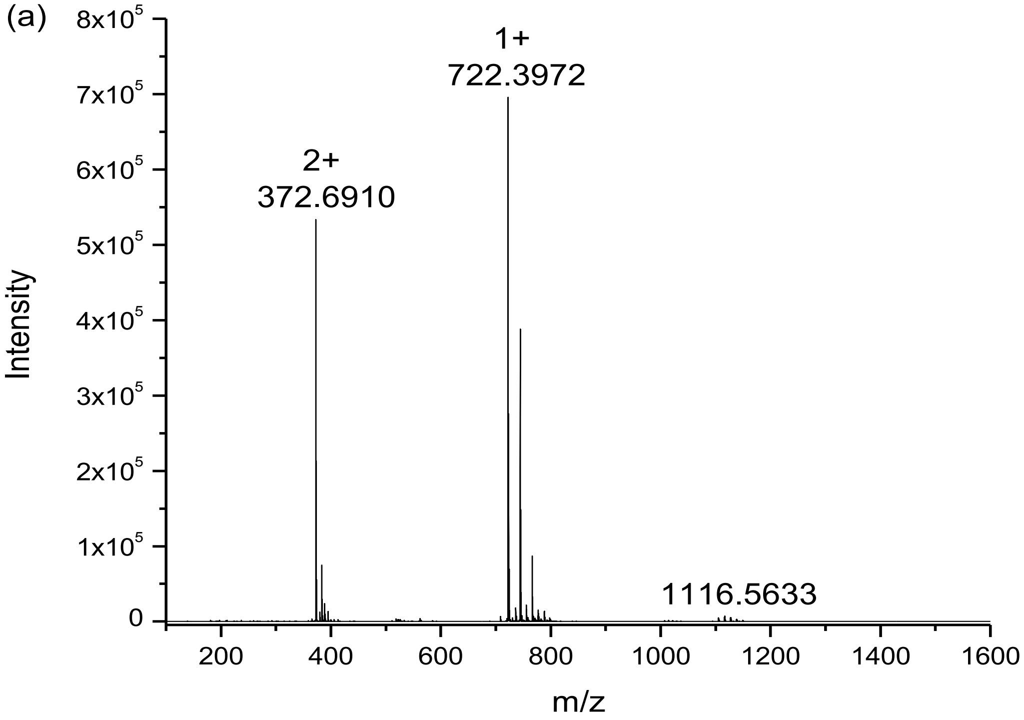

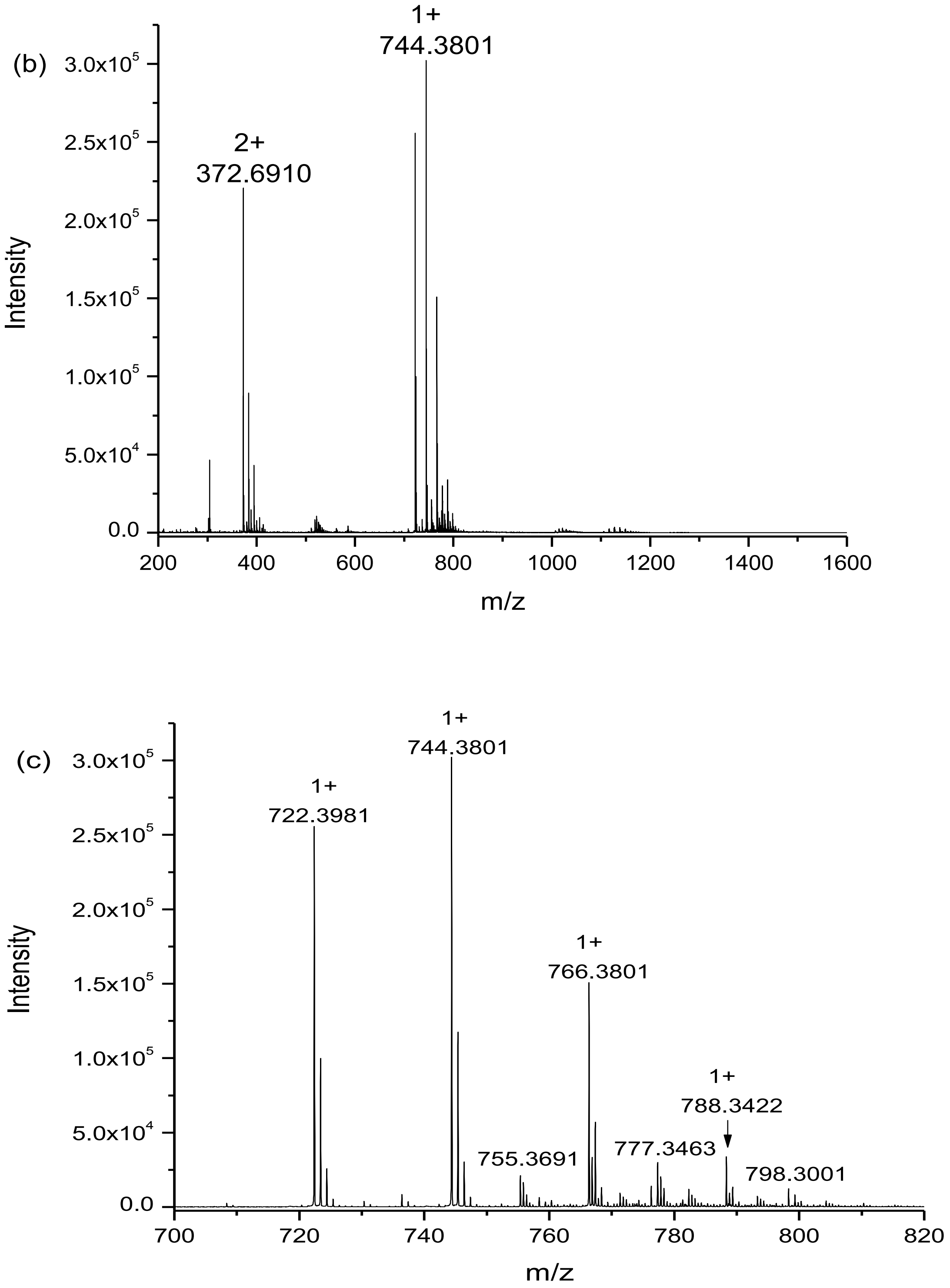

Figure 6.12: Mass Spectra of fumonisin B1: (a) Without irradiation, (b) With irradiation, and (c) Enlarged spectrum of (b) to show the clear peaks.

6.7 Summary

The self-assembly ability of different analytes to spontaneously organize into nanostructures mimicking the living cell membranes, appears as a suitable concept for the development of biomimetic membrane models. Langmuir monolayer of analyte like FB1 provides the potential of two-dimensional molecular self-assemblies, which have been extensively used as models to understand the role and the organization of biological membranes and its interaction. We found that the FB1 Langmuir monolayer was degraded with the effect of green LED light at 525 nm wavelength. This clearly means that the tendency of FB1 molecules to stay active on the cell membrane and their penetrating ability will get diminished. Furthermore, UV-vis absorption, emission, and mass spectra of the green LED light treated FB1 showed that there is change in their structure and the molecules get degraded. This finding will be a milestone in the treatment of fungal keratitis by *in vivo* method.

Chapter 7

Future Directions

7.1 Investigation of Reactivity of Monolayers

The reactivity of the monolayer can also be studied to unleash the properties of the monolayer. The study of the surface reactivity and many other is an active area of research in surface chemistry. It has been found that study of reactivity of monolayer helps in controlling the density of ligands that are to be immobilized. Here, the reactivity of the monolayer can be turned off by electrochemical reduction, this way it is possible to turn the reactivity of monolayer on and off. [175-177]

7.2 Understanding of Surface Reactions

We are also interested in the detailed mechanisms of reactions occurring at surfaces and interfaces. How chemical reactions take place at the air-water as well as air-solid, liquid-solid, and solid-solid interface is another aspect of our research to be focused. An understanding of this chemistry is inherently interesting because of the typical complexity of reactions at a surface or interface, and because interfacial processes are crucial in so many important technological applications. Surface reactions form the core of heterogeneous catalytic processes. Moreover, the construction of electronic devices relies on an understanding of the surface chemistry of silicon and other inorganic semiconductors. The development of organic electronic devices relies on a detailed understanding of the attachment of organic molecules to silicon surfaces, as well as an understanding of the organic-organic interfaces that comprise typical thin film organic electronic devices. Even applications as common as corrosion inhibition rely on an understanding of the surface oxidation of materials and their interactions with molecular systems. For this, our work will rely on obtaining molecular/atomic level information about the structure of surfaces and interfaces and coupling this structural information with detailed kinetic and mechanistic information obtained using a range of spectroscopic probes. Structural information is obtained using low energy electron diffraction, X-ray diffraction, electron microscopy or scanning probe microscopies, such as scanning tunneling microscopy (STM) or atomic force microscopy (AFM). Electron spectroscopies, such as UV and X-ray photoelectron spectroscopy, as well as optical probes such as reflection absorption infrared spectroscopy and surface enhanced Raman spectroscopy allow us to obtain surface composition and molecular level structural information about the surfaces and interfaces that we study. Electrochemical probes, such as cyclic voltammetry and electrochemical impedance spectroscopy, are used to study the kinetics of these processes at the liquid-solid interface.[178] Mass spectrometry and molecular spectroscopy are used to probe kinetics and dynamics of reactions at the gas-solid interface.

Several of the key questions which must be addressed for the eventual implementation of thin film organic electronic and opto-electronic devices fashioned inexpensively using solution processing approaches are related to the detailed mechanism of self-assembly of organic molecules at the liquid-solid interface. Understanding these structural motifs and their stabilities, and the design rules based on these observations, could lead to an improvement of the structure dependent electronic properties of these self-assembled layers utilized in organic electronic devices. Chemical reactions occurring at electrode surfaces, in particular the electrocatalytic reduction of CO_2 to form fuels and value added chemicals, will be another focus of our research. In this, electrochemical probes will be coupled with vacuum based photoelectron spectroscopy to provide a detailed understanding of the interaction of CO_2 and catalyst molecules, such as imidazole with electrode surfaces under aqueous conditions. This work also informs mechanistic studies of corrosion inhibition at active metal surfaces such as iron and copper using these same sorts of pyridine and substituted imidazole molecules in the presence of dissolved CO_2.

7.3 Carbon dots in Polymerization Process as Initiators

Due to the low toxicity, high water solubility, and bio-compatibility CDs are widely investigated. The fluorescent CDs have already been used in bio-imaging, drug delivery, medical diagnosis, catalysis, photovoltaic etc. We have predicted that CDs can also be used as initiators in polymerization process. Specially, polyaniline, polypyrrole, and co-polymerization of polyaniline and polypyrrole from monomers can be performed using CDs and UV light. This is because the CDs have many unshared or unpaired electrons and the positively charged aniline is attracted to the CDs. This strategy will be helpful in designing the synthetic route for polymerization of monomer through colloidal synthesis by economic, efficient, and green method. Moreover, this will shorten the preparation steps of ready-to-use material and will open a new route for polymerizing monomers with new properties and lead to economically efficient process application. The newly synthesized polymers can be used as supercapacitor in bioanalytical application, in sensors, and as the chemiresistors. Furthermore, the mechanism of catalytical activity of CDs can be investigated by masking the COOH, or OH, or C=O groups on the surface of CDs.

7.4 Quantification of Fumonisin B1 Toxin Using Carbon Dots

Researchers have been struggling to degrade the mycotoxins without the use of invasive techniques. In this regard, the important objective is to detect the mycotoxins. Besides this, primarily the detection of mycotoxins should proceed via the detection of specific strains of molds. Previously, some techniques like liquid-liquid extraction[179], solid phase extraction[180], ion-exchange columns[181], immunoaffinity columns[182] have been used for the detection of mycotoxins. These methods have the problems like time-consuming, labor-intensive, and needing large volume of solvents.[183] Moreover, the presence of mycotoxin can be superficially known by enzyme-linked immunosorbent assay (ELISA), PCR, and whole genome sequencing (WGS). But, ELISA has the limitation of antibody availability for various toxins, while PCR and WGS indicate the presence of mycotoxins at a genetic level only.

Till now, the conjugation of mycotoxins has been made to mask them[184] and in the removal of nonfermentable fractions in the ethanol production process.[185] To the best of our knowledge, the quantification of toxins has not been reported so far by using the nanoparticles as the conjugating precursor. Herein, we propose a facile method to quantify the Fumonisin B1 from mixture of different mycotoxins.

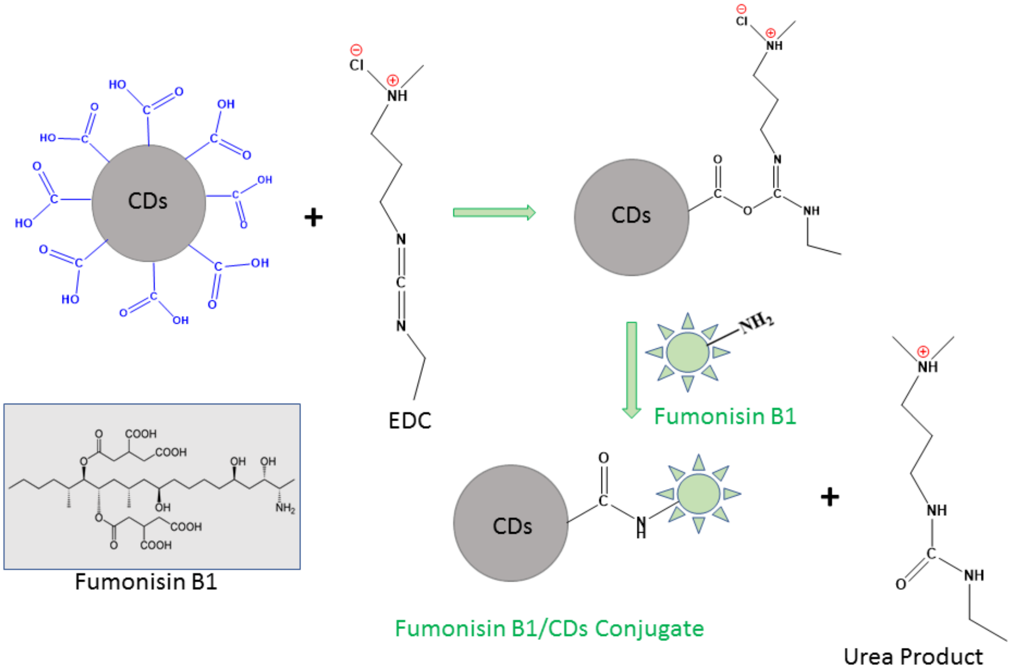

Scheme 7.1: Conjugation of Fumonisin B1 with CDs.

Usually, it is hard to quantify any mycotoxins when there is a mixture of many mycotoxins in a given sample of corneal tissue. We successfully conjugated fumonisin B1 with CDs as shown in **scheme 7.1.** We designed our method in such a way that the conjugation process can only bind the of fumonisin B1 with the CDs as shown in **equation 7.1** and later it's easier to quantify selectively. This is because the FB1 has only -NH2 group which other mycotoxins do not have to react with -COOH group of CDs make a C-N bond in the conjugation process.

CDs + Fumonisin B1 ⟹ CDs-Fumonisin Conjugate + Urea biproduct ……(7.1)

Once we are able to quantify the conjugate then we can relate the result to find the amount of fumonisin present in any sample. We will use following methods in quantification of thus obtained conjugates.

I. Nuclear Magnetic Resonance (NMR) Spectroscopy

In this method, the Nitrogen NMR, N-NMR spectra will be obtained with the integrated signals. From this, the number of nitrogen atoms present in the sample can be evaluated. We know that fumonisin B1 has only one nitrogen in its molecular structure. Evaluating the number of nitrogen in a specific concentration of sample taken can easily help in evaluating the actual concentration of fumonisin B1 present in the sample.

II. Circular Dichroism Spectroscopy (CD)

Earlier, our group members have been successful in determining the concentration of different protein conjugates by using the circular dichroism spectroscopy.[186-187] In this method, a calibration curve is used to determine the concentration of the conjugate. CD is based on the differential absorption of the left- and right-circularly polarized light when such light beams are passed through a chiral sample[188] (whose mirror images do not superimpose), such as fumonisin B1. The carbon dots is assumed as achiral in most cases, so it does not have the CD signal. Under this assumption, we can expect to determine the mycotoxin (fumonisin B1) concentration in the conjugates from a calibration curve obtained from the CD spectra as shown in **equation 7.2**.

$$\Delta A = A_L - A_R = \Delta \varepsilon \, c \, l \quad \ldots\ldots\ldots\ldots\ldots\ldots (7.2)$$

where ‘AL’ and ‘AR’ are the absorbance of the left- and right circularly polarized light by the chiral sample, respectively. ‘$\Delta\varepsilon$’ is the molar extinction coefficient of the sample; ‘c’ is the molar concentration, and ‘l’ is the path length in centimeters.

REFERENCES

1. McCash, E. M. *Surface Chemistry*. **2001**.

2. Bangham, A.; Standish, M. M.; Watkins, J. C. *J. Mole. Bio.* **1965,** *13*, 238.

3. Tien, H. T., *Bilayer Lipid Membranes (BLM): Theory and Practice*. M. Dekker: **1974**.

4. Micol, V.; Sánchez-Piñera, P.; Villalaín, J.; de Godos, A.; Gómez-Fernández, J. C. *Biophys. J.* **1999,** *76*, 916.

5. Matsuzaki, K. *BBA-Biomembranes* **2007,** *1768*, 1935.

6. Langmuir, I. *J. Am. Chem. Soc.* **1917,** *39*, 1848.

7. Roberts, G. *Langmuir-Blodgett Films*. Springer Science & Business Media: **2013**.

8. Ulman, A. *An Introduction to Ultrathin Organic Films: From Langmuir--Blodgett to Self--Assembly*. Academic Press: **2013**.

9. Harkins, W. D.; Boyd, E. *J. Phys. Chem.* **1941,** *45*, 20.

10. Harkins, W. D.; Boyd, E. *J. Chem. Phys.* **1940,** *8*, 129.

11. Dervichian, D. *Prog. Biophys. Mol. Biol.* **1964,** *14*, 263

12. Feng, S. *Langmuir* **1999,** *15*, 998

13. Chen, X.; Wang, J.; Shen, N.; Luo, Y.; Li, L.; Liu, M.; Thomas, R. K. *Langmuir* **2002,** *18*, 6222.

14. Sung, I.-H.; Yang, J. C.; Kim, D. E.; Shin, B. S. *Wear* **2003,** *255*, 808.

15. Singer, S. J.; Nicolson, G. L. *Science* **1972,** *175*, 720.

16. Simons, K.; Ikonen, E. *Nature* **1997,** *387*, 569.

17. Iwabuchi, K.; Yamamura, S.; Prinetti, A.; Handa, K.; Hakomori, S. *J. Biol. Chem.* **1998,** *273*, 9130.

18. Boucher, J.; Trudel, E.; Méthot, M.; Desmeules, P.; Salesse, C. *Colloids Surf. B: Biointerfaces* **2007,** *58*, 73.

19. Higuchi, Y.; Matsufuji, H.; Tanuma, M.; Arakawa, T.; Mori, K.; Yamada, C.; Shofia, R.; Matsunaga, E.; Tashiro, K.; Fushinobu, S. *Sci. Rep.* **2018,** *8*, 12013.

20. Fowler, A. V.; Zabin, I. *J. Biol. Chem.* **1978,** *253*, 5521.

21. Grosová, Z.; Rosenberg, M.; Rebroš, M. Czech J. Food Sci., Citeseer: **2008**.

22. Sharma, S. K.; Leblanc, R. M. *Ana. Biochem.* **2017,** *535*, 1.

23. Ingram, C. J.; Mulcare, C. A.; Itan, Y.; Thomas, M. G.; Swallow, D. M. *Human Genet.* **2009,** *124*, 579.

24. Abel, S. M.; Roose, J. P.; Groves, J. T.; Weiss, A.; Chakraborty, A. K., *J. Phys. Chem. B* **2012,** *116*, 3630.

25. Shih, S. C.; Goyal, G.; Kim, P. W.; Koutsoubelis, N.; Keasling, J. D.; Adams, P. D.; Hillson, N. J.; Singh, A. K. *ACS Synth. Biol.* **2015,** *4*, 1151.

26. Acton, Q. A. *Advances in beta-Galactosidase Research and Application: 2012 Edition: ScholarlyBrief*. ScholarlyEditions: **2012**.

27. Juers, D. H.; Jacobson, R. H.; Wigley, D.; Zhang, X. J.; Huber, R. E.; Tronrud, D. E.; Matthews, B. W. *Protein Sci.* **2000,** *9*, 1685.

28. Jain, V. K.; Magrath, I. T. *Anal. Biochem.* **1991,** *199*, 119.

29. Juers, D. H.; Heightman, T. D.; Vasella, A.; McCarter, J. D.; Mackenzie, L.; Withers, S. G.; Matthews, B. W. *Biochemistry* **2001,** *40*, 14781.

30. Leighton, P. A.; Mitchell, K. J.; Goodrich, L. V.; Lu, X.; Pinson, K.; Scherz, P.; Skarnes, W. C.; Tessier-Lavigne, M. *Nature* **2001,** *410*, 174.

31. Casadaban, M. J.; Martinez-Arias, A.; Shapira, S. K.; Chou, J. *Methods Enzymol.* **1983,** *100*, 293.

32. Yang, S.; Veide, A.; SO, E. *Biotechnol. Appl. Biochem.* **1995,** *22*, 145.

33. Ullmann, A. *Gene* **1984,** *29*, 27.

34. Benito, A.; Valero, F.; Lafuente, J.; Vidal, M.; Cairo, J.; Sola, C.; Villaverde, A. *Enzyme Microb. Technol.* **1993,** *15*, 66.

35. Sambrook, J.; Fritsch, E. F.; Maniatis, T., *Molecular Cloning*. Cold Spring Harbor Laboratory Press New York: **1989**, 2.

36. Villaverde, A. *FEBS Lett.* **2003,** *554*, 169.

37. Gaines, G. L., Jr. Insoluble Monolayers at Liquid-Gas Interfaces. **1966**.

38. Adamson, A.; Gast, A. *Electrical Aspects of Surface Chemistry. Physical Chemistry of Surfaces;* John Wiley & Sons: New York*,* **1997**.

39. Li, S.; Leblanc, R. M. *J. Phys. Chem. B* **2013,** *118*, 1181.

40. Orbulescu, J.; Micic, M.; Ensor, M.; Trajkovic, S.; Daunert, S.; Leblanc, R. M. *Langmuir* **2009,** *26*, 3268.

41. Li, S.; Micic, M.; Orbulescu, J.; Whyte, J. D.; Leblanc, R. M. *J. Royal Soc. Interface* **2012**, 20, 120.

42. Hasegawa, T.; Sato, Y.; Kakuda, H.; Li, C.; Orbulescu, J.; Leblanc, R. M. *J. Phys. Chem. B* **2008,** *112*, 1391.

43. Kaganer, V. M.; Möhwald, H.; Dutta, P. *Rev. Modern Phys.* **1999,** *71*, 779.

44. Vollhardt, D.; Fainerman, V. *Colloids Surf. A: Physicochem. Eng. Aspects* **2001,** *176*, 117.

45. Richmond, M.; Gray, J.; Stine, C. *J. Dairy Sci.* **1981,** *64*, 1759.

46. Holzmann, B.; Johnson, J. P. *J. Immunol. Methods* **1983,** *60*, 359.

47. Crawford, N. F.; Micic, M.; Orbulescu, J.; Weissbart, D.; Leblanc, R. M. *J. Colloid Interface Sci.* **2015,** *453*, 202.

48. Jagla, E. *Phys. Rev. E* **2001,** *63*, 61509.

49. Vidawati, S.; Bakowoski, U.; Rothe,U. *Adv. Biol. Chem.* **2012,** 0*2, 233*.

50. Matsumoto, Y.; Nakahara, H.; Moroi, Y.; Shibata, O. *Langmuir* **2007,** *23*, 9629.

51. Netto, C. G.; Toma, H. E.; Andrade, L. H. *J. Mol. Catal. B: Enzymatic* **2013,** *85*, 71.

52. Kiernan, J. *Biotech. Histochem.* **2007,** *82*, 73.

53. Dynarowicz-Łątka, P.; Dhanabalan, A.; Oliveira, O. N. *Adv. Colloid Interface Sci.* **2001,** *91*, 221.

54. Mendelsohn, R.; Mao, G.; Flach, C. R. *BBA-Biomembranes* **2010,** *1798*, 788.

55. Flach, C. R.; Brauner, J. W.; Mendelsohn, R. *Biophys. J.* **1993,** *65*, 1994.

56. Blaudez, D.; Buffeteau, T.; Cornut, J.; Desbat, B.; Escafre, N.; Pezolet, M.; Turlet, J. *Appl. Spect.* **1993,** *47*, 869.

57. Jacobson, R.; Zhang, X.; DuBose, R.; Matthews, B. *Nature* **1994,** *369*, 761.

58. Tello-Solís, S. R.; Jiménez-Guzmán, J.; Sarabia-Leos, C.; Gómez-Ruíz, L.; Cruz-Guerrero, A. E.; Rodríguez-Serrano, G. M.; García-Garibay, M. *J. Agri. Food Chem.* **2005,** *53*, 10200.

59. Meunier, J. *Colloids Surf. A: Physicochem. Eng. Asp.* **2000,** *171*, 33.

60. Hénon, S.; Meunier, J. *Rev. Sci. Instrum.* **1991,** *62*, 936.

61. Basu, I.; Mukhopadhyay, C. *Langmuir* **2014,** *30*, 15244.

62. Ye, S.; Luo, Y. *Sci. China Chem.* **2014,** *57*, 1646.

63. Niaura, G.; Kuprionis, Z.; Ignatjev, I.; Kazemekaite, M.; Valincius, G.; Talaikyte, Z.; Razumas, V.; Svendsen, A. *J. Phys. Chem. B* **2008,** *112*, 4094.

64. Miranda, P.; Shen, Y. *J. Phys. Chem. B* **1999,** *103*, 3292.

65. Buck, M.; Himmelhaus, M. *J. Vac. Sci. Technol. A* **2001,** *19*, 2717.

66. Chen, Z.; Shen, Y.; Somorjai, G. A. *Annu. Rev. Phys. Chem.* **2002,** *53*, 437.

67. Richmond, G. *Chem. Rev.* **2002,** *102*, 2693.

68. Grubb, S.; Kim, M. W.; Rasing, T.; Shen, Y. *Langmuir* **1988,** *4*, 452.

69. Juers, D. H.; Heightman, T. D.; Vasella, A.; McCarter, J. D.; Mackenzie, L.; Withers, S. G.; Matthews, B. W. *Biochemistry* **2001,** *40*, 14781.

70. Frisch, M. J.; Trucks, G. W.; Schlegel, H. B.; Scuseria, G. E.; Robb, M. A.; Cheeseman, J. R.; Scalmani, G.; Barone, V.; Mennucci, B.; Petersson, G. A.; Nakatsuji, H.; Caricato, M.; Li, X.; Hratchian, H. P.; Izmaylov, A. F.; Bloino, J.; Zheng, G.; Sonnenberg, J. L.; Hada, M.; Ehara, M.; Toyota, K.; Fukuda, R.; Hasegawa, J.; Ishida, M.; Nakajima, T.; Honda, Y.; Kitao, O.; Nakai, H.; Vreven, T.; Montgomery Jr., J. A.; Peralta, J. E.; Ogliaro, F.; Bearpark, M. J.; Heyd, J.; Brothers, E. N.; Kudin, K. N.; Staroverov, V. N.; Kobayashi, R.; Normand, J.; Raghavachari, K.; Rendell, A. P.; Burant, J. C.; Iyengar, S. S.; Tomasi, J.; Cossi, M.; Rega, N.; Millam, N. J.; Klene, M.; Knox, J. E.; Cross, J. B.; Bakken, V.; Adamo, C.; Jaramillo, J.; Gomperts, R.; Stratmann, R. E.; Yazyev, O.; Austin, A. J.; Cammi, R.; Pomelli, C.; Ochterski, J. W.; Martin, R. L.; Morokuma, K.; Zakrzewski, V. G.; Voth, G. A.; Salvador, P.; Dannenberg, J. J.; Dapprich, S.; Daniels, A. D.; Farkas, Ö.; Foresman, J. B.; Ortiz, J. V.; Cioslowski, J.; Fox, D. J. *Gaussian 09*, Gaussian, Inc.: Wallingford, CT, USA, **2009**.

71. Wang, J.; Wolf, R. M.; Caldwell, J. W.; Kollman, P. A.; Case, D. A. *J. Comput. Chem.* **2004,** *25*, 1157.

72. Wang, J.; Wang, W.; Kollman, P. A.; Case, D. A. *J. Mol. Graph. Model.* **2006,** *25*, 247.

73. Krieger, E.; Koraimann, G.; Vriend, G. *Proteins: Structure, Function, and Bioinformatics* **2002,** *47*, 393.

74. Lindahl, E.; Hess, B.; van der Spoel, D. *Mol. Model. Annual* **2001,** *7*, 306.

75. Oostenbrink, C.; Villa, A.; Mark, A. E.; Van Gunsteren, W. F. *J. Comput. Chem.* **2004,** *25*, 1656.

76. Case, D. A.; Cheatham, T. E.; Darden, T.; Gohlke, H.; Luo, R.; Merz, K. M.; Onufriev, A.; Simmerling, C.; Wang, B.; Woods, R. J. *J. Comput. Chem.* **2005,** *26*, 1668.

77. Jorgensen, W. L.; Chandrasekhar, J.; Madura, J. D.; Impey, R. W.; Klein, M. L. *The J. Chem. Phys.* **1983,** *79*, 926.

78. Miyamoto, S.; Kollman, P. A. *J. Comput. Chem.* **1992,** *13*, 952.

79. Darden, T.; York, D.; Pedersen, L. *J. Chem. Phys.* **1993,** *98*, 10089.

80. Petrucci, R. H.; Harwood, W. S.; Herring, G. F.; Madura, J. D., *General Chemistry: Principles and Modern Applications*. Pearson Education International: **2007**.

81. Mahmoud, M. A.; O'Neil, D.; El-Sayed, M. A. *Chem. Mater.* **2013,** *26*, 44.

82. Dhakshinamoorthy, A.; Asiri, A. M.; Garcia, H. *ACS Catalysis* **2017,** *7*, 2896.

83. Zhou, M.; Tian, M.; Li, C. *Bioconjugate Chem.* **2016,** *27*, 1188.

84. Miao, Q.; Xie, C.; Zhen, X.; Lyu, Y.; Duan, H.; Liu, X.; Jokerst, J. V.; Pu, K. *Nat. Biotechnol.* **2017,** *35*, 1102.

85. Yao, X.; Niu, X.; Ma, K.; Huang, P.; Grothe, J.; Kaskel, S.; Zhu, Y. *Small* **2017,** *13*, 2.

86. Maeki, M.; Kimura, N.; Sato, Y.; Harashima, H.; Tokeshi, M. *Advanced Drug Delivery Reviews* **2018**.

87. Iannazzo, D.; Pistone, A.; Salamò, M.; Galvagno, S.; Romeo, R.; Giofré, S. V.; Branca, C.; Visalli, G.; Di Pietro, A. *Int. J. Pharm.* **2017,** *518*, 185.

88. Derfus, A. M.; Chan, W. C.; Bhatia, S. N. *Adv. Mater.* **2004,** *16*, 961.

89. Sapsford, K. E.; Pons, T.; Medintz, I. L.; Mattoussi, H. *Sensors* **2006,** *6*, 925.

90. Li, J.; Zhu, J. J. *Analyst* **2013,** *138*, 2506.

91. Luo, X.; Morrin, A.; Killard, A. J.; Smyth, M. R. *Electroanalysis* **2006,** *18*, 319.

92. Derfus, A. M.; Chan, W. C.; Bhatia, S. N. *Nano Lett.* **2004,** *4*, 11.

93. Gwinn, M. R.; Vallyathan, V. *Env. Health Perspect.* **2006,** *114*, 1818.

94. Gaonkar, A. G.; Vasisht, N.; Khare, A. R.; Sobel, R., *Microencapsulation in the Food Industry: a Practical Implementation Guide*. Elsevier: **2014**.

95. Pollard, D. J.; Woodley, J. M. *Trends Biotechnol.* **2007,** *25*, 66.

96. Fjerbaek, L.; Christensen, K. V.; Norddahl, B. *Biotechnol. Bioeng.* **2009,** *102*, 1298.

97. Garcia-Galan, C.; Berenguer-Murcia, Á.; Fernandez-Lafuente, R.; Rodrigues, R. C. *Adv. Synth. Catal.* **2011,** *353*, 2885.

98. Wang, M.; Qi, W.; Yu, Q.; Su, R.; He, Z. *Biochem. Eng. J.* **2010,** *52*, 168.

99. Li, Y.; Liu, W.; Sun, C.; Zheng, M.; Zhang, J.; Liu, B.; Wang, Y.; Xie, Z.; Xu, N., *J. Colloid Interface Sci.* **2018,** *523*, 226.

100. Pradhan, N.; Jana, N. R.; Jana, N. R. *ACS Appl. Nano Mater.* **2018,** *1*, 1094.

101. Hosseinzadeh, G.; Maghari, A.; Farniya, S. M. F.; Keihan, A. H.; Moosavi-Movahedi, A. A. *Mater. Sci. Eng. C* **2017,** *77*, 836.

102. Zhou, Y.; Desserre, A.; Sharma, S. K.; Li, S.; Marksberry, M. H.; Chusuei, C. C.; Blackwelder, P. L.; Leblanc, R. M. *ChemPhysChem* **2017,** *18*, 890.

103. Wang, J. *Chem. Rev.* **2008,** *108*, 814.

104. Mazaheri, M.; Simchi, A.; Aashuri, H. *Microchim. Acta* **2018,** *185*, 178.

105. Sharma, S. K.; Seven, E. S.; Micic, M.; Li, S.; Leblanc, R. M. *Langmuir* **2018,** *34*, 2557.

106. Sharma, S. K.; Li, S.; Micic, M.; Orbulescu, J.; Weissbart, D.; Nakahara, H.; Shibata, O.; Leblanc, R. M. *J. Phys. Chem. B* **2016,** *120*, 12279.

107. Kissinger, P. T.; Heineman, W. R. *J. Chem. Edu.* **1983,** *60*, 702.

108. Holmgren, J. *Nature* **1981,** *292*, 413.

109. Leitch, J. J.; Brosseau, C. L.; Roscoe, S. G.; Bessonov, K.; Dutcher, J. R.; Lipkowski, J. *Langmuir* **2013,** *29*, 965.

110. Lopez, P. H.; Schnaar, R. L. *Curr. Opin. Struct. Biol.* **2009,** *19*, 549.

111. Conte, W. L.; Kamishina, H.; Reep, R. L. *Nat. Protoc.* **2009,** *4*, 1157.

112. Haan, L. D.; Hirst, T. R. *Mol. Membr. Biol.* **2004,** *21*, 77.

113. Chakraborty, S. K.; Fitzpatrick, J. A.; Phillippi, J. A.; Andreko, S.; Waggoner, A. S.; Bruchez, M. P.; Ballou, B. *Nano Lett.* **2007,** *7*, 2618.

114. Zhou, N.; Hao, Z.; Zhao, X.; Maharjan, S.; Zhu, S.; Song, Y.; Yang, B.; Lu, L. *Nanoscale* **2015,** *7*, 15635.

115. Lanciego, J. L.; Wouterlood, F. G. *J. Chem. Neuroanat.* **2011,** *42*, 157.

116. Sanchez, J.; Holmgren, *J. Proc. Natl. Acad. Sci.* **1989,** *86*, 481.

117. Sanchez, J.; Johansson, S.; Löwenadler, B.; Svennerholm, A.; Holmgren, J. *Res. Microbiol.* **1990,** *141*, 971.

118. Zhang, B.; Li, H.; Zhang, L.; Tan, S.; Cai, W.; Men, X.; Huang, Y.; Shan, Y.; Lin, Y.; Lu, Z. *J. Neuroinflammation* **2016,** *13*, 147.

119. Sun, J.-B.; Holmgren, J.; Czerkinsky, C. *Proc. Natl. Acad. Sci.* **1994,** *91*, 10795.

120. Holmgren, J.; Adamsson, J.; Anjuère, F.; Clemens, J.; Czerkinsky, C.; Eriksson, K.; Flach, C.-F.; George-Chandy, A.; Harandi, A. M.; Lebens, M. *Immunol. Lett.* **2005,** *97*, 181.

121. Harokopakis, E.; Childers, N. K.; Michalek, S. M.; Zhang, S. S.; Tomasi, M. *J. Immunol. Methods* **1995,** *185*, 31.

122. Porras, M. A. G.; Durfee, P. N.; Gregory, A. M.; Sieck, G. C.; Brinker, C. J.; Mantilla, C. B. *J. Neurosci. Methods* **2016,** *273*, 160.

123. Nichols, N. L.; Vinit, S.; Bauernschmidt, L.; Mitchell, G. S. *Exp. Neurol.* **2015,** *267*, 18.

124. Matsuzaki, K.; Kato, K.; Yanagisawa, K. *BBA-Mol. Cell Biol. Lipids* **2010,** *1801*, 868.

125. Yanagisawa, K. *BBA-Biomembranes* **2007,** *1768*, 1943.

126. Thakur, G.; Micic, M.; Leblanc, R. M. *Colloids Surf. B: Biointerfaces* **2009,** *74*, 436.

127. Craig, L.; Taylor, R. K. *Bacterial Pili: Structure, Synthesis and Role in Disease* **2014,** *27*, 1.

128. Day, C. A.; Kenworthy, A. K. *Essays Biochem.* **2015,** *57*, 135.

129. Zhang, R.-G.; Scott, D. L.; Westbrook, M. L.; Nance, S.; Spangler, B. D.; Shipley, G. G.; Westbrook, E. M. *J. Mole. Biol.* **1995,** *251*, 563.

130. Branson, T. R.; McAllister, T. E.; Garcia-Hartjes, J.; Fascione, M. A.; Ross, J. F.; Warriner, S. L.; Wennekes, T.; Zuilhof, H.; Turnbull, W. B. *Angew. Chemie Int. Edit.* **2014,** *53*, 8323.

131. Baldauf, K. J.; Royal, J. M.; Hamorsky, K. T.; Matoba, N. *Toxins* **2015,** *7*, 974.

132. Terrettaz, S.; Stora, T.; Duschl, C.; Vogel, H. *Langmuir* **1993,** *9*, 1361.

133. Lauer, S.; Goldstein, B.; Nolan, R. L.; Nolan, J. P. *Biochemistry* **2002,** *41*, 1742.

134. Miller, C.; Majewski, J.; Faller, R.; Satija, S.; Kuhl, T. *Biophys. J.* **2004,** *86*, 3700.

135. Williams, T. L.; Jenkins, A. T. A. *J. Am. Chem. Soc.* **2008,** *130*, 6438.

136. Kuziemko, G. M.; Stroh, M.; Stevens, R. C. *Biochemistry* **1996,** *35*, 6375.

137. Sun, H.; Chen, L.; Gao, L.; Fang, W. *Langmuir* **2015,** *31*, 9105.

138. Munishkina, L. A.; Phelan, C.; Uversky, V. N.; Fink, A. L. *Biochemistry* **2003,** *42*, 2720.

139. Cherepanov, D. A.; Feniouk, B. A.; Junge, W.; Mulkidjanian, A. Y. *Biophys. J.* **2003,** *85*, 1307.

140. Jiang, D.; Dinh, K. L.; Ruthenburg, T. C.; Zhang, Y.; Su, L.; Land, D. P.; Zhou, F. *J. Phys. Chem. B* **2009,** *113*, 3160.

141. Lee, K. Y. C. *Annu. Rev. Phys. Chem.* **2008,** *59*, 771.

142. Krieger, E., YASARA. **2003**.

143. Lee, I.; Justus, B. L.; Lee, J. W.; Greenbaum, E. *J. Phys. Chem. B* **2003,** *107*, 14225.

144. Teale, F.; Weber, G. *Biochem. J.* **1957,** *65*, 476.

145. Ma, G.; Allen, H. C. *Langmuir* **2006,** *22*, 5341.

146. Crawford, N.; Micic, M.; Orbulescu, J.; Weissbart, D.; Leblanc, R. *J. Colloid Interface Sci.* **2015,** *453*, 202.

147. Hasegawa, T. *Quantitative Infrared Spectroscopy for Understanding of a Condensed Matter*. Springer: **2017**.

148. Jackson, M.; Mantsch, H. H. *Crit. Rev. Biochem. Mole. Biol.* **1995,** *30*, 95.

149. Vagharchakian, L.; Desbat, B.; Hénon, S. *Macromolecules* **2004,** *37*, 8715.

150. Naiker, S.; Odhav, B. *Mycoses* **2004,** *47*, 50.

151. Shetty, P. H. *Natural Occurrence and Management of Fumonisin Mycotoxins*. Lambert Academic Publishing: **2011**.

152. Thomas, P.; Kaliamurthy, J. *Clin. Microbiol. Infect.* **2013,** *19*, 210.

153. Desjardins, A.; Proctor, R. *Int. J. Food Microbiol.* **2007,** *119*, 47.

154. Marasas, W. F. O.; Nelson, P. E.; Toussoun, T. A., *Toxigenic Fusarium species. Identity and mycotoxicology*. Pennsylvania State University: **1984**.

155. Seo, J.-A.; Proctor, R. H.; Plattner, R. D. *Fungal Genet. Biol.* **2001,** *34*, 155.

156. Rheeder, J. P.; Marasas, W. F.; Vismer, H. F. *Appl. Env. Microbiol.* **2002,** *68*, 2101.

157. Blackwell, B.; Edwards, O.; Fruchier, A.; ApSimon, J.; Miller, J. *In Fumonisins in Food*, Springer: **1996**, 75.

158. Plattner, R. D.; Weisleder, D.; Poling, S. M. *In Fumonisins in Food*, Springer: **1996**, 57.

159. Momany, F. A.; Dombrink-Kurtzman, M. A. *J. Agric. Food Chem.* **2001,** *49*, 1056.

160. Xie, L.; Dong, X.; Shi, W. *Brit. J. Ophthalmol.* **2001,** *85*, 1070.

161. Galperin, G.; Berra, M.; Tau, J.; Boscaro, G.; Zarate, J.; Berra, A. *Cornea* **2012,** *31*, 176.

162. Bunya, V. Y.; Hammersmith, K. M.; Rapuano, C. J.; Ayres, B. D.; Cohen, E. *J. Am. J. Ophthalmol.* **2007,** *143*, 151.

163. Yoon, K.-C.; Jeong, I.Y.; Im, S.K.; Chae, H.J.; Yang, S.Y. *Cornea* **2007,** *26*, 814.

164. Chang, H.-Y. P.; Chodosh, J. *Int. Ophthalmol. Clin.* **2011,** *51*, 33.

165. Shih, M.-H.; Huang, F.-C. *Invest. Ophthalmol. Vis. Sci.* **2011,** *52*, 223.

166. Kharkwal, G. B.; Sharma, S. K.; Huang, Y. Y.; Dai, T.; Hamblin, M. R. *Lasers Surg. Med.* **2011,** *43*, 755.

167. Arboleda, A.; Miller, D.; Cabot, F.; Taneja, M.; Aguilar, M. C.; Alawa, K.; Amescua, G.; Yoo, S. H.; Parel, J.-M. *Am. J. Ophthalmol.* **2014,** *158*, 64.

168. Amescua, G.; Arboleda, A.; Nikpoor, N.; Durkee, H.; Relhan, N.; Aguilar, M. C.; Flynn, H. W.; Miller, D.; Parel, J.-M. *Cornea* **2017,** *36*, 1141.

169. Höfs, S.; Mogavero, S.; Hube, B. *J. Microbiol.* **2016,** *54*, 149.

170. Hostetter, M. K. *Clin. Microbiol. Rev.* **1994,** *7*, 29.

171. Bonanno, J. A.; Polse, K. *Invest. Ophthalmol. Vis. Sci.* **1987,** *28*, 522.

172. Šegvić, M.; Pepeljnjak, S. *Veterinarski Arhiv* **2001,** *71*, 299.

173. Thakur, G.; Wang, C.; Leblanc, R. M. *Langmuir* **2008,** *24*, 4888.

174. Wang, Y.; He, C.-H.; Zheng, H.; Zhang, H.-B. *Int. J. Mol. Sci.* **2011,** *13*, 84.

175. Quinn, B. M.; Liljeroth, P.; Kontturi, K. *J. Am. Chem. Soc.* **2002,** *124*, 12915.

176. Wong, G.; Concepcion, M.; Vohs, J. M. *Surf. Sci.* **2003,** *526*, 211.

177. Ahmad, J.; Astin, K. B. *J. Am. Chem. Soc.* **1988,** *110*, 8175.

178. Wieckowski, A., *Interfacial Electrochemistry: Theory: Experiment, and Applications*. Routledge: **2017**.

179. Hayashi, Y.; Yoshizawa, T. *Food Chem.* **2005,** *93*, 215.

180. Medina, Á.; González, G.; Sáez, J. M.; Mateo, R.; Jiménez, M. *Syst. Appl. Microbiol.* **2004,** *27*, 261.

181. Monbaliu, S.; Van Poucke, C.; Van Peteghem, C.; Van Poucke, K.; Heungens, K.; De Saeger, S. *Rapid Communications in Mass Spectrometry: An International Journal Devoted to the Rapid Dissemination of Up‐to‐the‐Minute Research in Mass Spectrometry* **2009,** *23*, 3.

182. Zinedine, A.; Brera, C.; Elakhdari, S.; Catano, C.; Debegnach, F.; Angelini, S.; De Santis, B.; Faid, M.; Benlemlih, M.; Minardi, V. *Food Control* **2006,** *17*, 868.

183. Rahmani, A.; Jinap, S.; Soleimany, F. *Compr. Rev. Food Sci. F.* **2009,** *8*, 202.

184. Hildebrand, A. A.; Kohn, B. N.; Pfeiffer, E.; Wefers, D.; Metzler, M.; Bunzel, M. *J. Agric. Food Chem.* **2015,** *63*, 4728.

185. Dzuman, Z.; Stranska-Zachariasova, M.; Vaclavikova, M.; Tomaniova, M.; Veprikova, Z.; Slavikova, P.; Hajslova, J. *J. Agric. Food Chem.* **2016,** *64*, 5085.

186. Li, S.; Peng, Z.; Leblanc, R. M. *Anal. Chem.* **2015,** *87*, 6455.

187. Peng, Z.; Li, J.; Li, S.; Pardo, J.; Zhou, Y.; Al-Youbi, A. O.; Bashammakh, A. S.; El-Shahawi, M. S.; Leblanc, R. M. *Anal. Chem.* **2018,** *90*, 2255.

188. Greenfield, N. J.*Nature Protocols* **2006,** *1*, 2876.

VITA

Shiv K Sharma was born in 3rd February 1987 in Tulsipur Sub-Metropolitan City of Nepal, a small Himalayan country sandwiched in between China and India. His parents are Pareshwar Sharma and Krishna K. Sharma. He received his elementary education in Govt. Primary Schools at Salliban & Ashwara and Dang Valley B. School, Tulsipur. He completed his secondary education (School Leaving Certificate) from Tulasi Secondary School in 2003. In July 2003, he entered the Orchid Science College, Chitwan for 10+2 college studies. In August 2005, he was admitted to Tri-Chandra Multiple Campus, the oldest campus of Nepal, located in the capital city of Kathmandu and completed the work for B.Sc. in Chemistry in 2008. He then pursued M.Sc. degree in Central Department of Chemistry, Tribhuvan University in 2012. In August 2014, he was admitted to the Graduate School of the University of Miami (UM), where he joined Department of Chemistry. In December 2014, he joined Dr. Roger M. Leblanc's group and was granted Ph.D. degree in December 2018. Following are the major publications related to his research works at UM:

I. Sharma, S. K.; Li, S.; Micic, M.; Orbulescu, J.; Weissbart, D.; Nakahara, H.; Shibata, O.; Leblanc, R. M. *J. Phys. Chem. B*, **2016**, 120, 12279.
II. Sharma, S.K.; Leblanc, R.M. *Anal. Biochem.*, **2017**, 535, 1.
III. Sharma, S. K.; Seven, E. S.; Micic, M.; Li, S.; Leblanc, R. M. *Langmuir*, **2018**, 34, 2557.
IV. Zhou, Y.; Desserrre, A.; Sharma, S.K.; Li, S.; Marskberry, M. H.; Chusuei, C.; Blackwelder, P. L., Leblanc, R. M. *ChemPhysChem*, **2017**, 18, 890.
V. Sharma, S. K.; Poudel Sharma, S.; Miller, D.; Parel, J. M.; Leblanc, R. M., *ACS Applied Bio Materials*, **2018** (submitted)
VI. Sharma, S. K.; Hoar, B.; Zahran, E. M. E.; Zhou, Y.; Paudyal, P.; Mintz, K.; and Leblanc, R. M. *Biosensors and Bioelectronics*, **2018** (submitted)
VII. Sharma, S. K.; Hoar, B.; Sharma Poudel, S.; Zhou, Y.; Leblanc, R. M., *Senosrs* **2018** (submitted).